

of infection, the number of EphA2^{low} infected cells decreased over time (Fig. 2A). This difference could not be accounted for by division rates, because we observed lower levels of host cell division among EphA2^{low} cells. Thus, our results may in fact underestimate the impact of EphA2 on infected cell survival (fig. S5). When we infected *EphA2*^(-/-) and wild-type mice with 10^5 *P. yoelii* sporozoites, we observed a large decrease in liver-stage burden after 42 hours in *EphA2*^(-/-) mice (Fig. 2B). *EphA2*^(-/-) mice also exhibited a delay in the onset of blood-stage infection by 1 to 3 days (Fig. 2C). Thus, without EphA2, the host is far less susceptible to productive parasite liver infection.

The parasitophorous vacuole membrane (PVM) is critical for liver-stage development. One liver-stage PVM-resident protein, UIS4, is highly expressed after invasion when it is exported to the PVM (11), making it a useful marker. We constructed a *P. yoelii* parasite line, *PyUIS4-Myc*, which expressed a UIS4-Myc fusion protein driven by the endogenous UIS4 promoter (Fig. 2D). This allowed us to monitor PVM prevalence (UIS4^{pos}) in infected cells by flow cytometry. Most of the UIS4^{pos} infected host cells were in the EphA2^{high} category (Fig. 2E). Similarly, the level of EphA2 expression was higher in UIS4^{pos} infected cells than in UIS4^{neg} infected cells (Fig. 2F). Thus, sporozoites not only preferentially entered EphA2^{high} cells, but invasion accompanied by PVM formation was far more effective in these cells. UIS4^{neg} infected hepatocytes suffered a higher frequency of cell death (Fig. 2G).

Two members of the 6-Cys family of parasite proteins (12, 13), P52 and P36, are expressed in sporozoites, are important for the invasion of hepatocytes (14–16), and are critical for PVM formation (14). In mouse livers, parasites without P52 or P36 were almost entirely eliminated within 3 hours after infection (fig. S6). We tested whether the lack of P52 and P36 phenocopies the lack of host EphA2 and found that *p52^{-/-}/p36^{-/-}* *P. yoelii* sporozoites exhibited a reduced preference for EphA2^{high} cells (Fig. 3A). The related 6-Cys protein PI2 shows structural similarity to the mammalian ligand for EphA2, EphrinA1 (10).

We showed that an interaction in the extracellular region of EphA2 was required for sporozoite entry using an EphA2-blocking antibody (Fig. 1K). Therefore, we next asked whether the presence of P36 and P52 was required for the antibody to block sporozoite entry. The EphA2 antibody blocked infection for wild-type *P. yoelii* sporozoites, but *p52^{-/-}/p36^{-/-}* sporozoite entry was not affected (Fig. 3B). These data suggest that P36 or P52 engages EphA2 at the point of host cell invasion. We next tested whether P52 or P36 could directly impede the interaction between EphrinA1 and EphA2 on the hepatocyte surface, which results in EphA2 activation. When we added EphrinA1 in the presence of P36 to Hepal-6 cells, P36 blocked the activation of EphA2 (Fig. 3, C and D). P52, however, did not block EphrinA1-mediated activation of EphA2 (Fig. 3, C and D). To determine whether the interaction between EphA2 and P36 also occurs in human parasites, we assessed levels of EphA2 in *P. falciparum*

wild-type or *p52^{-/-}/p36^{-/-}/sap1^{-/-}* parasite-infected HC-04 cells. The P52-P36-deficient *P. falciparum* sporozoites exhibited partially reduced selectivity for EphA2^{high} HC-04 cells compared with *P. falciparum* wild-type sporozoites (Fig. 3E). Thus, P36 engages EphA2 but does not trigger its activation in rodent and human parasites.

We have shown that both host EphA2 and parasite 6-Cys proteins have a role in sporozoite invasion of hepatocytes and the establishment of the growth-permissive intracellular niche. Without either component, the parasite can still enter hepatocytes, but it does so without a PVM, which can result in death of the infected hepatocyte. The convergence of infection-permissive phenotypes is best explained by an interaction between parasite P36 and hepatocyte EphA2 when the PVM is formed. This role for EphA2 in hepatocyte infection does not preclude the possibility that additional hepatocyte receptors may be critical for infection. Interventional strategies aimed at either EphA2 or sporozoite 6-Cys proteins might block parasite infection before the onset of clinical malaria.

REFERENCES AND NOTES

1. S. H. Kappe, A. M. Vaughan, J. A. Boddey, A. F. Cowman, *Science* **328**, 862–866 (2010).
2. A. Coppi et al., *Cell Host Microbe* **2**, 316–327 (2007).
3. U. Frevert et al., *J. Exp. Med.* **177**, 1287–1298 (1993).
4. O. Silvie et al., *Nat. Med.* **9**, 93–96 (2003).
5. S. Yalaoui et al., *Cell Host Microbe* **4**, 283–292 (2008).
6. C. D. Rodrigues et al., *Cell Host Microbe* **4**, 271–282 (2008).
7. L. S. Austin, A. Kaushansky, S. H. Kappe, *Cell. Microbiol.* **16**, 784–795 (2014).
8. A. Kaushansky et al., *Infect. Immun.* **83**, 39–47 (2015).
9. E. M. Lisabeth, G. Falivelli, E. B. Pasquale, *Cold Spring Harb. Perspect. Biol.* **5**, a009159 (2013).
10. S. A. Arredondo et al., *Proc. Natl. Acad. Sci. U.S.A.* **109**, 6692–6697 (2012).
11. A. K. Mueller et al., *Proc. Natl. Acad. Sci. U.S.A.* **102**, 3022–3027 (2005).
12. T. Annoura et al., *FASEB J.* **28**, 2158–2170 (2014).
13. M. R. van Dijk et al., *PLOS Pathog.* **6**, e1000853 (2010).
14. M. Labaied et al., *Infect. Immun.* **75**, 3758–3768 (2007).
15. M. R. van Dijk et al., *Proc. Natl. Acad. Sci. U.S.A.* **102**, 12194–12199 (2005).
16. K. M. VanBuskirk et al., *Proc. Natl. Acad. Sci. U.S.A.* **106**, 13004–13009 (2009).

ACKNOWLEDGMENTS

We are grateful to W. Betz for mosquito and sporozoite production. We thank the vivarium staff of the Center for Infectious Disease Research for their work with mice. This work was funded by a NIH Research Project Grant (R01) to S.H.I.K. and A.K. (grant no. 1R01GM101183-01A1). A.K. is also a recipient of a Transition to Independence Award (award no. 1K99AI11785-01A1), which partially funded this work. A.K., N.A., A.N.D., V.V., N.D., H.K., and L.S.A. performed the experiments. A.K., D.N.S., and S.H.I.K. supervised the research. A.K. and S.H.I.K. wrote the paper. A provisional U.S. patent application (application no. 62/110018) has been filed by the Center for Infectious Disease Research, covering interventions that exploit the described host-parasite interaction. The data are included in the main manuscript and in the supplementary materials.

SUPPLEMENTARY MATERIALS

www.sciencemag.org/content/350/4264/1089/suppl/DC1
Materials and Methods
Figs. S1 to S7
Table S1

28 August 2015; accepted 13 October 2015
10.1126/science.aad3318

GENOMICS

Gene essentiality and synthetic lethality in haploid human cells

Vincent A. Blomen,^{1*} Peter Májek,^{2*} Lucas T. Jae,^{1*} Johannes W. Bigenzahn,² Joppe Nieuwenhuis,¹ Jacqueline Staring,¹ Roberto Sacco,² Ferdy R. van Diemen,¹ Nadine Olk,² Alexey Stukalov,² Caleb Marceau,³ Hans Janssen,¹ Jan E. Carette,³ Keiryn L. Bennett,² Jacques Colinge,^{2,4†} Giulio Superti-Furga,^{2,5†} Thijn R. Brummelkamp^{1,2,6†}

Although the genes essential for life have been identified in less complex model organisms, their elucidation in human cells has been hindered by technical barriers. We used extensive mutagenesis in haploid human cells to identify approximately 2000 genes required for optimal fitness under culture conditions. To study the principles of genetic interactions in human cells, we created a synthetic lethality network focused on the secretory pathway based exclusively on mutations. This revealed a genetic cross-talk governing Golgi homeostasis, an additional subunit of the human oligosaccharyltransferase complex, and a phosphatidylinositol 4-kinase β adaptor hijacked by viruses. The synthetic lethality map parallels observations made in yeast and projects a route forward to reveal genetic networks in diverse aspects of human cell biology.

Single-cell organisms can often tolerate inactivating mutations in the majority of genes (1–3), but it is unclear whether human cells require more essential genes because of increased complexity, or fewer because of added redundancy. To study this, we used mutagenesis in the near-haploid chronic myeloid leu-

kemia (CML) cell line KBM7 (karyotype 25, XY, +8, Ph+), and its nonhematopoietic derivative HAPI, which is haploid for all chromosomes (fig. S1A) (4). More than 34.3 million and 65.9 million gene-trap integrations were identified in KBM7 and HAPI cells, respectively. The gene-trap vector we used was unidirectional by design (fig. S1B),

and for most genes, the number of intronic insertions in the sense direction was similar to that in the antisense direction (for example, pro-apoptotic factor *BBC3*) (Fig. 1, A and B) (5–7). For a fraction of genes, however, disruptive muta-

¹Netherlands Cancer Institute, Plesmanlaan 121, 1066 CX, Amsterdam, Netherlands. ²CeMM Research Center for Molecular Medicine of the Austrian Academy of Sciences, 1090 Vienna, Austria. ³Department of Microbiology and Immunology, Stanford University School of Medicine, 299 Campus Drive, Stanford, CA 94305, USA. ⁴University of Montpellier, Institut de Recherche en Cancérologie de Montpellier Inserm U1194, Institut régional du Cancer Montpellier, 34000 Montpellier, France.

⁵Center for Physiology and Pharmacology, Medical University of Vienna, Vienna, Austria. ⁶Cancer Genomics Center (CGC.nl), Plesmanlaan 121, 1066CX, Amsterdam, Netherlands.
*These authors contributed equally to this work. †Corresponding author. E-mail: jacques.colinge@inserm.fr (J.C.); gsuperti@cemm.at (G. S.-F.); t.brummelkamp@nki.nl (T.R.B.)

tions were underrepresented, which is indicative of impaired fitness: Some genes (such as *STAT5B*) appeared essential in one cell type (fig. S1C), whereas others appeared essential in both (such as *RPL13A*) (Fig. 1, A and B, and tables S1 to S3).

In KBM7 cells, 2054 genes (table S1 and figs. S2 and S3) and in HAP1, 2181 genes (table S2 and figs. S2 and S3) appeared to be needed for viability or optimal fitness under the experimental growth conditions (referred to as “essential,” although the approach does not distinguish between the two). The 1734 genes identified in both cell lines were designated as “core essentialome” (table S3). In KBM7 cells, genes on chromosome 8 (present in two copies) tolerated disruptive mutations, underscoring the specificity of the approach (fig. S1D). Furthermore, nearly all subunits of the proteasome were identified as es-

sential (fig. S4). In general, essential genes are overrepresented in categories such as translation or transcription but not signaling (Fig. 1C and figs. S5 and S6).

Many genes required for fitness in yeast were also essential in human cells. Exceptions were largely explained by paralogs in the human genome or by yeast-specific requirements (fig. S7A and table S4) (I). We estimated the evolutionary age of essential genes and found that 77% emerged in premetazoans (“old” essential genes) (fig. S7B). Essential genes had fewer paralogs and higher protein abundance and contained fewer single-nucleotide polymorphisms (SNPs) predicted to impair function (Fig. 1D). Proteins encoded by essential genes displayed more protein-protein interactions (fig. S8, A to D), and these occurred more frequently with other essential proteins (49.8%) (fig. S9A) and within the same functional

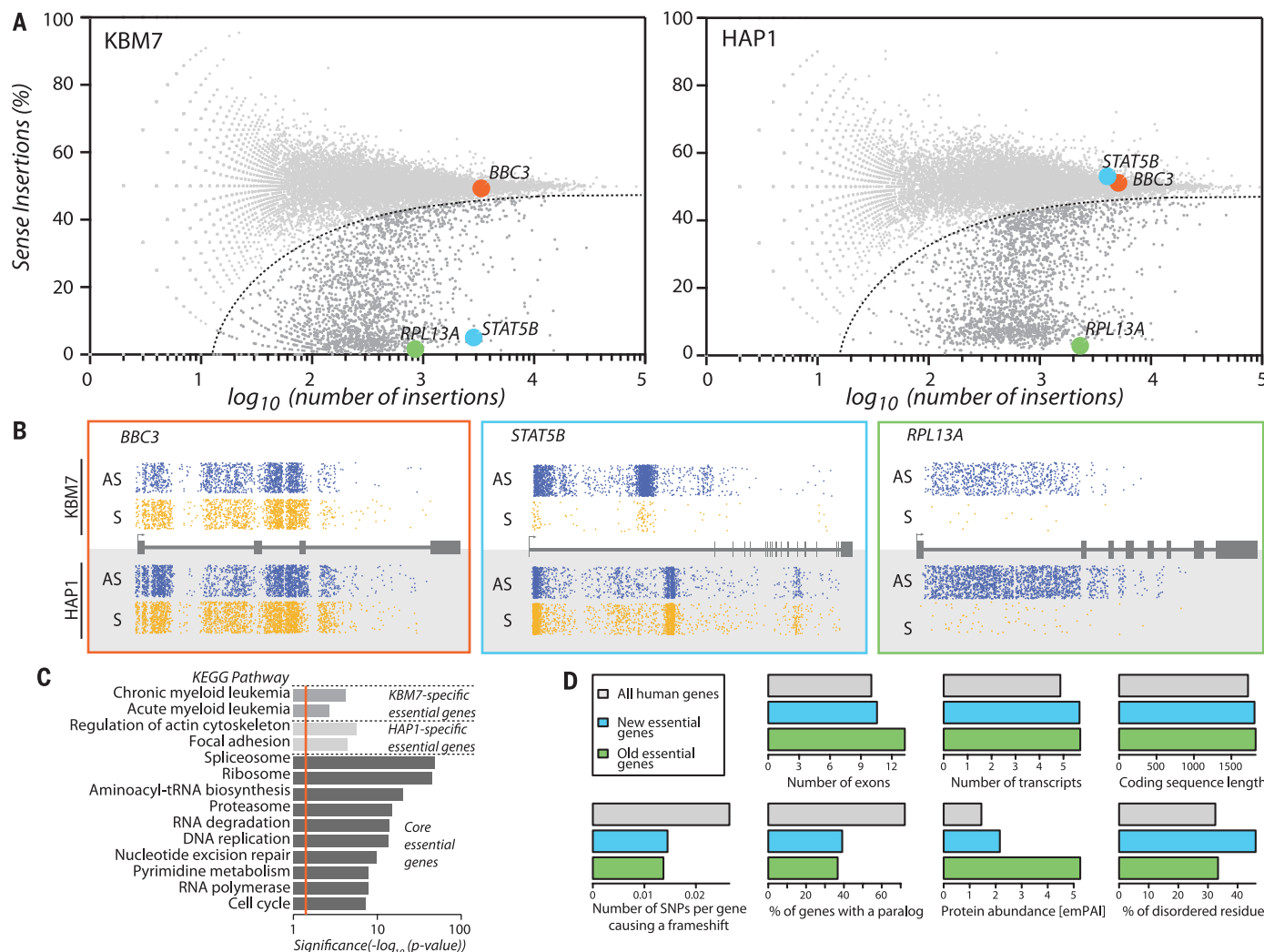


Fig. 1. Identification of genes required for fitness in KBM7 and HAP1 cells through insertional mutagenesis. (A) Distinct gene-trap insertions were mapped in KBM7 and HAP1 cells, and their orientation relative to the affected genes was counted. Per gene, the percentage of sense orientation gene-trap insertions (y axis) and the total number of insertions in a particular gene (x axis) are plotted. (B) Gene-trap insertions identified in the sense (S, yellow) or antisense orientation (AS, blue) in a nonessential gene

(*BBC3*), a gene essential only in KBM7 cells (*STAT5B*), and a gene essential in both cell lines (*RPL13A*). (C) KEGG pathway enrichment analysis of essential genes shared between or specific to KBM7 or HAP1 cells. (D) Properties of new and old essential genes compared with the human genome. Averages for the sets are displayed, except for protein abundance, in which median Exponentially Modified Protein Abundance Index (emPAI) values are shown.

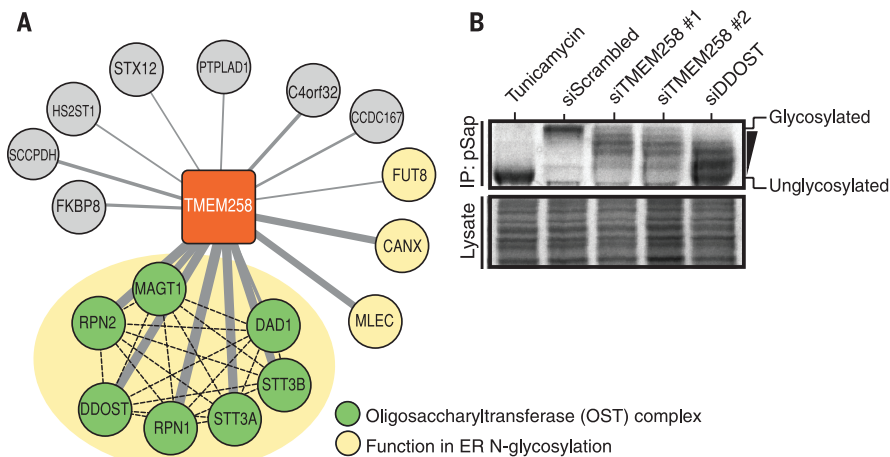


Fig. 2. The essential gene *TMEM258* encodes a component of the OST complex. (A) High-confidence protein-protein interactions associated with *TMEM258*. Green proteins indicate members of the OST complex. Dashed lines indicate the OST complex subnetwork. **(B)** Effects of depletion of *TMEM258* with small interfering RNAs on the glycosylation of endogenous prosaposin. Cells were pulsed with ^{35}S -methionine/cysteine, lysed, and subjected to immunoprecipitation by using antibodies to prosaposin. Precipitated proteins were detected by means of phosphorimaging, and hypoglycosylated prosaposin species are indicated. Tunicamycin treatment and depletion of the established OST subunit *sDDOST* served as positive controls.

category (fig. S5B). Remarkably, the products of “new” essential genes are more often connected with old rather than other new essential gene products, suggesting that they largely function within ancient molecular machineries (fig. S9, B and C).

To identify proteins interacting with products of 18 uncharacterized essential genes, we used tandem affinity purification coupled to mass spectrometry (fig. S10). Interactors were frequently essential proteins (52.4%, $P < 2.5 \times 10^{-36}$, hypergeometric test) involved in processes such as splicing, translation, and trafficking (fig. S11 and table S5). The small transmembrane protein *TMEM258* associated with components of the conserved oligosaccharyltransferase (OST) complex (Fig. 2A and fig. S12A) that are essential for protein N-glycosylation (8). *TMEM258* localized to the endoplasmic reticulum (fig. S12B), and depletion (fig. S12, C and D) impaired OST catalytic activity as monitored by means of hypoglycosylation of prosaposin (Fig. 2B) (9). This also rationalizes the observed clustering of *TMEM258* with OST complex subunits in a recent genetic screen (10). Thus, *TMEM258* constitutes a subunit of the

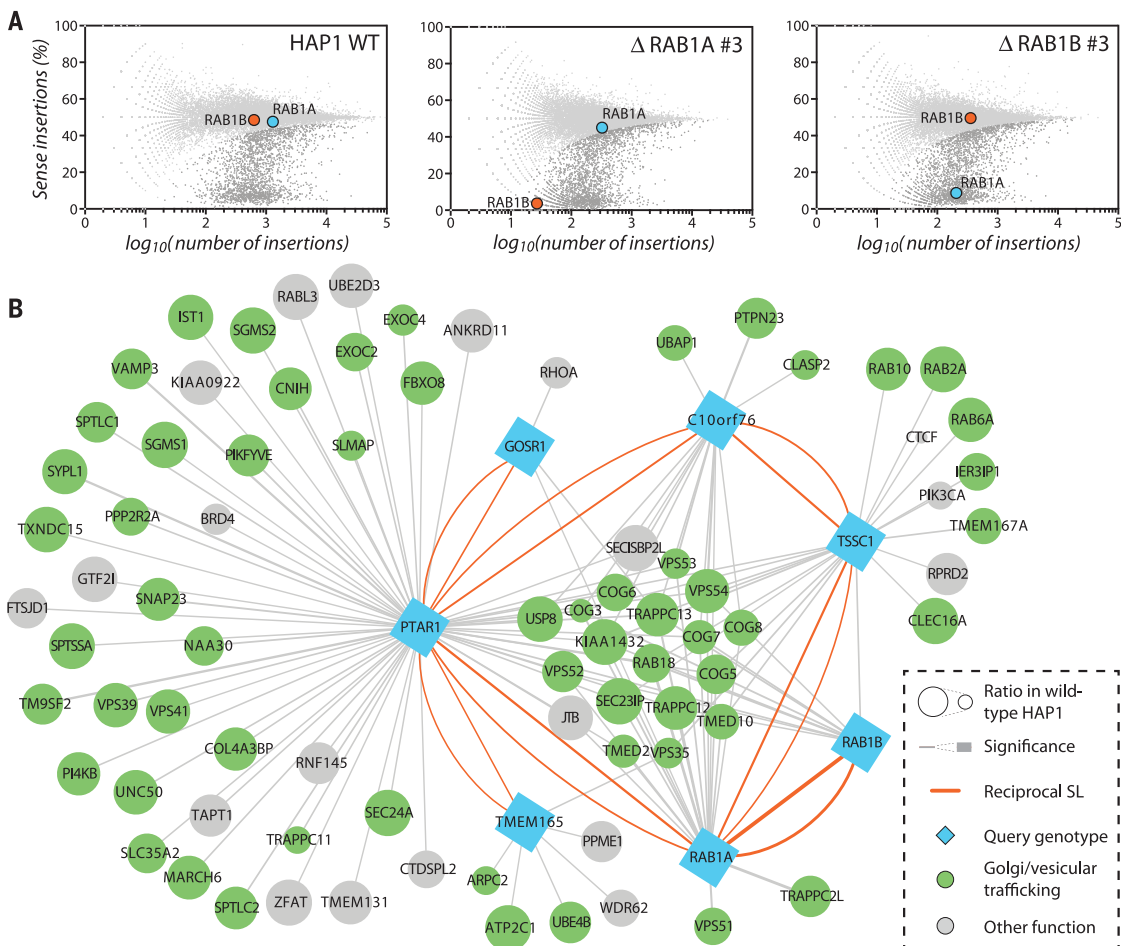


Fig. 3. Synthetic lethality network generated based on mutations. (A) Essentiality of *RAB1A* and *RAB1B* in wild-type HAP1 cells and cells deficient for *RAB1A* or *RAB1B*. **(B)** Genetic interaction network indicating synthetic lethal/sick interactions that were identified by scoring genes for fitness reduction in three nuclease-generated knockout clones per genotype. This revealed an interconnected network, with many genes that could be functionally assigned to the secretory pathway (labeled in green). Reciprocal interactions, scored in either query genotype, are indicated by orange edges. Edge thickness reflects the effect size of the interaction (compared with wild-type cells).

human OST complex, and although homology searches (fig. S12E) do not identify a yeast ortholog, TMEM258 may relate to the similarly sized yeast transmembrane protein OST5 (21).

Whereas most genes appear nonessential, their function may be buffered by other genes so that only simultaneous disruption is lethal (12–15). The frequency of such synthetic lethal interactions between human genes is debated and challenging to address experimentally (16, 17). We studied the small guanosine triphosphatases (GTPases) RAB1A and RAB1B by creating individual knockout lines and assessing the genes needed for fitness in these backgrounds (Fig. 3A and fig. S13A). Whereas neither *RAB1A* nor *RAB1B* were essential in wild-type cells, *RAB1A* became indispensable in *RAB1B* knockout cells and vice versa (Fig. 3A and fig. S13B). To explore the breadth of synthetic lethality, we probed the secretory pathway using three independent knockout cell lines (fig. S14) for *RAB1A*, *RAB1B*, *GOSR1* [a subunit of the Golgi soluble *N*-ethylmaleimide-sensitive factor attachment protein (SNAP) receptor] (18), and *TMEM165* (a Golgi-resident $\text{Ca}^{2+}/\text{H}^+$ antiporter whose deficiency impairs glycosylation) (Fig. 3B, figs. S15 and S16, and table S6) (19). Most of their genetic interactions impinged on the secretory pathway (Fig. 3B and table S7), and many were found synthetic lethal with *PTARI*. Synthetic lethality screens in *PTARI*-deficient cells confirmed these genetic interactions and additionally identified the uncharacterized gene *C10orf76* (Fig. 3B and fig. S17A). Validation by use of *C10orf76* as query gene confirmed synthetic lethality with *PTARI* and (reciprocally) identified

TSSC1, which was recently reported to interact with the Golgi-associated retrograde protein complex (GARP) (Fig. 3B) (20). The human genes we studied display on average ~20 synthetic lethal interactions, a number comparable with that in yeast (12), although this varies between genes, with *PTARI* (causing a fitness defect when deleted alone) having close to 60 interactions (fig. S17B). This illustrates that synthetic lethal interactions can be identified and validated by using reciprocal haploid screens and that, similarly to yeast, interactions frequently occur between genes whose products act in related processes (fig. S17B) (13, 16). However, we acknowledge a caveat that this approach cannot readily distinguish between synthetic lethal or synthetic “sick” interactions.

The impaired growth of *PTARI*-deficient cells (table S2) was suppressed by loss of the Golgi factor *GOLGA5* (Fig. 4A and fig. S18) (21). *PTARI*-deficient cells had an abnormally dilated Golgi morphology (fig. S19A), which was partially corrected by codeletion of *GOLGA5* (Fig. 4B and fig. S19B). Functionally, *PTARI* deficiency impaired glycosylation (fig. S19C) (7), possibly owing to dysregulation of RAB proteins (22). Indeed, *PTARI*-deficient cells showed attenuated geranylgeranylation of RAB1A and RAB1B (fig. S19D). Partial correction of the Golgi morphology in cells lacking both *PTARI* and *GOLGA5* could relate to the effect of *GOLGA5*, itself a RAB effector, on Golgi fragmentation (21, 23). Thus, the interaction map reveals *PTARI* and *GOLGA5* as opposing handles tuning Golgi morphology and homeostasis.

Genetic analysis suggested a link between the unstudied gene *C10orf76* and *PI4KB*, which were

both synthetic lethal with *PTARI* (Fig. 3B). A host factor screen with coxsackievirus A10 also identified *C10orf76* as well as *PI4KB* (fig. S20, A and B), and a proteomics survey (24) suggested association between *C10orf76* and *PI4KB*. We confirmed this interaction in immunoprecipitation experiments with cells expressing FLAG-tagged *C10orf76* (Fig. 4C). Phosphatidylinositol 4-kinase β (*PI4KB*) regulates abundance of phosphatidylinositol 4-phosphate [*PI(4)P*] (25) and has a role in genome replication of various RNA viruses, including coxsackieviruses (26). Infection studies confirmed that cells in which *C10orf76* was knocked out were particularly resistant to coxsackievirus A10 (fig. S20C). Although virus entry occurred normally, replication of viral RNA was decreased in cells in which *C10orf76* was knocked out (Fig. 4D and fig. S20D). Enteroviruses hijack *PI4KB* activity to construct “replication factories,” which were abundant in wild-type cells but rare in *C10orf76*-deficient cells (fig. S20E). Amounts of *PI(4)P* were decreased in these cells, and Golgi retention of *PI4KB* after chemical inhibition (27) was largely dependent on *C10orf76*, which also localized to this compartment under these conditions (fig. S21, A and B). Thus, *C10orf76* is a *PI4KB*-associated factor hijacked by specific picornaviruses for replication.

This study identifies ~2000 genes required for optimal fitness of cultured haploid human cells. Despite technical limitations, the identification of gene essentiality shows high concordance with the gene-trap and clustered regularly interspaced short palindromic repeats (CRISPR) data reported in the accompanying manuscript of Wang *et al.*

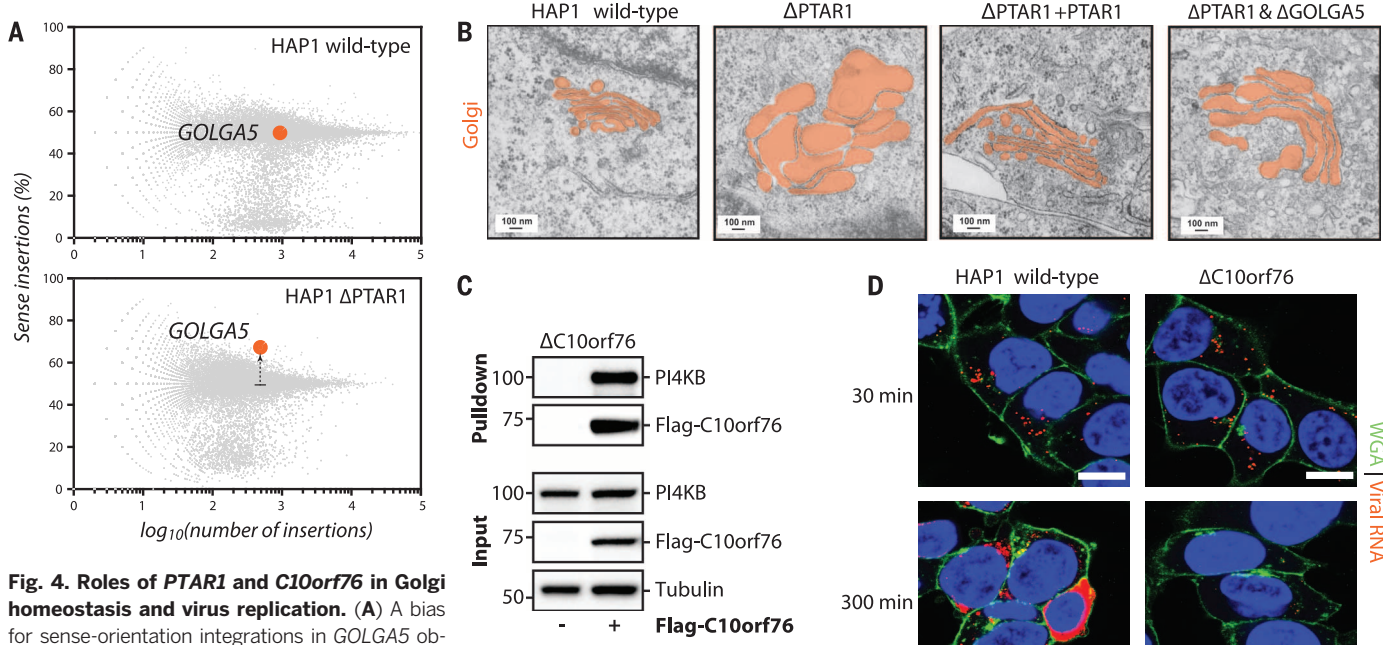


Fig. 4. Roles of *PTARI* and *C10orf76* in Golgi homeostasis and virus replication. (A) A bias for sense-orientation integrations in *GOLGA5* observed in *PTARI*-deficient HAP1 cells but not wild-type cells. (B) Electron micrographs of the Golgi apparatus (orange highlight) in the indicated genotypes. (C) Interaction of FLAG-tagged *C10orf76* with *PI4KB* in HAP1 cells detected with immunoprecipitation by using antibodies to FLAG. (D) Coxsackievirus A10 amplification in wild-type and *C10orf76*-deficient cells measured by means of single molecule fluorescent in situ hybridization (smFISH) to localize individual viral genomes (red). Intracellular viral RNA was first detected after 30 min. Increased RNA signal after 300 min indicates RNA replication.

(supplementary text and fig. S22) (28). This suggests that the increase in total number of genes in humans as compared with that in yeast yielded a system of higher complexity rather than more robustness through added redundancy. Non-essential human genes appear to frequently engage in synthetic lethal interactions. Our studies start to reveal an interconnected module of genetic interactions affecting the secretory pathway and link it to uncharacterized genes. The experimental strategy is applicable to various cellular processes and may help unravel the genetic network encoding a human cell.

REFERENCES AND NOTES

- Giaever et al., *Nature* **418**, 387–391 (2002).
- A. H. Tong et al., *Science* **294**, 2364–2368 (2001).
- S. M. Mnaimneh et al., *Cell* **118**, 31–44 (2004).
- J. E. Carette et al., *Nature* **477**, 340–343 (2011).
- J. E. Carette et al., *Nat. Biotechnol.* **29**, 542–546 (2011).
- J. E. Carette et al., *Science* **326**, 1231–1235 (2009).
- L. T. Jae et al., *Science* **340**, 479–483 (2013).
- D. J. Kelleher, R. Gilmore, *Glycobiology* **16**, 47R–62R (2006).
- A. Dumax-Vorzet, P. Roboti, S. High, *J. Cell Sci.* **126**, 2595–2606 (2013).
- O. Parnas et al., *Cell* **162**, 675–686 (2015).
- G. Reiss, S. te Heesen, R. Gilmore, R. Zufferey, M. Aeby, *EMBO J.* **16**, 1164–1172 (1997).
- A. H. Tong et al., *Science* **303**, 808–813 (2004).
- J. L. Hartman 4th, B. Garvik, L. Hartwell, *Science* **291**, 1001–1004 (2001).
- C. Boone, H. Bussey, B. J. Andrews, *Nat. Rev. Genet.* **8**, 437–449 (2007).
- M. Schuldiner et al., *Cell* **123**, 507–519 (2005).
- S. M. Nijman, S. H. Friend, *Science* **342**, 809–811 (2013).
- J. Tischler, B. Lehner, A. G. Fraser, *Nat. Genet.* **40**, 390–391 (2008).
- V. N. Subramaniam, F. Peter, R. Philip, S. H. Wong, W. Hong, *Science* **272**, 1161–1163 (1996).
- D. Demaeijer et al., *Proc. Natl. Acad. Sci. U.S.A.* **110**, 6859–6864 (2013).
- E. L. Huttlin et al., *Cell* **162**, 425–440 (2015).
- A. Diao, D. Rahman, D. J. Pappin, J. Lucocci, M. Lowe, *J. Cell Biol.* **160**, 201–212 (2003).
- W. L. Charnq et al., *PLOS Biol.* **12**, e1001777 (2014).
- A. Rejman Lipinski et al., *PLOS Pathog.* **5**, e1000615 (2009).
- A. L. Greninger, G. M. Knudsen, M. Betegon, A. L. Burlingame, J. L. DeRisi, *MBio* **4**, e00098–e00013 (2013).
- T. R. Graham, C. G. Burd, *Trends Cell Biol.* **21**, 113–121 (2011).
- N. Y. Hsu et al., *Cell* **141**, 799–811 (2010).
- H. M. van der Schaaf et al., *Cell Res.* **22**, 1576–1592 (2012).
- T. Wang et al., *Science* **350**, 1096–1101 (2015).

ACKNOWLEDGMENTS

We thank T. Sixma, S. Nijman, J. Roix, J. Neefjes, and members of the Brummelkamp group for discussion and K. Sandhoff for antibodies directed against saposin. This work was supported by the Cancer Genomics Center (CGC.nl), Nederlandse Organisatie voor Wetenschappelijk Onderzoek (NWO)—VIDI grant 917.11.316, European Research Council (ERC) Starting Grant (ERC-2012-STG 309634) to T.R.B., the Austrian Academy of Sciences and the Advanced ERC grant i-FIVE and Austrian Science Fund grant (FWF SFB F4711) to G.S.-F., and the ARC Foundation grant PJA 20141201975 to J.C. Sequence data have been deposited at the National Center for Biotechnology Information Sequence Read Archive with accession number SRP058962.

SUPPLEMENTARY MATERIALS

www.sciencemag.org/content/350/6264/1092/suppl/DC1

Materials and Methods

Supplementary Text

Figs. S1 to S23

Tables S1 to S8

References (29–62)

28 September 2014; accepted 1 October 2015

Published online 15 October 2015

10.1126/science.aac7557

GENOMICS

Identification and characterization of essential genes in the human genome

Tim Wang,^{1,2,3,4} Kivanç Birsoy,^{1,2,3,4*} Nicholas W. Hughes,³ Kevin M. Krupeckak,^{2,3,4} Yorick Post,^{2,3,4} Jenny J. Wei,^{1,2} Eric S. Lander,^{1,3,5†‡} David M. Sabatini^{1,2,3,4,6†‡}

Large-scale genetic analysis of lethal phenotypes has elucidated the molecular underpinnings of many biological processes. Using the bacterial clustered regularly interspaced short palindromic repeats (CRISPR) system, we constructed a genome-wide single-guide RNA library to screen for genes required for proliferation and survival in a human cancer cell line. Our screen revealed the set of cell-essential genes, which was validated with an orthogonal gene-trap-based screen and comparison with yeast gene knockouts. This set is enriched for genes that encode components of fundamental pathways, are expressed at high levels, and contain few inactivating polymorphisms in the human population. We also uncovered a large group of uncharacterized genes involved in RNA processing, a number of whose products localize to the nucleolus. Last, screens in additional cell lines showed a high degree of overlap in gene essentiality but also revealed differences specific to each cell line and cancer type that reflect the developmental origin, oncogenic drivers, paralogous gene expression pattern, and chromosomal structure of each line. These results demonstrate the power of CRISPR-based screens and suggest a general strategy for identifying liabilities in cancer cells.

The systematic identification of essential genes in microorganisms has provided critical insights into the molecular basis of many biological processes (1). Similar studies in human cells have been hindered by the lack of suitable tools. Moreover, little is known about how the set of cell-essential genes differs across cell types and genotypes. Differentially essential genes are likely to encode tissue-specific modulators of key cellular processes and important targets for cancer therapies. We used two independent approaches for inactivating genes at the DNA level to define the cell-essential genes of the human genome.

The first approach uses the clustered regularly interspaced short palindromic repeats (CRISPR)/Cas9-based gene editing system, which has emerged as a powerful tool to engineer the genomes of cultured cells and whole organisms (2, 3). We and others have shown that lentiviral single-guide RNA (sgRNA) libraries can enable pooled loss-of-function screens and have used the technology to uncover mediators of drug resistance and pathogen toxicity (4–6). To systematically identify cell-essential genes, we constructed

a library, which was optimized for high cleavage activity, and performed a proliferation-based screen in the near-haploid human KBM7 chronic myelogenous leukemia (CML) cell line (Fig. 1, table S1, and supplementary text S1).

The unusual karyotype of these cells also allows for an independent method of genetic screening. In this approach, null mutants are generated at random through retroviral gene-trap mutagenesis, selected for a phenotype, and monitored by sequencing the viral integration sites to pinpoint the causal genes (7). Positive selection-based screens by use of this method have identified genes underlying processes such as epigenetic silencing and viral infection (7–9). We extended this technique by developing a strategy for negative selection and conducted a screen for cell-essential genes (Fig. 1 and supplementary text S2).

For both methods, we computed a score for each gene that reflects the fitness cost imposed by inactivation of the gene. We defined the CRISPR score (CS) as the average \log_2 fold-change in the abundance of all sgRNAs targeting a given gene, with replicate experiments showing a high degree of reproducibility [correlation coefficient (r) = 0.90] (Fig. 2A, fig. S1A, and table S2). Of the 18,166 genes targeted by the library, 1878 scored as essential for optimal proliferation in our screen, although this precise number depends on the cutoff chosen (Fig. 2A and tables S2 and S3). Overall, this fraction represents ~10% of genes within our data set or roughly 9.2% of the entire genome (many of the genes not targeted by our library encode olfactory receptors that are unlikely to be cell-essential). Gene products that act in a non-cell-autonomous manner are not expected to score as essential in this pooled setting (fig. S1B).

*Department of Biology, Massachusetts Institute of Technology, Cambridge MA 02139, USA. [†]Whitehead Institute for Biomedical Research, 9 Cambridge Center, Cambridge, MA 02142, USA.

[‡]Broad Institute of MIT and Harvard, 7 Cambridge Center,

Cambridge, MA 02142, USA. [§]David H. Koch Institute for

Integrative Cancer Research at MIT, Cambridge, MA 02139, USA. [¶]Department of Systems Biology, Harvard Medical School, Boston, MA 02115, USA. ^{||}Howard Hughes Medical Institute, Department of Biology, Massachusetts Institute of Technology, Cambridge, MA 02139, USA.

^{*}Present address: Laboratory of Metabolic Regulation and

Genetics, The Rockefeller University, New York, NY 10065, USA.

†These authors contributed equally to this work.

‡Corresponding author. E-mail: lander@broadinstitute.org (E.S.L.); sabatini@wi.mit.edu (D.M.S.).

Supplementary Material for **Gene essentiality and synthetic lethality in haploid human cells**

Vincent A. Blomen, Peter Májek, Lucas T. Jae, Johannes W. Bigenzahn,
Joppe Nieuwenhuis, Jacqueline Staring, Roberto Sacco, Ferdy R. van Diemen,
Nadine Olk, Alexey Stukalov, Caleb Marceau, Hans Janssen, Jan E. Carette,
Keiryn L. Bennett, Jacques Colinge,* Giulio Superti-Furga,* Thijn R. Brummelkamp*

*Corresponding author. E-mail: jcolinge@cemm.oeaw.ac.at (J.C.); gsuperti@cemm.at (G. S.-F.);
t.brummelkamp@nki.nl (T.R.B.)

Published 15 October 2015 on *Science* Express
DOI: 10.1126/science.aac7557

This PDF file includes:

Materials and Methods
Supplementary Text
Figs. S1 to S23
Full Reference List

Other Supplementary Material for this manuscript includes the following:
(available at www.sciencemag.org/content/science.aac7557/DC1)

Tables S1 to S8

Materials and Methods

Cells

HAP1 cells and KBM7 cells were cultured in IMDM supplemented with 10% fetal calf serum (FCS, Thermo Scientific, HyClone cat. SV30160.03, lot. RWB35889), penicillin–streptomycin and L-glutamine. HeLa cells and HEK-293T cells were grown in DMEM supplemented with 10% FCS, penicillin–streptomycin and L-glutamine. HAP1 cells and KBM7 cells were used for the identification of essential genes, and HAP1 cells and knockout derivatives were used for follow-up experiments. HeLa cells were used for follow-up experiments. HEK293 Flip-In T-Rex cells were used for the inducible expression of tagged proteins to be analyzed for interacting factors by tandem affinity purification mass spectrometry.

Haploid Genetic Screen to identify essential genes

Gene-trap retrovirus required for the mutagenesis of HAP1 cells was produced in HEK293T cells using the gene-trap vector described previously (7) and a similar gene-trap retrovirus was used in which green fluorescent protein (GFP) was exchanged for blue fluorescent protein (BFP). Cells were seeded in 12 T175 flasks at 40% confluence. The next day the medium was replaced with DMEM supplemented with 30% fetal calf serum (FCS) prior to transfection with 6.6 µg gene-trap plasmid per T175 flask, in combination with the packaging plasmids Gag-pol, VSVg, and pAdv (6). The medium was harvested 48 hours post transfection and subsequently concentrated by ultracentrifugation at 21,000 rpm for 2 hours at 4°C. The supernatant was discarded and

the pellets were resuspended in 200 uL phosphate buffered saline (PBS, Life technologies) overnight at 4°C. Retrovirus-containing medium was collected and concentrated twice daily for three consecutive days.

To generate a mutagenized HAP1 cell population, 40 million HAP1 cells were seeded and transduced with gene-trap retrovirus from two combined harvests on three consecutive days in the presence of 8 µg/mL protamine sulfate (Sigma). The mutagenized library was subsequently expanded and passaged for a period of 10 days after mutagenesis while maintaining at least 3-fold library complexity.

The non-adherent KBM7 cells (40 million cells) were similarly transduced with gene-trap retrovirus on three consecutive days in the presence on 8 µg/mL protamine sulfate. Following each addition of the retrovirus, cells were seeded in a 6-well plate and centrifuged for 1.5 hours at 2,200 rpm at room temperature. Following mutagenesis, KBM7 cells were passaged at cell densities between 1·10⁶ and 8·10⁶ cells/mL while maintaining at least 3-fold complexity.

After passaging, at least 6·10⁸ cells were fixed using BD fix buffer I (BD biosciences) for 10 minutes at 37°C. Following a wash with PBS containing 10% FCS cells were filtered through a 40 µm strainer (BD FalconTM). In order to minimize potential confounding effects of diploid cells which are heterozygous for alleles carrying gene-trap integrations, DNA content was stained using either 3 µM 4',6-diamidino-2-phenylindole (DAPI) or 10 µg/mL propidium iodide (Life Technologies) solution. In the latter case, cells were also

treated with 100 µg/mL RNase A (Qiagen) at room temperature for 30 minutes. Subsequently, cells were sorted on either a Biorad S3 Cell sorter (PI-stained DNA) or an Astrios Moflo (DAPI stained DNA content) based on DNA content (1n) until approximately 30 million cells were collected.

Sorted cells were pelleted by centrifugation (2,500 rpm 10 min.) and genomic DNA was isolated using Qiagen DNA mini kit. To facilitate de-crosslinking pellets were resuspended in PBS (200 µL/10 million cells) and after the addition of Proteinase K (Qiagen) and lysis buffer (buffer AL, Qiagen) incubated overnight at 56°C with agitation. The following day DNA was isolated according to manufacturer's specifications and measured by Nanodrop2000 spectrophotometer (Thermo fisher).

Insertion site mapping

Insertion sites were amplified using a Linear AMplification polymerase chain reaction (LAM-PCR) using the total genomic DNA isolated from 30 million haploid cells (1-2 µg/reaction), with each 50 uL reaction (rxn) containing 1 mM MgSO₄, 0.75 pmol double-biotinylated primer (5'-/double biotin/ggtctccaaatctcggtggaac-3'), Accuprime Taq HiFi (0.4 µL/rxn) and the supplied buffer II (Life technologies). The reaction was performed in 120 cycles with an annealing temperature of 58°C for 30 seconds and an extension temperature of 68°C for 60 seconds. To capture biotinylated single-stranded DNA (ssDNA) products, PCR reactions were combined with M270 streptavidin-coated magnetic beads (Life technologies) in 2x binding buffer (6 M LiCl, 10 mM Tris, 1 mM EDTA, pH=7.5) for 2 hours at room temperature and subsequently captured using a

magnet. Prior to binding, the beads were washed once in PBS-containing 0.1% bovine serum albumin (BSA) in 1.5 mL non-stick tubes (Life technologies). Following magnetic precipitation, beads were washed three times with PBS containing 0.05% Triton X-100 (Sigma) prior to linker ligation.

A ssDNA linker (

5'/phospho/atcgatgccgtttctgcttgactcagtagttgtgcgatggattgatg/dideoxycytidine/3') was ligated to the 3' end of biotinylated products in N x 10uL reactions containing 2.5 mM MnCl₂, 1 M betaine, 12.5 pmol linker, 1 μ L and 0.5 μ L of Circligase II (Illumina) buffer and enzyme respectively, with N = number of LAM-PCR reactions. Alternatively, a preadenylated linker (5'-/Adenyl/atcgatgccgtttctgcttgactcagtagttgtgcgatggattgatg/dideoxycytidine/-3') was ligated to the single stranded amplified DNA product using E. coli-purified TS2126 thermostable RNA ligase 1 from Thermus scotoductus bacteriophage (32) patent WO 2010/094040 A1) in N x 10 μ L reactions containing 12.5 pmol adenylated-linker, 18.75% PEG6000, 2.5 μ g BSA, 2.5 mM MnCl₂, 1 uL buffer (500 mM MOPS, 100 mM KCl, 50 mM MgCl₂, 10 mM dithiothreitol (DTT)), and 2 μ g RNA ligase. All ligation reactions occurred at 60°C for 2 hours in non-stick 1.5 mL tubes (Life technologies) and were followed by three washes with PBS with 0.05% Triton X-100 (Sigma) after 20 minutes incubation at room temperature. Subsequently, a PCR reaction was performed that introduced the adaptors sequences required for Illumina sequencing (P5 and P7) N x 50 μ L reactions containing 25pmol of each primer, 5 μ L buffer II and 0.6 μ L Accuprime Taq HiFi (Life technologies) with N = 0.5 X No. of LAM-PCR reactions).

This final amplification was carried out using 18 cycles and an annealing temperature of 55°C for 30s followed by an extension (at 68°C) for 105 s using primers: 5'-aatgatacggcgaccaccgagatctgatggttctctagcttgcc-3' and 5'- caagcagaagacggcatacga-3'. Products were purified (PCR purification kit, Qiagen) and sequenced as 51bp or 65bp single-reads (18 picomolar loading concentration) on an Illumina HiSeq2000 (Illumina) or HiSeq2500 (Illumina) using sequencing primer 5'-ctagcttgccaaacctacaggtgggtctttca-3'.

Insertion sites were defined by aligning reads to the human genome (hg19) using bowtie (33) and selecting for reads that uniquely align allowing for a single mismatch. On average, ±16 million insertion sites were mapped per experiment albeit with some variation (table S8).

Sequencing data processing and mapping of insertions to genes

All protein coding transcripts from Ensembl 72 that have identical annotations in Ensembl and VEGA (34) (aka gold transcripts) that do not undergo nonsense-mediated decay were tested for the enrichment of antisense trap insertions. For each such transcript, sense and antisense insertions in its pre-mRNA region excluding the 3'-UTR and all exon segments were counted. Importantly, we excluded from the analysis any insertions that are located in genomic regions where two or more genes on the same or opposite strand overlap, as the insertion bias in these overlapping regions cannot be attributed to a single gene in a straightforward way. For the purpose of essential genes selection, for each gene we considered only one gold transcript, either the one with most

significant depletion of sense insertions or if none of the golden transcripts was depleted for sense insertions then the transcript with largest number of insertions was considered. For the synthetic lethality analysis, all gold transcripts were considered. Graphics depicting gene-specific insertion patterns were produced by plotting the genomic coordinates of all insertion sites falling within the transcript coordinates. All insertion sites were assigned a random but unique Y-coordinate, and subsequently the x-axis replaced with a scaled illustration of the gene.

Identification of essential genes

Data from three independent experiments (replicates) for KBM7 cells and four experiments for HAP1 cells were used to select significant fitness-reducing genes in each cell line as follows. The replicates were first exploited to model sense insertion versus total insertion ratio variability. In fig. S2A we see that differences between ratios obtained from different replicates have a typical magnitude that depends on the total number of insertions. The gene-trap insertion ratios are thus heteroscedastic meaning that the variance is not constant. For a vertical “slice” in fig. S2A, i.e. a pool of gene ratios with close total number of insertions, the distribution of ratio difference is close to normal (fig. S2B). We therefore model ratio differences with a normal distribution whose mean is 0 and standard deviation varies according to log-transformed total number of insertions. Standard deviation is modeled by a so-called noise function of the form $\sigma(x) = a + re^{-\lambda x}$, with x the log of the total number of insertions. In fig. S2A we plotted curves representing $\pm 2.326\sigma(x)$ (1% of the points outside each curve). Namely, given two replicates, each gene i is associated with $s_{i,j}$ sense insertions and $a_{i,j}$ antisense

insertions ($j = 1,2$). Ratios are $r_{i,j} = s_{i,j}/(s_{i,j} + a_{i,j})$ and differences $d_i = r_{i,1} - r_{i,2}$ with log of average total insertions $x_i = \log_{10}[(s_{i,1} + a_{i,1} + s_{i,2} + a_{i,2})/2]$. The likelihood function for observing differences d_i according to the normal model with standard deviation $\sigma(x)$ is thus

$$L(a, r, \lambda) = \prod_i \frac{e^{-\frac{d_i^2}{2[\sigma(x_i)]^2}}}{\sqrt{2\pi}\sigma(x_i)}.$$

Parameters a, r, λ are learnt by maximizing $L(a, r, \lambda)$, which was done in R with the function nlm. For each pair of replicates $k \in \{1; \dots; n\}$ we obtain a set of parameters a_k, r_k, λ_k and hence a slightly different function $\sigma_k(x)$. An average function $\sigma(x) = \frac{1}{n} \sum_k \sigma_k(x)$ is obtained with $a = \frac{1}{n} \sum_k a_k$ (by setting $x \rightarrow +\infty$), $r = \frac{1}{n} \sum_k r_k$ (by setting $x = 0$), and $\lambda = -\ln\left(\frac{1}{n} \sum_k r_k e^{-\lambda_k}\right) + \ln(r)$ (by setting $x = 1$). In the case of KBM7 cells, three replicates were available, i.e. $n = 3$, and fig. S2C features the three corresponding noise functions $\sigma_k(x)$ as well as the average. In the case of HAP1 cells, four replicates could be combined in six pairs, fig. S2D. The two average KBM7 and HAP1 $\sigma(x)$, which were computed and used separately, are compared in fig. S2E.

Having this model for ratio differences, and following ideas we already exploited for quantitative mass spectrometry data (35) we derived a statistical test for individual gene ratios. We have $\text{Var}(d_i) = \text{Var}(r_{i,1} - r_{i,2}) = \text{Var}(r_{i,1}) + \text{Var}(r_{i,2}) = 2\text{Var}(r_{i,1}) = \sigma^2(x_i)$ if we assume the biological replicates to be independent experiments. Therefore, $\text{Var}(r_{i,1}) = \sigma^2(x_i)/2$ and each ratio can be associated with a P-value computed from a normal distribution with mean 0.5 and variance equal to $\sigma^2(x_i)/2$. These P-values where multiple hypothesis corrected according to Benjamini-Hochberg procedure (FDR).

Compared to a less conservative binomial test that would assume 0.5 probability of insertion in each orientation, this approach takes into account experimental variability and logically results in a more stringent selection, fig. S2F. Genes that pass 1% threshold after the FDR correction are considered as essential for fitness in either of the cell lines. Genes identified to be essential in both cell lines are considered as core essentialome. The number of insertions, the corresponding P-values and Q-values are reported for each gene in Tables S1-3.

Sequence analysis of essential genes

The 1,734 genes of the core essentialome were analyzed for conservation using eggNOG 3.0 database. 1,319 genes could be mapped to orthologous groups of proteins in opisthokonta and are defined as ‘old’ essential genes, 415 map to metazoans or younger taxonomic groups (fig. S7B), and are referred to as ‘new’ essential genes. We analyzed the set of ‘old’ and ‘new’ essential genes for the following properties. Ensembl 72 was used to analyze the sets for the length of the longest transcript, the number of exons, the number of protein coding transcripts, and the number of paralogs. Ensembl Variation Database was used to analyze the number of SNP’s per gene. IUPRED (36) server was used to analyze the proportion of unstructured regions. The protein abundance was analyzed using the quantitative proteomics data from (37). In all of the analyses of the human genome we considered only genes with a protein coding gold transcript, excluding genes of chromosome 8, as only those could be detected as essential by our pipeline.

Gene annotation enrichment analysis

KEGG pathway enrichment analysis was performed using DAVID (38, 39) using the KBM7-specific set (top 2 shown), the HAP1-specific set (top 2 shown), and the shared set of essential genes (top 10 shown) as queries and their P-values plotted. Additionally, DAVID was used for GO cellular component enrichment to identify compartments enriched for synthetic lethal interactions. For each uncharacterized genotype the 4 highest scoring GO terms were graphically represented and their respective P-value plotted.

Network analysis

The human interactome was assembled integrating several public PPI repositories: IntAct (40), BioGRID (41), HPRD (42), DIP (43), MINT (44), innateDB(45), MatrixDB (46). Protein accession codes were converted to UniprotKB/Swissprot primary accession codes to avoid redundancy and facilitate matching with MS identifications. We also included in the network co-occurrences of proteins in protein complexes from the CORUM (47) and NCI-PID (48). Interaction repositories versions were the most recent at the time of this data compilation (1st of January 2013). We used the largest connected component of the resulting network which comprised of 12,967 proteins and 112,985 PPIs. The topological parameters were computed at each node of this network using R. The generation of null (random) distributions for the proportion of PPIs towards other essential genes used 10,000 random sets of proteins from the network, none of them being essential, having the same node degree distribution as the various essential gene sets considered. Core essentialome genes as well as all human genes (fig. S5-6) were functionally classified using eggNOG 3.0 (49).

Strengths of interaction between functional categories, (fig. S6) were determined by considering all essential genes in a category C2 reached from essential genes in another category C1 following the edges of the core essential network. Depending on the total number of proteins reached from C1 proteins and the total number of core essential proteins with annotation C2, we computed a hypergeometric P-value. Depending on connectivity, P-values from C1 to C2 or C2 to C1 are not symmetric. We took the minimum of the two P-values to represent functional association over the core essential network. Functional categories ‘unknown’ and ‘other’ were omitted for this network.

Expression of tagged cDNAs in cell lines

For the generation of inducible cell lines ORFs were PCR amplified from KBM7 cDNA and cloned into the Gateway-compatible pDONR201 entry vector using BP recombination (Invitrogen, Carlsbad, CA, USA). Following sequence verification, cDNAs were transferred to the inducible N-terminal Strep-HA tag expression vector pTO-HA-StrepII-GW-FRT-HygroR (50) via LR recombination (Invitrogen). In order to generate stable inducible cell lines, HEK293 Flip-In T-Rex cells (Invitrogen) maintained in DMEM (Sigma) supplemented with 10% FCS (Gibco), 100 U/mL penicillin, 100 µg/mL Streptomycin (Sigma), 100 µg/mL Zeocin (Invitrogen) and 15 µg/mL blasticidin (Invivogen, San Diego, CA, USA) were co-transfected with the expression vector and pOG44 vector (Invitrogen) using Fugene6 transfection reagent (Promega, Fitchburg, WI, USA). Two days after transfection, cells that stably integrated expression constructs were selected using 100 µg/mL hygromycin (Invivogen) for 2-3 weeks and expanded. Bait

expression was induced upon addition of 1 µg/mL doxycycline for 24 h and verified by anti-HA immunoblotting (HA; Y11, Santa Cruz, Dallas, TX, USA or HA7-HRP; Sigma, St. Louis, MO, USA).

C-terminally Flag-tagged PTAR1 cDNA was recovered by PCR from a HAP1 cDNA library generated using SuperScript First Strand Synthesis System (Invitrogen) using the following primers: 5'-gatcGGATCCaccatggccgagaccagcgaggag-3' and 5'-gatcCTCGAGttacttgtcatcgctgcctttagtcttgactcaaagttaaccagcca-3', digested with BamHI and XhoI restriction enzymes and cloned into pBabe-Puro retroviral vector digested with BamHI and SalI. N-terminally Flag-tagged C10orf76 was generated by gene synthesis (Life technologies) based on NCBI transcript NM_024541.2, digested with EcoRI and XhoI restriction enzymes and cloned into modified retroviral vector pMX-2A-BLAST described previously (51). C-terminal HA-tagged TMEM258 cloned form cDNA using primers: 5'- catgGGATCCatggagcttgaggccatg-3' and 5'-catgGTCGACagcgtaatctggaacatcgatggtagacacgttagatgccaacccagag-3'. The product was digested with BamHI and SalI and ligated into pMX-IRES-Blasticidin, which had been digested with BamHI and XhoI. The plasmid encoding TAP1-RFP was a kind gift of Prof. dr. Jacques Neefjes.

The mouse STT3B ORF was PCR-amplified from the cDNA clone BC052433 using primers 5'-CACCatggcggagccctcgcc-3' and 5'-ttacttatcgctcatcctttagatcaacagtcttttagaggcttc-3' to include a C-terminal Flag epitope. This PCR product was introduced in the Gateway compatible entry vector pENTR/D-TOPO (Life technologies). Subsequently STT3B was cloned into pLenti CMV Puro DEST (Addgene #17452) (52) using LR clonase according to manufacturers protocol

(Life technologies). Flag-tagged DAD1 with pcDNA3.1(-) homology (5'-end 5'-
CTAGACTCGAGCGGCCGCACTGTGGCCACC-3', 3'-end 5'-
CACACTGGACTAGTGGATCCGAGCT-3') for Gibson cloning was generated by gene
synthesis (Life technologies) and cloned in BstXI digested pcDNA3.1(-) using Gibson
Assembly Kit (New England BioLabs NEB #E2611).

Tandem affinity purification, liquid chromatography mass spectrometry and data analysis

Tandem affinity purifications (TAP) and liquid chromatography mass spectrometry (LCMS) analyses were performed as previously described (53, 54). Briefly, five confluent 15 cm dishes were incubated with 1 µg/mL doxycyline for 24 h. Cells were harvested and lysed in 50 mM HEPES pH 8.0, 150 mM NaCl, 5 mM EDTA, 0.5% NP-40, 50 mM NaF, 1 mM Na₃VO₄, 1 mM PMSF and protease inhibitor cocktail. Insoluble material was removed by centrifugation at 13,000 r.p.m. for 20 min at 4°C and 50 mg total lysate (measured by Bradford assay using γ-globin as the standard; BioRad, Hercules, CA, USA) was incubated with StrepTactin sepharose beads (IBA, Goettingen, Germany). Tagged bait proteins were eluted with D-biotin (Alfa Aesar, Karlsruhe, Germany) followed by immunopurification with anti-HA-agarose beads (Sigma). Protein complexes were eluted with 100 mM formic acid and immediately neutralized with triethylammonium bicarbonate (TEAB, Sigma). Affinity purifications were performed as biological replicates and cell lines expressing Strep-HA tagged GFP were used as negative controls. The samples were digested with trypsin (Promega Corp, Madison, WI), peptides purified and concentrated on C18 reversed-phase material and analyzed by LC-MSMS using a 1200 series high-performance liquid chromatography system (Agilent

Technologies, Santa Clara, CA, USA) coupled to a linear trap quadrupole (LTQ) Orbitrap Velos mass spectrometer (ThermoFisher Scientific, Waltham, MA, USA). Details of the LCMS configuration and methodology are described elsewhere (55). To identify the proteins, acquired MS data files were converted into Mascot generic format (.mgf) files, searched against the human SwissProt protein database (v. 2013.01) using the search engines Mascot (v2.3.02, MatrixScience, London, UK) (56) and Phenyx (v2.6, GeneBio, Geneva, Switzerland) (57). One missed tryptic cleavage site was allowed. Carbamidomethyl cysteine was set as a fixed modification, and oxidized methionine was set as a variable modification. Mascot and Phenyx identifications were merged to ensure < 1% FDR according to a previously described procedure (58).

Filtering of non-specific protein interactions was performed using a modified version of the Decontaminator algorithm (59), where the algorithm was applied three times on spectral counts, Phenyx protein scores, and Mascot protein scores (the original method only used Mascot protein scores) and the three P-values obtained for each identified prey in a pulldown were then combined into single P-value using the Fisher method. Furthermore, the original Decontaminator used scores directly, whereas our modification first transformed protein scores and spectral counts into their quantiles before proceeding according to the original method. Multiple GFP pulldowns as well as one NADKD1 pulldown (which gave no sign of real interactors) were used as negative controls for Decontaminator calculations. To account for variable numbers of identified proteins in each bait pulldown, we adjusted the P-values for multiple hypotheses accordingly. The cut for calling an interaction true was adjusted P-value<0.05. Two last requirements were

imposed on interactions passing this filter. We eliminated known MS contaminants such as trypsin and keratin and a protein *A* identified in the pulldown of a bait *B* was marked as carryover if *A* was the bait analyzed immediately before *B* due to general high expression levels of baits and associated carryover risk. Supplementary table S5 provides the data used for each prey in each pulldown.

N-glycosylation assay

HeLa cells were transfected on two consecutive days with siRNAs against *TMEM258* (D-012822-01 and D-012822-04, Thermo Scientific) and *DDOST* (SI04134802, Qiagen, Venlo, The Netherlands) as well as a non-targeting siRNA (D-001810, Thermo Scientific) using Lipofectamine RNAiMAX (Life technologies, Carlsbad, USA). As a control, untransfected HeLa cells were treated with tunicamycin for 4 hours prior to lysis at 1 µg/mL. For radiolabelling, culture medium was replaced with methionine and cysteine free DMEM (Life Technologies, Carlsbad, USA) supplemented with 10% dialyzed fetal calf serum for 20 minutes before adding 200 µCi/mL of ³⁵S-labelled methionine/cysteine for a period of 10 minutes. Cells were lysed using RIPA buffer (10 mM Tris-HCl (pH 8.5), 1% NP-40, 140mM NaCl, 0.5% sodium deoxycholate, 1 mM MgCl₂) supplemented with EDTA-free Protease Inhibitor Cocktail (Roche, Basel, Switzerland). Lysates were cleared by centrifugation at max speed for 10 minutes twice and precleared using Protein-A Sepharose conjugate beads (Life Technologies, Carlsbad, USA) for 1 hour. Pre-cleared lysates were incubated with Saponin antibody, bound to Protein-A Sepharose beads for 16 hours. Beads were washed five times with RIPA buffer, boiled for 7 minutes in sample buffer containing 2-mercaptoethanol. Dried gels

were exposed to imaging plate BAS-TR2040 (Fuji Photo Film Co. LTD) and images taken using BASReader.

Colony outgrowth assay

For assessing viability after TMEM258 depletion, HeLa cells were transfected with two siRNAs against TMEM258 (D-012822-01 and D-012822-04, Thermo Scientific) or a non-targeting siRNA (D-001810, Thermo Scientific) as described before. Two days following transfection cells were passaged for three days before staining with crystal violet solution (0.5% crystal violet, 25% methanol in H₂O).

Generation of HAP1 knockout cell lines

CRISPRs were designed targeting *RAB1A* (exon4; 5'-caccgcatacacaactatgatgcca-3'), *RAB1B* (exon4; 5'-caccggggctatggcatcatcg-3'), *GOSR1* (exon2; 5'-caccgcaggaaacaggctcgacagc-3'), *C10orf76* (exon5; 5'-caccgagtcatagcagtacccgaga-3'), *TSSC1* (exon2; 5'-caccgcgtcccaacaaaaaccgaa-3'), *GOLGA5* (exon10; 5'-caccgcgaacagcagatgaactccg-3'), and *TMEM165* (exon4; 5'-caccgtacccgttcaacatctcc-3') and cloned into PX330 (60). HAP1 cells were transfected with the gene-specific PX330 vectors in addition to a vector containing a guide RNA to the zebrafish *TIA* gene (5'-ggtatgtcggaacctctcc-3') and a cassette of a 2A sequence followed by a blasticidin resistance gene, flanked by two TIA target sites. Co-transfection with PX330 results in excision of the cassette from the plasmid and subsequent sporadic incorporation at the site of the targeted genomic locus by non-homologous end joining (61). Successful integration of the cassette into the targeted gene disrupts the allele, renders cells resistant

to blasticidin, and provides a tag at the location of the mutation. Four days following transfection the culture medium was supplemented with blasticidin (10 µg/mL). Surviving colonies were clonally expanded, screened for cassette integration into the query gene by PCR, and their mutations verified by Sanger sequencing (fig. S14). The generation of *TSSC1*-deficient cells was identical with the exception of a targeting cassette with a puromycin-resistance gene. Selection occurred at 750 ng/ul puromycin in the culture medium. For *RAB1B*, a targeting cassette was used with a CMV-promoter preceding the blasticidin-resistance gene.

For *PTARI* a TALEN was designed targeting exon 3 (5'-tcccacagaaagggcacagc-3'; 5'-agatggaggctgtggtaa-3') and transfected into HAP1 cells in combination with pMX-IRES-Blasticidin. Two days post-transfection the culture medium was supplemented with 30µg/mL blasticidin (Invivogen, San Diego, USA). Cells surviving the selection were subcloned, genotyped by PCR, and their mutations verified by Sanger sequencing (fig. S14).

Synthetic lethality network

We used mutagenesis data of four wild-type (WT) HAP1 replicates and three biological replicates for each of the query knockout (KO) genotype. To identify synthetic lethality interactions we analyzed the proportions of sense and antisense insertions in all gold gene transcripts in all WT and query KO replicates. We observed, as demonstrated in fig. S22A, that the level of sense depletion between any two replicates can vary. For example, for most of the depleted transcripts in the *RAB1B*-3 replicate, the depletion is better than

that in WT-1 replicate, as most of the transcripts lie under the highlighted red diagonal. As this systematic drop in the ratio of sense insertions is not caused by inactivation of a single gene but rather by different overall depletion level in the two experiments caused by experimental variation, we pre-normalized the data such that the median depletion of genes on the genome scale is preserved (fig. S22B). We normalized the insertion counts for the purposes of the synthetic lethality analysis in the following manner. The aggregated insertion counts from the 4 WT replicates were used as a reference set that each replicate, including each WT replicate, was normalized against. The gold transcripts were sorted based on their ratio of sense insertions in the reference set into bins of 200 transcripts, then the insertion numbers in each bin were adjusted independently such that the median sense ratio of the 200 transcripts in a bin was same in each replicate and equal to the median ratio of those genes in the reference set. For a given replicate to be normalized, let m be an observed median ratio and m^* be the reference median ratio of sense insertions in a bin of 200 transcripts. Then for a given transcript in the bin, its observed number of sense insertions, s , and antisense insertions, a , were normalized to integers s' and a' such that $a' + s' = a + s$ and $s'/(a' + s')$ was as close as possible to r' defined as

$$r' = \begin{cases} \frac{m^*}{m} r & \text{iff } r < m \\ 1 - \left[(1 - r) \frac{1-m^*}{1-m} \right] & \text{iff } r \geq m \end{cases},$$

where, $r = s/(a + s)$. Observed insertion counts of transcripts with less than 20 insertions in the reference set or in the replicate being normalized were not altered by the above normalization protocol and also were not considered for median calculations. The normalized insertion counts in each gold transcript were then analyzed for synthetic

lethality. We considered a gene transcript passing the following three criteria to be synthetic lethal with the query: (i) the transcript showed significant bias for antisense insertions in each of the three query KO datasets (three Binomial tests, each at P-value cutoff 0.05); (ii) each query KO dataset showed increased depletion of sense insertions as compared against each WT dataset (12 Fisher's exact tests, between the 4 WT and the 3 KO datasets, each at P-value cutoff 0.1); and (iii) the overall proportion of sense insertions in the data aggregated from all WT replicates was at least 1.3 times larger than that in the query KO replicates $\left(\frac{\sum_{i \in \text{WT}} s_i}{\sum_{i \in \text{WT}} a_i} \geq 1.3 \frac{\sum_{i \in \text{KO}} s_i}{\sum_{i \in \text{KO}} a_i} \right)$. As the last step, the detected transcripts are projected into corresponding genes and the results of synthetic lethality analysis are reported on the genes level. Interestingly, we observed that our selection criterion that required passing 12 individual Fisher's tests at the significance cutoff of 0.1 is more stringent than a single Fisher's exact test at $1 \cdot 10^{-4}$ P-value cutoff on aggregated data from all replicates would have been (data not shown). However, the advantage of 12 separate Fisher's tests against a single Fisher's test on aggregated data is that it ensures that the decrease in sense ratio is reproducibly observed in all replicates and thus allowed us to better filter away false positive interactions.

Immunofluorescence Microscopy

One day prior to the experiments cells were seeded onto poly-L-lysine (Sigma Aldrich, St. Louis, USA) or gelatin-coated cover slips. Cells were then fixed with PBS containing 4% paraformaldehyde and permeabilized with PBS 0.1% Triton X-100 (Sigma Aldrich). Next, cells were pre-incubated with PBS 10% horse serum after which primary antibodies were added in the same buffer. Golgi morphology was visualized using an

antibody directed against Giantin (PRB-114C, Covance, Princeton, New Jersey, USA). GOLGA5 was detected with a specific antibody (HPA000992, Sigma Aldrich, St. Louis, USA). For detecting PI(4)P and PI4KB, cells were permeabilized in 10 µg/mL digitonin in 100mM Glycine containing PBS, stained in 1% BSA in PBS and incubated with primary antibody (PI4KB, 06-578, Millipore, Billerica, USA; PI(4)P (Z-P004, Echelon Biosciences, Salt Lake City, USA) overnight at 4°C. Exogenous TMEM258, and C10orf76 were detected using an antibody directed against hemagglutinin (HA) tag (H6908, Sigma Aldrich, St. Louis, USA) and Flag-tag (M2, Sigma Aldrich, St. Louis, USA) respectively. Specifically for Flag-tag staining, cells were permeabilized and stained in 3% BSA/PBS containing 0.3% triton X-100 and 10% goat serum. After labeling with primary antibodies, cells were washed and incubated with secondary antibodies coupled to Alexa Fluor 488 or Alexa Fluor 568 (Life Technologies, Carlsbad, USA). Finally, coverslips were mounted on glass slides using DAPI-containing mounting medium (Vector Labs, Burlingame, California, USA) and analyzed on a Leica-Microsystems confocal microscope using LCS software (Leica-Microsystems, Vienna, Austria).

For visualizing Coxsackie A10 viral particles, cells were seeded on IbiTreat slides µ-slide 18-wells (Ibidi, Martinsried, Germany) one day prior to infection. Infection and binding occurred on ice (MOI=±50) for 60 minutes, washed 3 times with ice cold PBS and subsequently cells were incubated at 37°C for 0, 30, and 300 minutes. At each time point, wheat germ agglutinin (Alexa 488, Life technologies) was added for 10 min at RT prior to 3 washes with PBS and fixation in PBS containing 4% paraformaldehyde. Cells were permeabilized overnight in 70% EtOH and viral RNA was visualized using *in situ*

hybridization of 48 fluorescent RNA probes complementary to the genome of Coxsackie A10 (accession no. AY421767.1) according to manufacturer's specification (Stellaris RNA FISH, Biosearch technologies, Petaluma, USA).

Flow cytometry

PBS supplemented with 5mM EDTA was used to detach cells from the dishes, after which cells were stained with an antibody directed against heparan sulfate (clone 10E4, US Biological, Salem, Massachusetts, USA) in the presence of 1% bovine serum albumin (BSA). Cells were then washed three times and incubated with secondary antibody coupled to Alexa Fluor 568 (Invitrogen). Stained cells were measured on a BD LSRII flow cytometer (BD, Franklin Lakes, New Jersey, USA) and data was analyzed using FlowJo software (TreeStar Inc, Ashland, Oregon, USA).

Immunoprecipitations and immunoblotting

For detection of protein-protein interactions, cells were lysed on ice using CHAPS buffer (30 mM Tris-Cl pH 7.5, 150 mM NaCl, 1% CHAPS). Lysates were then cleared twice by centrifugation and incubated with anti-Flag M2 agarose beads (Sigma-Aldrich) at 4°C for 2 hours. A portion of the lysates was kept separate as input. Beads were washed four times, mixed with sample buffer containing 100 mM dithiothreitol (DTT) and 2% sodium dodecyl sulfate (SDS) and boiled.

For detection of geranylgeranylation of proteins, cells were incubated in the presence of 50 µM azido-geranylgeranyl (Life Technologies, Carlsbad, USA) for 48 hours, lysed in 1% SDS in 50 mM Tris-HCl, pH 8.0 containing protease inhibitor cocktail. Azido-

geranylgeranyled proteins were labeled using biotin-alkynes and immobilized on streptavidin-coated M280 beads (Life Technologies, Carlsbad, USA) following manufacturer's instructions. Beads were washed four times, bound complexes were mixed with sample buffer and boiled.

Protein lysates in sample buffer were subsequently separated by SDS polyacrylamide gel-electrophoresis (SDS-PAGE) and transferred onto polyvinylidene fluoride (PVDF) membranes (Millipore) by wet Western blotting. Membranes were then blocked with PBS 0.1% Tween-20 and 5% non-fat milk powder and subsequently incubated with primary antibodies in the same buffer. Endogenous RAB1A and RAB1B were detected using specific antibodies (Rab 1A (C-19) and Rab 1B (G-20), Santa Cruz Biotechnology, Santa Cruz, USA), and so were TMEM258 (TMEM258 (E15)), CDK4 (Cdk4 (C-22)), Tubulin (Tubulin (B-7)) and PI4K-beta (PI4-Kinase β 06-578, Merck Millipore). Flag-tagged STT3B, DAD1, and C10orf76 were detected using an antibody directed against the Flag-tag (F3165, Sigma-Aldrich).

Following washing, membranes were incubated with secondary antibodies coupled to horse radish peroxidase (HRP) and analyzed using enhancer and peroxide solutions (Thermo-Scientific, Waltham, Massachusetts, USA) on a gel imaging system (Bio-Rad).

Electron microscopy (EM)

Cells were fixed using Karnovsky's fixative (2.0% paraformaldehyde 2.5% glutaraldehyde in 100mM cacodylate buffer at pH 7.2). Post-fixation was carried out with 1% osmiumtetroxide in 100mM cacodylatebuffer. Following washing, cell pellets were stained en bloc using Ultrastain 1 (Leica, Vienna, Austria) and subjected to an ethanol

dehydration series. Cell pellets were embedded in DDSA/NMA/Embed-812 (EMS, Hatfield, Pennsylvania, USA) and sectioned. Sections were stained with Ultrastain 2 (Leica) and analyzed on a CM10 electron microscope (FEI, Eindhoven, Netherlands). For examining virus replication factories, cells were infected with Coxsackie A10 virus (MOI=±10) and incubated at 37°C for 8 hours prior to fixation.

Virus Infectivity Assay.

For testing the role of C10orf76 in virus susceptibility, HAP1 wild-type cells, HAP1 cells deficient for *C10orf76*, and *C10orf76*-deficient cells expressing FLAG-C10orf76 were seeded in 96-well plates at ±50% confluence. The next day, cells were challenged with Coxsackie A10 (Cox A10), Coxsackie B1 (Cox B1), herpes simplex virus 1 (HSV1), and vesicular stomatitis virus (VSV) at an MOI of approximately 5 and incubated at 37°C for two days prior to formaldehyde fixation and crystal violet staining.

Supplementary Discussion

Comparison of the essential genes identified in KBM-7 cells using gene-trap mutagenesis in the Wang *et al.* study and this study.

Wang *et al.* also used random gene-trap mutagenesis in KBM-7 cells to identify essential genes. In both cases the directionality of the gene-trap was used to gauge essentiality for a given locus. Based on our triplicate datasets in KBM-7 cells we modeled the overall technical and biological variability between samples and applied a noise model to identify essential genes in the merged dataset containing 34.3 million unique mutations. When the gene-trap data in KBM-7 cells from Wang *et al.* were analyzed in the same way 1,196 genes scored as essential for fitness compared to 2,054 genes in this study (fig. S22A). Due to the difference in the number of identified genes these datasets overlap for $\pm 50\%$ when calculated from the larger dataset, however, when viewed from the perspective of the smaller dataset $\pm 90\%$ of the genes identified by Wang *et al.* were present in the gene set identified in this manuscript, thus supporting high technical and biological reproducibility of the used method (fig. S22B). The difference in dataset size can be explained by an additional experimental step in our protocol that was implemented to **enrich for haploid cells** (using flow cytometric cell sorting) prior to deep sequencing of the insertion sites, as well as to the use of a different gene-trap vector, and the number of interrogated mutants.

Comparison of the essential genes identified by Wang *et al.* using CRISPR mutagenesis in KBM-7 cells and the essential genes identified in this study using gene-trap mutagenesis.

To assess the degree of overlap, the analysis was limited to 16,246 genes that could in principle be identified by both technologies as (i) they are not located on chromosome 8, (ii) a corresponding guide RNA is present in the library used by Wang et al., and (iii) an Ensembl Gold Transcript is annotated. The comparison shows that entirely different techniques yield an overlap of $\pm 77\%$ viewed from the perspective of the smaller CRISPR dataset by Wang *et al.*, and $\pm 66\%$ from the perspective of the gene-trap-based data in this manuscript, underlining the validity of both approaches (fig. S22C). Differences could be attributed to limitations of either approach (limitations of gene trapping are discussed below). Furthermore, the high number of unique gene-trap mutations measured in many genes may enable the detection of subtle fitness defects.

Limitations of the employed gene-trap mutagenesis approach to identify essential genes.

First, retroviral integration is biased and therefore some genes are mutated more frequently than others and this also affects the location within the gene where gene-trap insertions are found. Although this complicates equal comparison of all genes, the bias of retroviral integration towards the 5' end of active genes likely facilitates the disruption of expressed genes. However, sense integrations at the 3' could result in (partially) functional gene products, which would therefore not score as essential. Furthermore the approach that we used is based on the unidirectional design of the gene-trap vector. This has several shortcomings: in intronless essential genes, for example, all integrations (regardless of orientation) are likely to be disruptive and therefore we exclude these from the analysis. Also, not all sense orientation insertions of the gene-trap in intronic regions

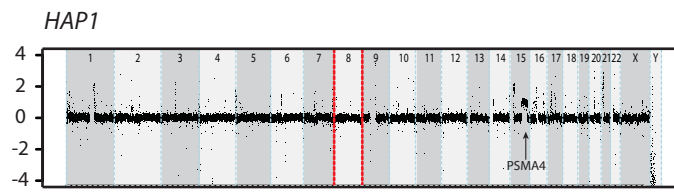
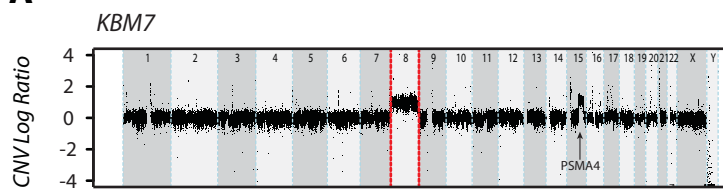
create full knockout alleles because alternative splicing may result in the formation of hypomorphic alleles.

Some complications arise from the sequence of the human genome itself. The presence of repetitive regions hinders unique alignment to the genome (and affected insertion events were not used in this study), while genes whose genomic location overlaps with other genes confounds the interpretation of observed orientation biases. In order to account for the latter, only integrations in non-overlapping genomic regions are considered for this study. As gene essentiality is determined on transcript level, the quality of transcript annotation additionally affects conclusions. For this, ENSEMBL gold transcripts were used, however, a number of genes either do not have an annotated gold transcript, have multiple gold transcripts, or the gold transcript does not necessarily reflect the transcript that is expressed in KBM-7 or HAP1 cells.

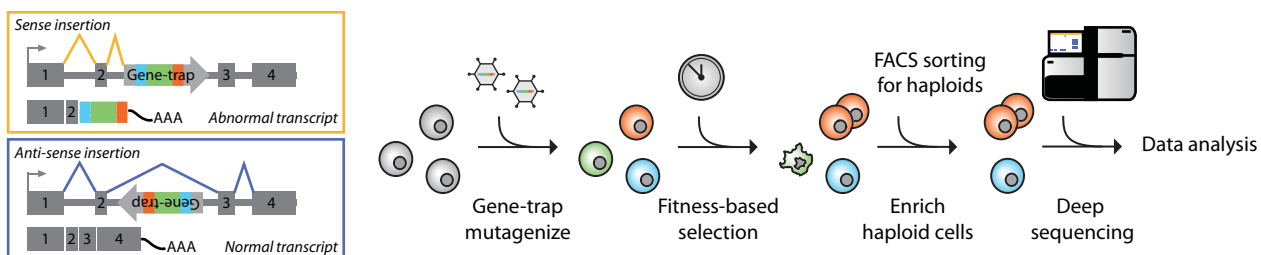
Finally, it is challenging to distinguish mutations in genes that lead to cell death from those mutations that cause more subtle fitness defects. Especially the measurement of large numbers of mutations in genes enables the identification of subtle fitness defects associated with gene loss as well as complete cell death. Also, essentiality is scored 10 days after introduction of the mutation in some cases long-lived proteins may maintain viability in low copy numbers. Together, it is difficult to make an absolute separation between the genes that cause cell lethality upon loss versus those that induce sickness.

Figure S1

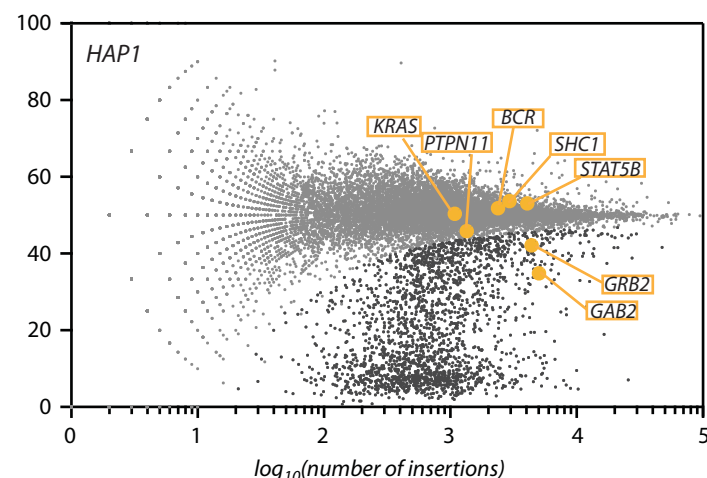
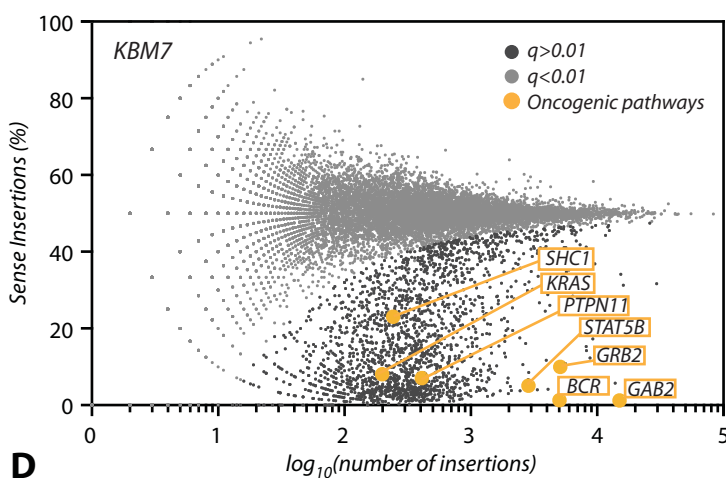
A



B



C



D

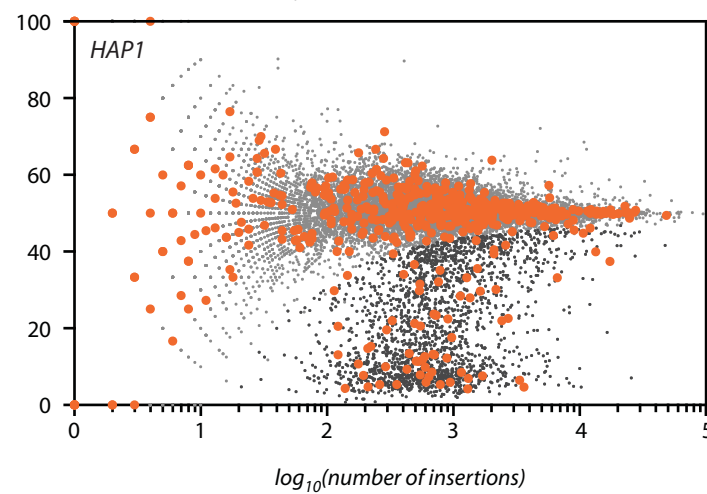
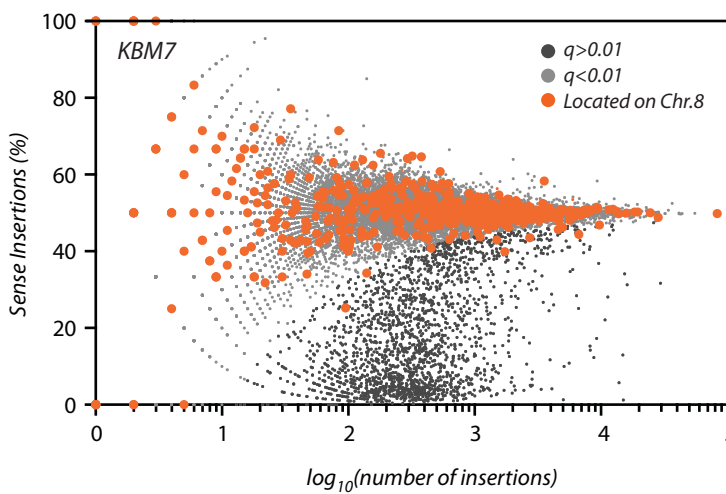


Fig. S1. The identification of essential genes depends on haploidy and signaling context. **(A)** Genome sequencing of KBM7 and HAP1 cells illustrates that KBM7 cells are diploid for chromosome 8 whereas no increased copy number of chromosome 8 is observed in HAP1 cells. **(B)** Schematic outline of the experimental strategy to identify genes that are essential for fitness. Sense-orientation insertion of the gene-trap vector into intronic sequences is likely to disrupt gene function. **(C)** KBM7 cells are highly dependent on BCR-ABL signaling and components of this signaling pathway were found to be highly depleted for sense-orientation gene-trap insertions in KBM7 cells but not in HAP1 cells. **(D)** The same plots as presented in Figure 1B were re-colored to highlight genes located on chromosome 8. In contrast to HAP1 cells, no chr. 8 genes were strongly depleted for sense-orientation gene-trap insertions in KBM7 cells.

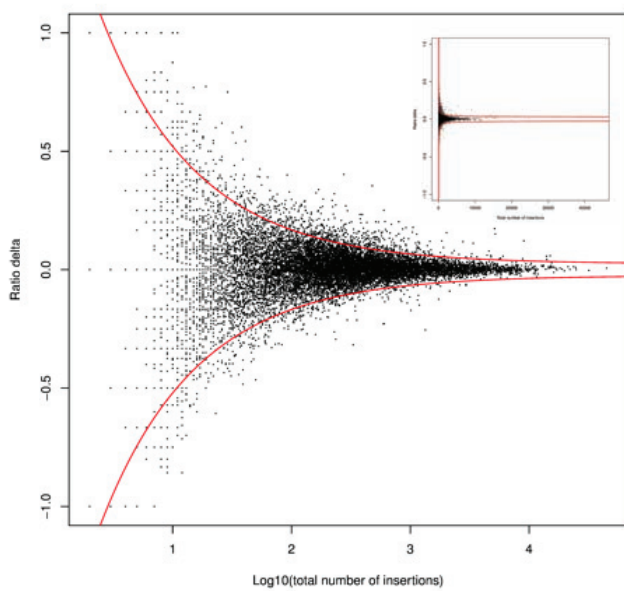
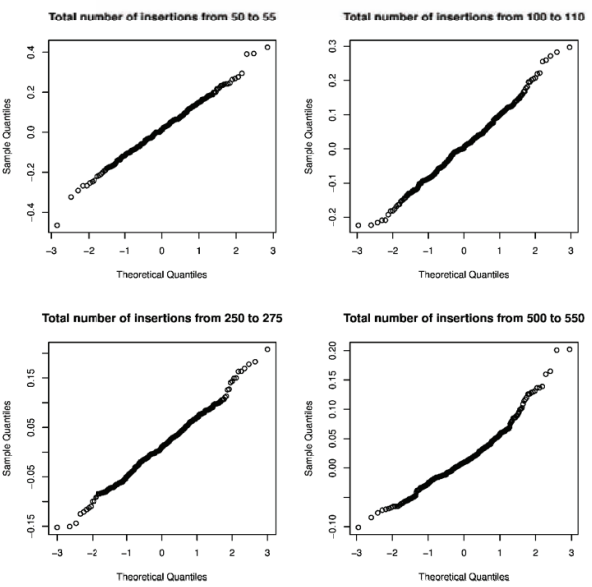
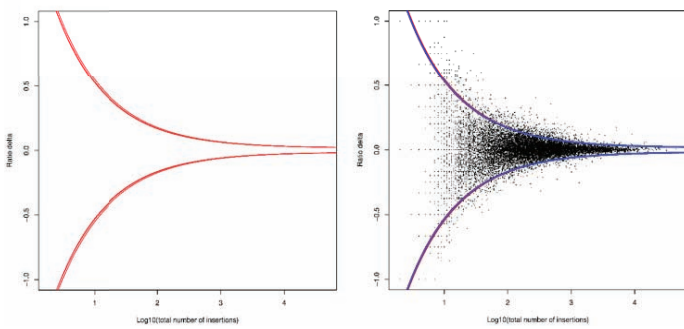
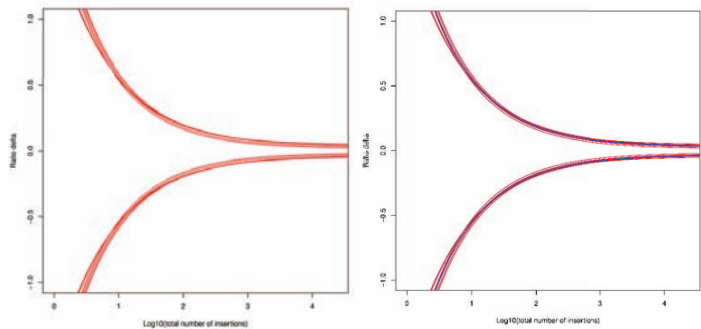
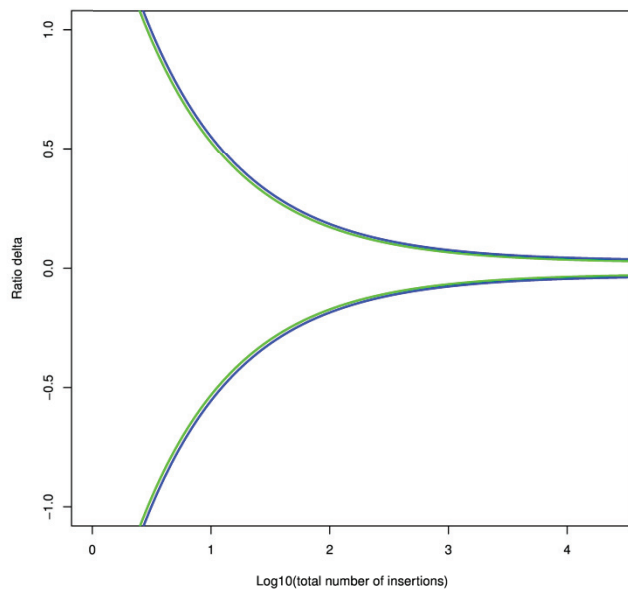
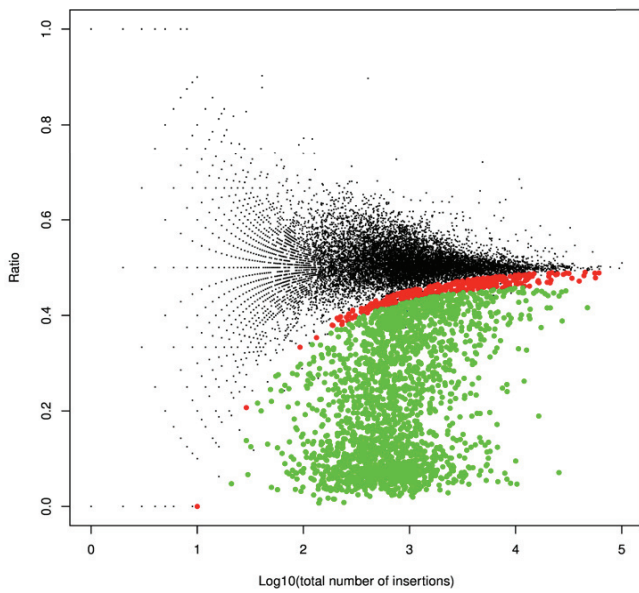
Figure S2**A****B****C****D****E****F**

Fig. S2. Noise function for filtering experimental variation in mutagenesis-based essentiality screens. **(A)** Ratio differences between KBM7 replicates 1 and 2 (black dots). The red curves represent $\pm 2.326\sigma(x)$, 1% significant one-sided test, with $\sigma(x)$ the standard deviation of ratio differences as a function of the logarithm of the total insertion counts. In the inset, is the same plot with total insertion counts in the linear scale instead of logarithmic. **(B)** Normality distribution of ratio differences. Quantile-quantile plots comparing a normal distribution with ratio differences for genes with total insertion numbers close to 50, 100, 250, and 500. A straight line indicates perfect match with a normal distribution. For large total insertion numbers it is difficult to collect enough close numbers to obtain reliable qq-plots and normality is thus assumed. **(C)** Definition of an average KBM7 noise function. We observe that the three red curves from the three possible pairs of KBM7 replicates are almost confounded (left), which shows highly reproducible data quality. The average model is featured in blue in the right panel (black dots are replicates 1 and 2 ratio differences for visualization purpose as in (A)). **(D)** Definition of an average HAP1 noise function, see (C). **(E)** Comparison of HAP1 (blue) and KBM7 (green) noise functions. The two noise functions do not need to be identical and are potentially cell type dependent. They are very close actually, which indicates a high stability of the experimental protocol on those two cell types. HAP1 data are slightly more variable. **(F)** Comparison of selection based on a one-sided binomial test and our more conservative model in HAP1 data. Green dots represent the genes we called fitness-reducing and red dots represent genes that the one-sided binomial test with 0.5 probability of sense insertion would additionally call as fitness reducing. This shows

increased stringency and the effect of the noise function that limits the selection of genes with ratios close to 0.5 based solely on the large number of integrations.

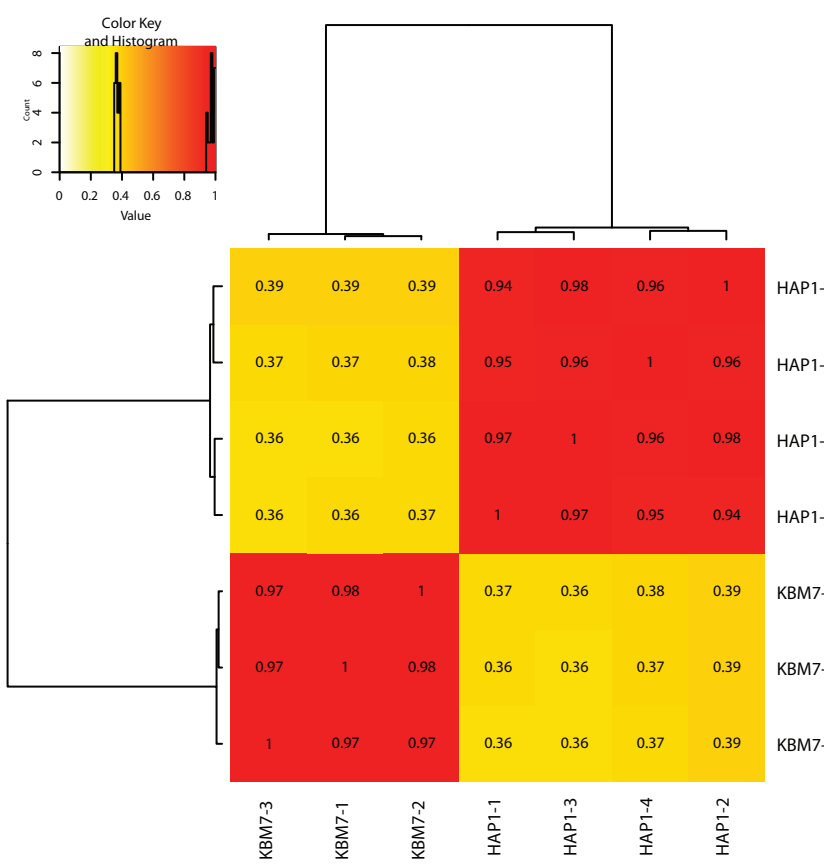
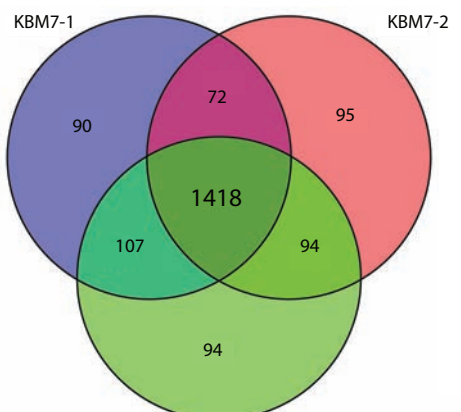
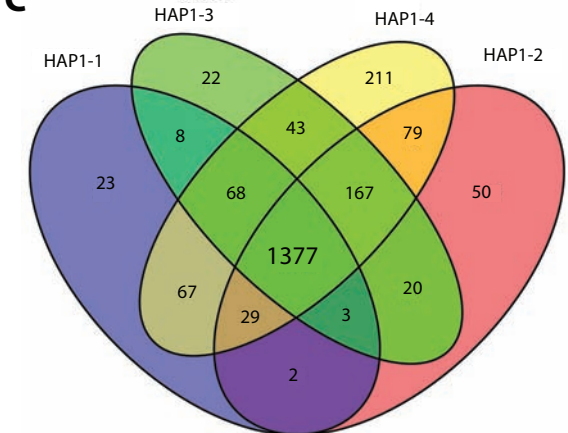
Figure S3**A****B****C**

Fig. S3. Comparison between independent replicates for wild-type KBM7 and HAP1

essentiality datasets. **(A)** To determine the reproducibility of the number of sense and antisense insertions across KBM7 and HAP1 samples as well as to show specific difference between cell lines, we considered insertions in all genes selected as essential for any of the two cell lines. We selected 2,054 and 2,181 genes in KBM7 and HAP1 cells respectively, and the union of those two lists resulted in 2,501 genes. For each biological replicate (3 KBM7 and 4 HAP1), we created a numerical vector made of the number of sense and antisense insertions for these 2,501 genes. We computed the correlation matrix of these 7 vectors and plotted it as a heatmap. This shows highly reproducible insertion profiles within one cell line and differences across the two. Moreover, correlation values are very similar switching from one replicate to the next.

(B) Venn diagram depicting overlap between the individual replicates for KBM7. **(C)** Venn diagram depicting overlap between the individual replicates for HAP1.

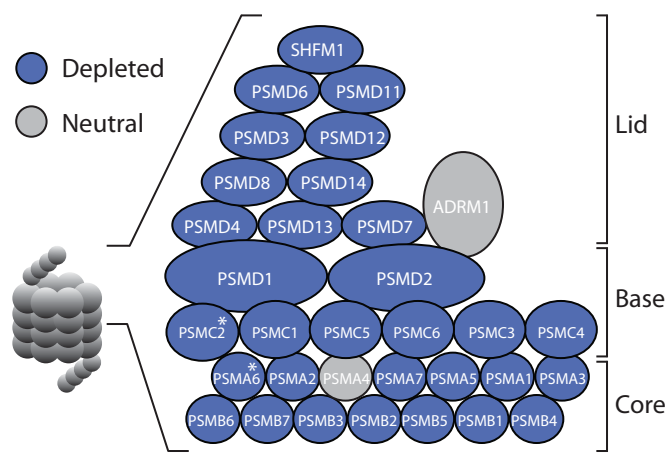
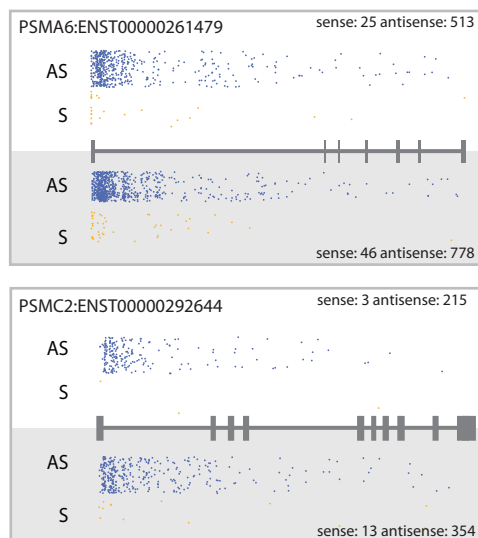
Figure S4**A****B****C**

Fig. S4. Insertion sites in proteasome subunits without annotated Ensembl Gold transcript. **(A)** Identification of the different subunits of the proteasome, an exemplary multi-subunit protein complex known to be essential for mammalian cells. Subunits that scored as essential are colored in blue and others in grey. Genes marked with * do not have an annotated Ensembl Gold transcript, but show strong depletion of disruptive insertions for other transcripts. **(B)** Depicted are all insertion sites found in transcript ENST00000261479 of *PSMA6* for both KBM7 and HAP1, showing a strong bias for antisense orientation insertions. **(C)** Similar illustration showing all insertion sites found in transcript ENST00000292644 of *PSMC2* for both KBM7 and HAP1, showing a similar bias for antisense orientation insertions.

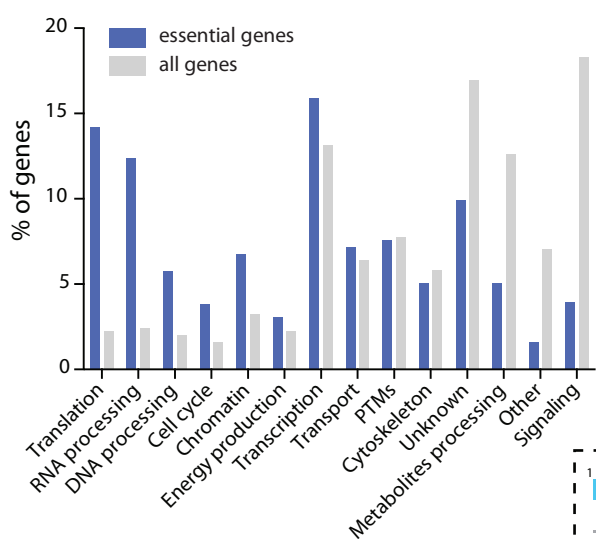
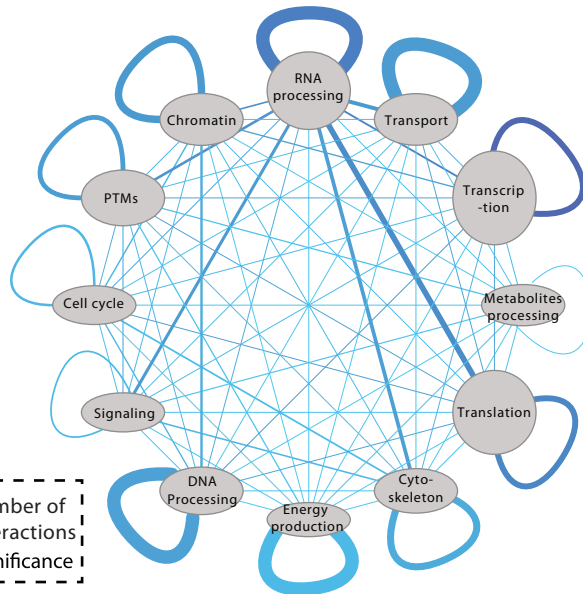
Figure S5**A****B**

Fig. S5. Functional properties of core essential genes. **(A)** Distribution of essential genes to biological functions (as defined by eggNOG database). **(B)** Core essentialome interaction network summarized according to the functional annotations (eggNOG database) of each essential gene.

Figure S6

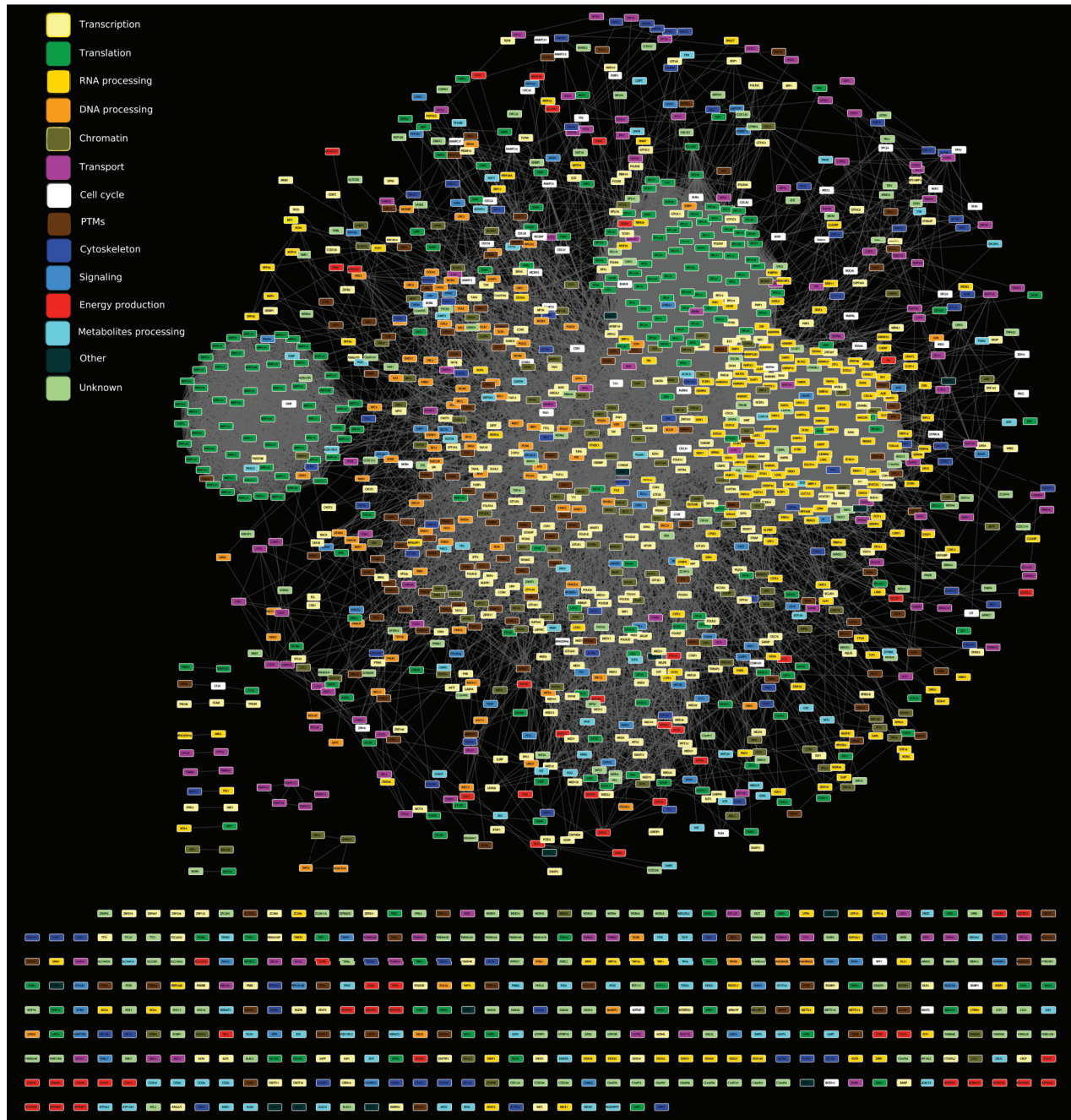
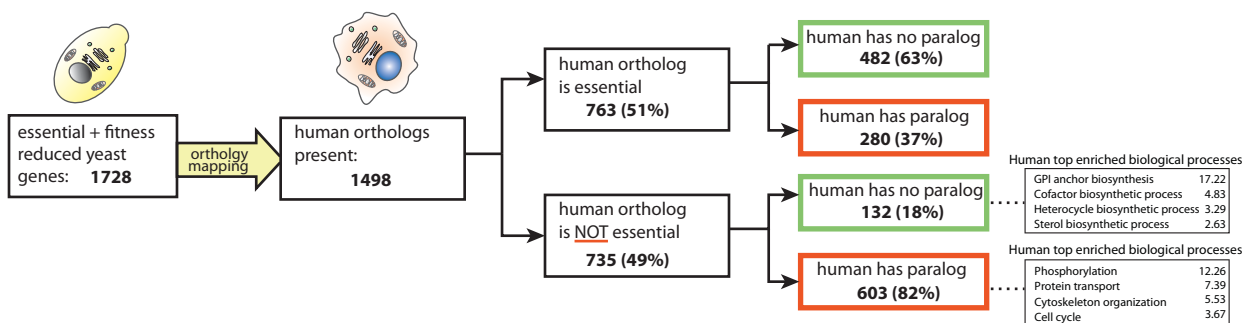
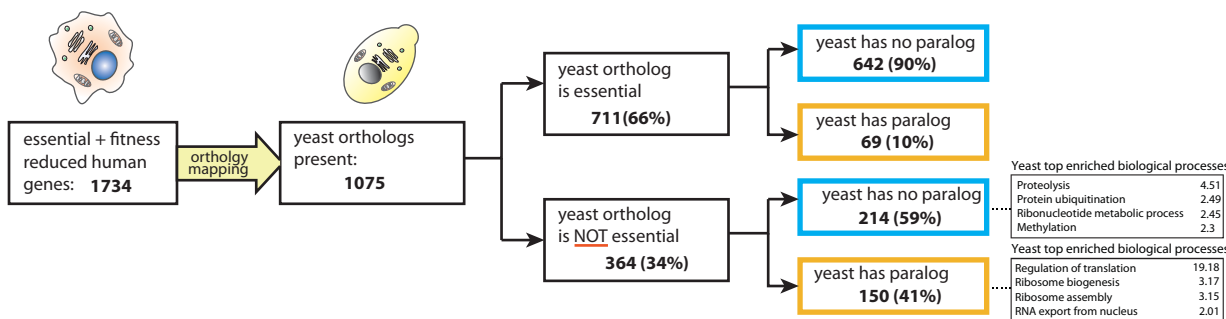


Fig. S6. Core essentialome interaction network. The protein-protein interaction (PPI) network of protein products of core essentialome genes is shown. The PPI's data are integrated from public databases (IntAct, MINT, HPRD, InnateDB, DIP, MatrixDB, BioGRID, NCI-PID, CORUM).

Figure S7

A



B

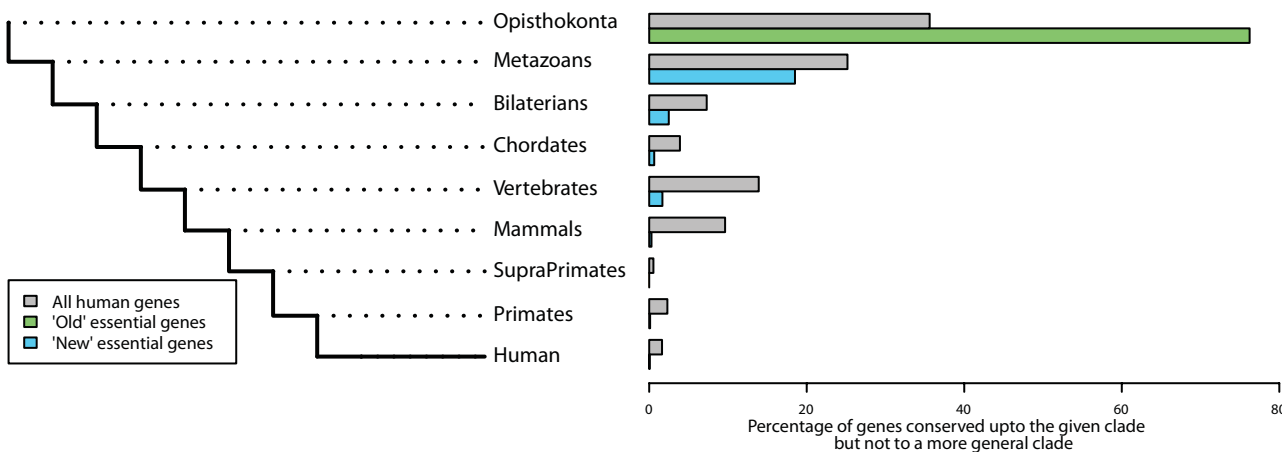


Fig. S7. Comparison of the human essentialome to yeast essential genes and their time of occurrence. (A) Yeast genes orthologous to human genes were mapped using the Ensembl database and queried for fitness in yeast (*I*) or human cells. In both species, genes were categorized based on the absence or presence of paralogs using the Ensembl database. Subsequently, biological process cluster enrichment was performed using DAVID on human genes with or without paralogs for yeast-unique essential genes and vice versa. For non-essential orthologs whose dispensability is not explained by paralogs, the top four enriched functional clusters that pass 5% Benjamini corrected *P*-value threshold are listed. (B) Age of the essential genes compared to the human genome based on mapping of genes' transcripts to most general homologous clusters of proteins via eggNOG 3.0.

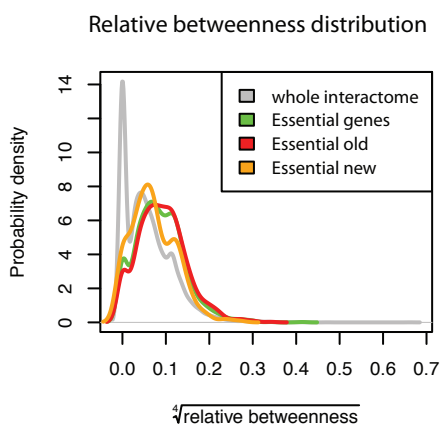
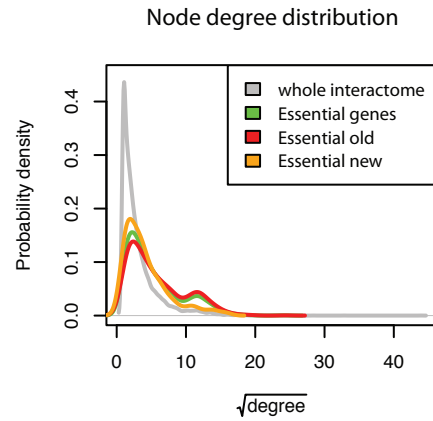
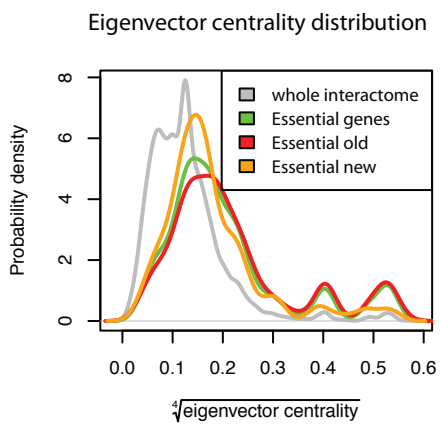
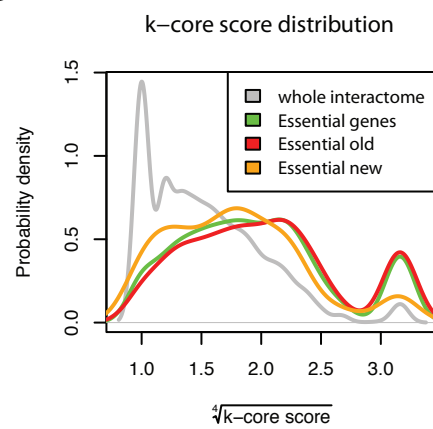
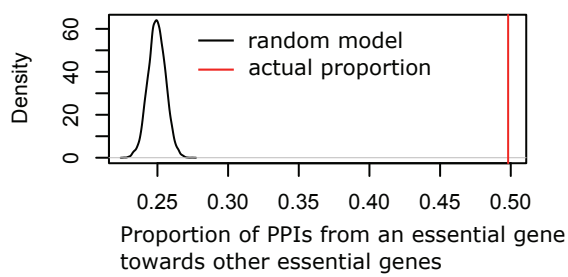
Figure S8**A****B****C****D**

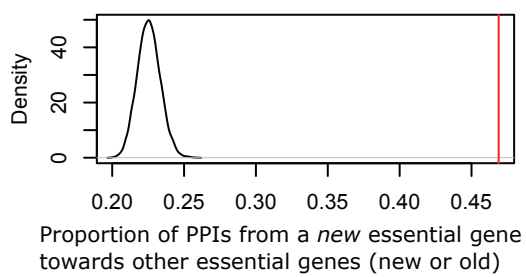
Fig. S8. Network connectivity of essential genes. Local topology measures characterizing the essential gene products within the human interactome (28, 29); (square or quartic roots were applied to scale data). **(A)** Relative betweenness, the proportion of shortest paths in the interactome between all pairs of nodes that go through a given node, and **(B)** eigenvector centrality, a notion of being central when one's neighbors are central as well, characterize how centrally essential gene products are located in the interactome. The node degree **(C)** is the number of PPIs at one gene product, a raw connectivity measure. **(D)** K-cores are highly interconnected sub-networks of the interactome, which usually correspond to protein complexes. Hence, a high k-core score indicates likelihood to form complexes with other proteins. We note that the essential gene products tend to be more central and connected than average nodes of the interactome, a trend that is amplified at *new* essential genes. All differences but one were statistically significant (Kolmogorov-Smirnov test): relative betweenness (all genes vs. essential $P=0$, *new* essential vs. essential $P=9.0E-6$); node degree ($P=0$, $P=5.9E-4$); eigenvector centrality ($P=0$, $P=1.1E-4$); k-core score ($P=0$, $P=6.8E-4$).

Figure S9

A



B



C

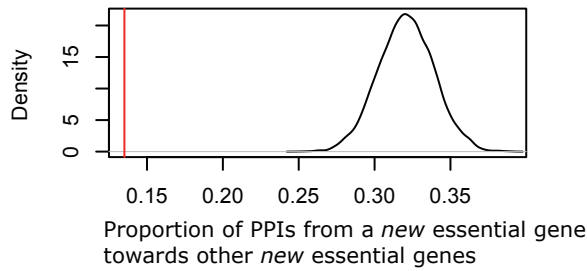


Fig. S9. Essential genes embedded in the human protein-protein interactome. (A)

Average proportions of PPIs towards essential genes originating from an essential gene compared with 10,000 random selections of a set of genes with the same connectivity as the essential genes. The essential genes significantly connect more to themselves than expected by chance ($P<10^{-4}$). **(B)** The same analysis for the proportion of PPIs towards the essential genes originating from *new* essential genes. We again note strong significance towards more connections with the essential genes ($P<10^{-4}$). **(C)** Proportion of PPIs from new essential genes towards other new essential genes ($P<10^{-4}$). From (B) and (C) we conclude that new essential genes connect preferentially with old essential genes.

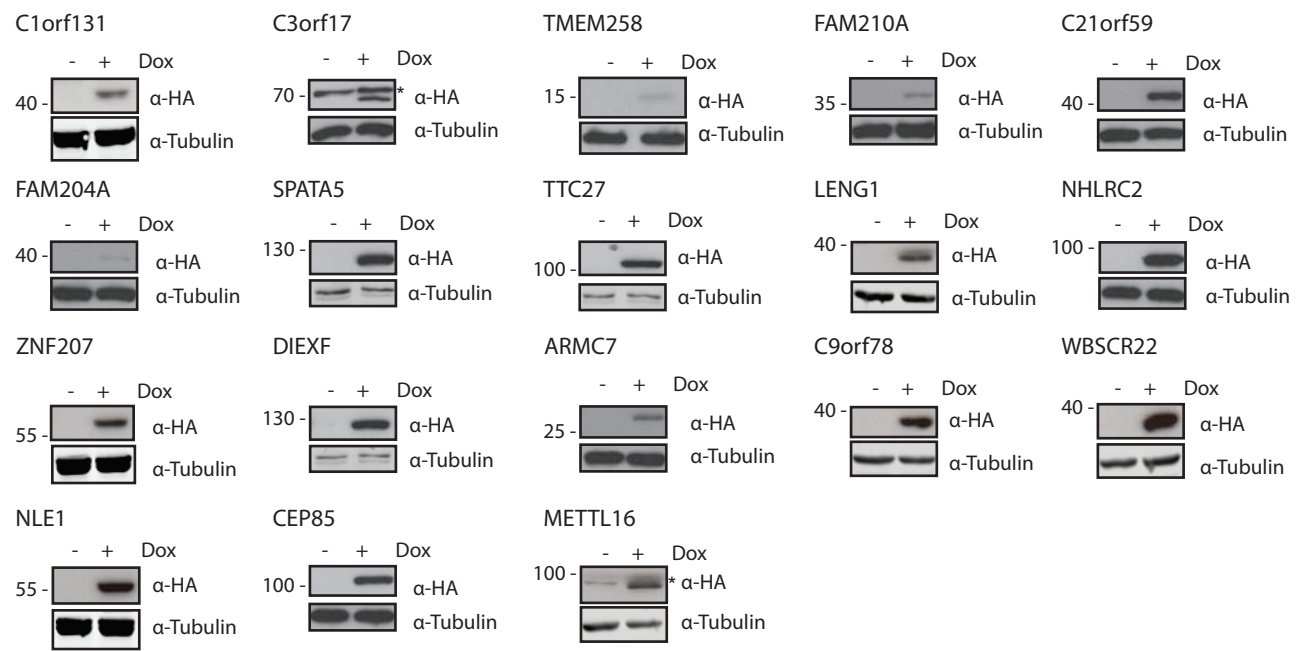
Figure S10

Fig. S10. Expression of the bait proteins for the isolation of protein complexes.

Correct expression of Strep-HA tagged bait proteins in HEK293 Flip-In T-Rex cell lines was verified by western blot. Bait expression in stable cell lines (-) was induced upon treated with 1 µg/mL doxycycline for 24 h (+) and subsequently visualized with anti-HA immunoblotting. Tubulin was used as loading control. Marks on the left side of each blot indicate corresponding molecular weight (kDa) and asterisks indicate non-specific bands.

Figure S11

A

bait prey essential gene
--- known PPI prey non-essential gene

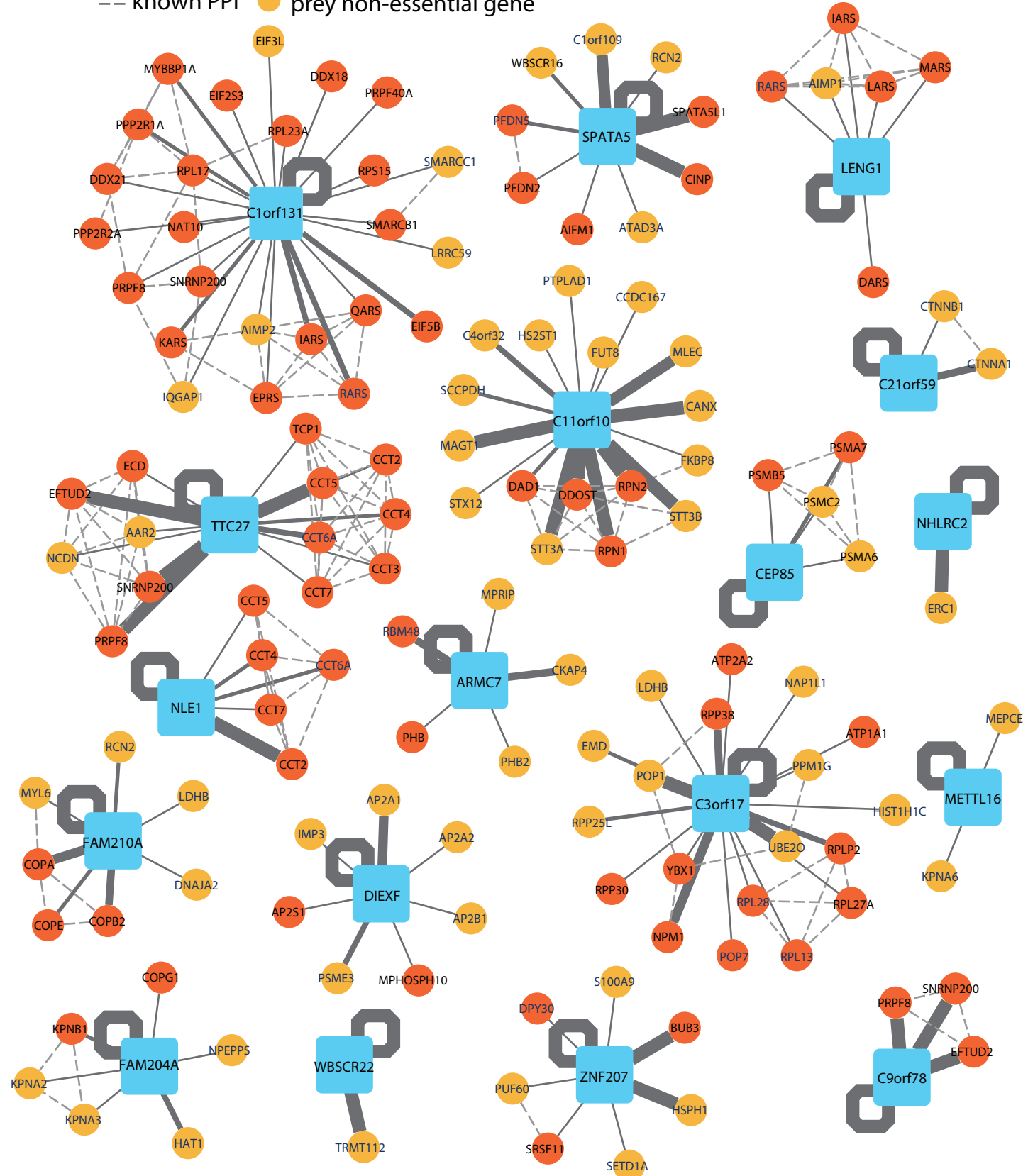


Fig. S11. Protein complexes of selected essential genes (A) High-confidence interactors of each selected essential protein (solid lines) and their known PPIs (dashed lines). Proteins that interacted with products of poorly annotated essential genes were detected by tandem affinity purification coupled to liquid chromatography mass spectrometry. A large proportion of preys were found to be essential themselves (52.4%, $P < 2.5E-36$, hypergeometric), in line with our global analysis of all the 1,734 essential genes mapped to the human interactome. ZNF207 was identified as an interactor of BUB3 during preparation of this manuscript and renamed BuGZ (30, 31).

Figure S12

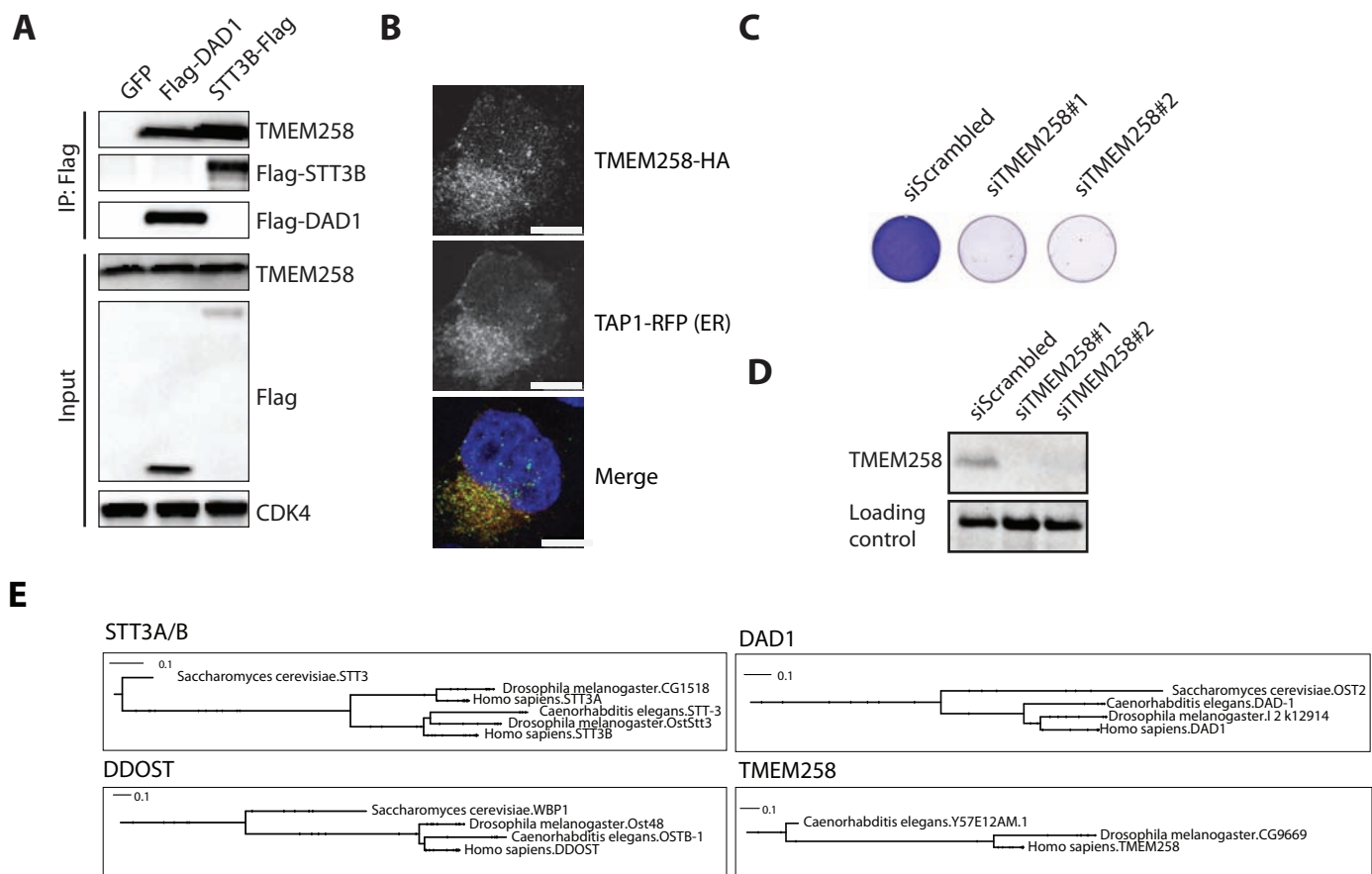
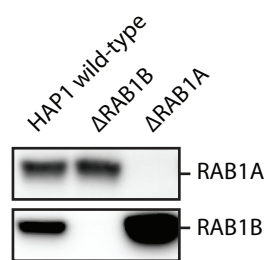


Fig. S12. Localization of TMEM258 and its association with the conserved OST complex.

(A) Association of TMEM258 with Flag-tagged subunits OST complex (DAD1 and STT3B) as assessed by immunoblot analysis with antibodies directed against TMEM258. **(B)** Localization of hemagglutinin (HA)-tagged TMEM258 with the endoplasmic reticulum-resident transporter TAP1 fused to red fluorescent protein (RFP). Cells were stained with HA-specific antibodies (upper picture) and imaged for RFP (middle image). **(C)** Viability of HeLa cells transfected with control siRNAs and siRNAs targeting *TMEM258* stained after 8 days using crystal violet. **(D)** Immunoblot showing depletion of TMEM258 following transfection of HeLa. **(E)** Phylogenetic trees from eggNOG 3.0 of human genes *STT3A/B*, *DADI*, *DDOST*, and *TMEM258* pruned to the selected species. *TMEM258* appears to have a lower degree of conservation in phylogenetic comparisons.

Figure S13

A



B

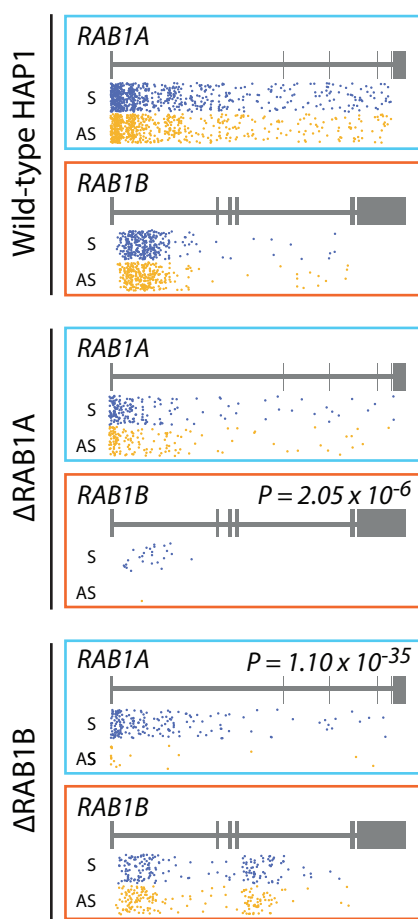


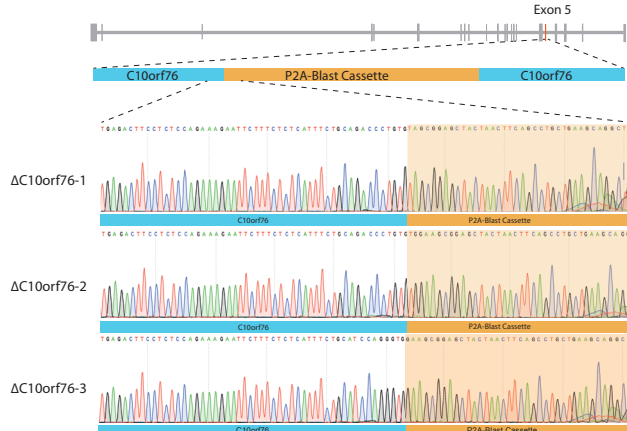
Fig. S13. Expression of RAB1A and RAB1B in HAP1 cells and knockout derivatives.

(A) HAP1 cells and cells deficient for either *RAB1A* or *RAB1B* were analyzed by immunoblotting using antibodies directed against RAB1A or RAB1B. **(B)** Unique gene-trap integrations in *RAB1A* and *RAB1B* mapped in wild-type HAP1 and respective RAB knockout cell lines.

Figure S14

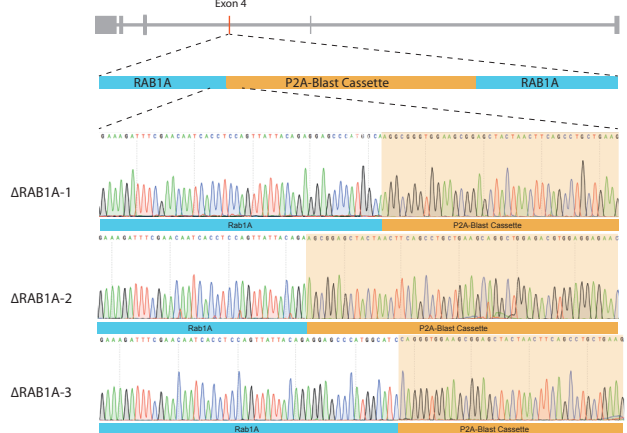
A

$\Delta C10orf76$



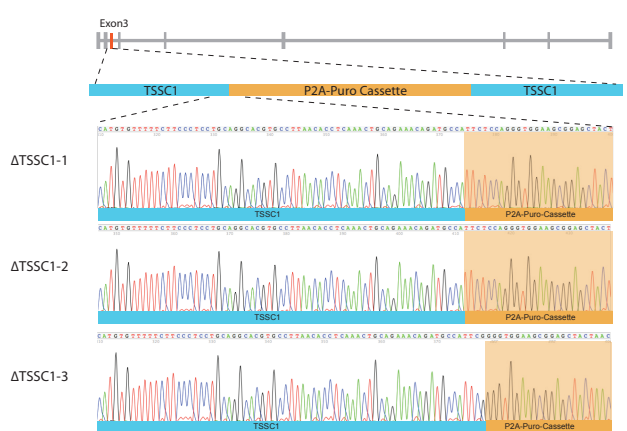
C

$\Delta RAB1A$



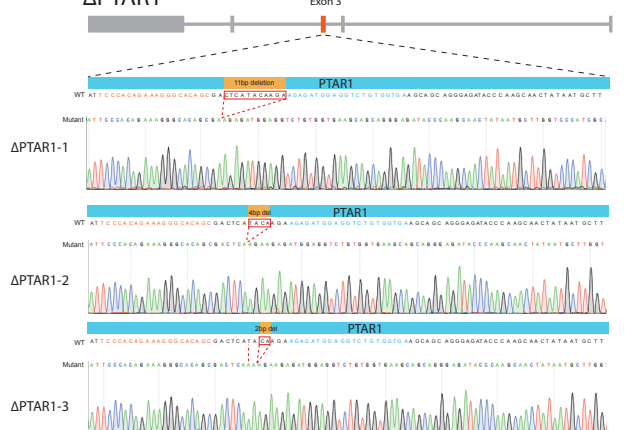
E

$\Delta TSSC1$



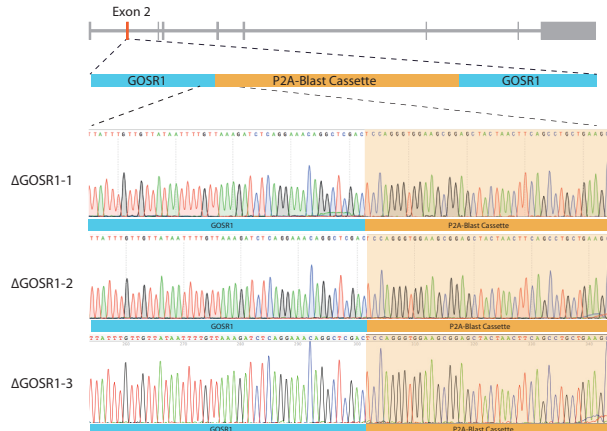
G

$\Delta P T A R 1$



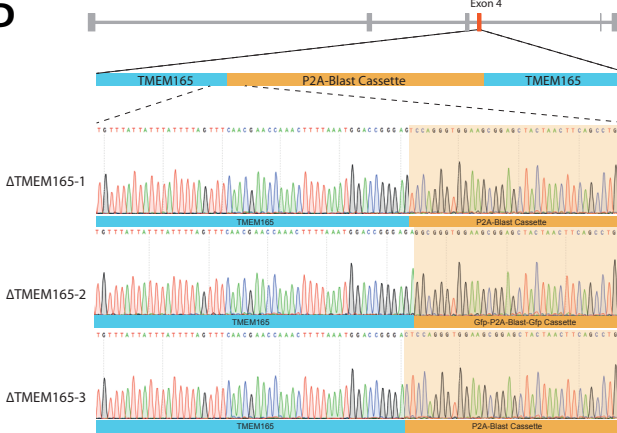
B

$\Delta G O S R 1$



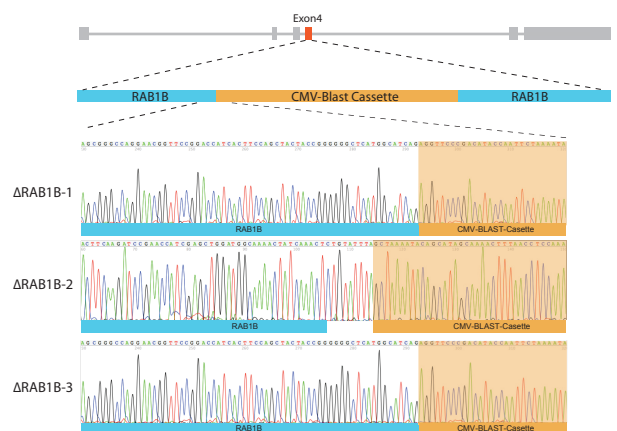
D

$\Delta T M E M 1 6 5$



F

$\Delta R A B 1 B$



H

$\Delta P T A R 1 / \Delta G O L G A 5$

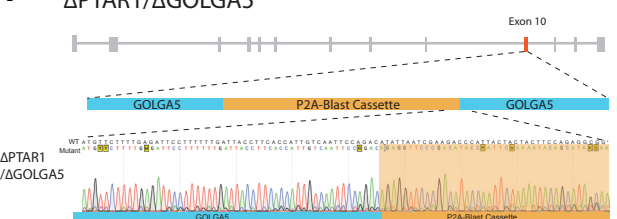


Fig. S14. Generation of HAP1 knockout cells for the indicated genes using genome editing. CRISPR sequences were designed to cleave into coding exons located at the 5' region of the indicated genes. Most mutant alleles were generated by co-transfection of a plasmid that contains a U6-expression cassette directing the expression of a guide RNA to program CAS9-induced cleavage of the same plasmid. This releases a DNA fragment containing the 2A sequence fused to a promoter-less Blasticidin resistance cassette that contained a stop codon and polyadenylation signal. Subsequently, cells were selected with Blasticidin, resistant clones were expanded and this led to identification of cell lines that carried the resistance cassette inserted into the endogenous CRISPR-targeted exonic sequence. *TSSC1*-deficient cells were generated using the same method, except using a puromycin-resistance gene instead of Blasticidin. For *RAB1B* a similar strategy was used but a cassette was integrated that also contained a CMV promoter to direct expression of a Blasticidin-resistance gene. *PTARI*-deficient cells were generated using TALENs and clonal cell lines were identified that carried indels leading to frameshift mutations in the coding sequences as indicated.

Figure S15

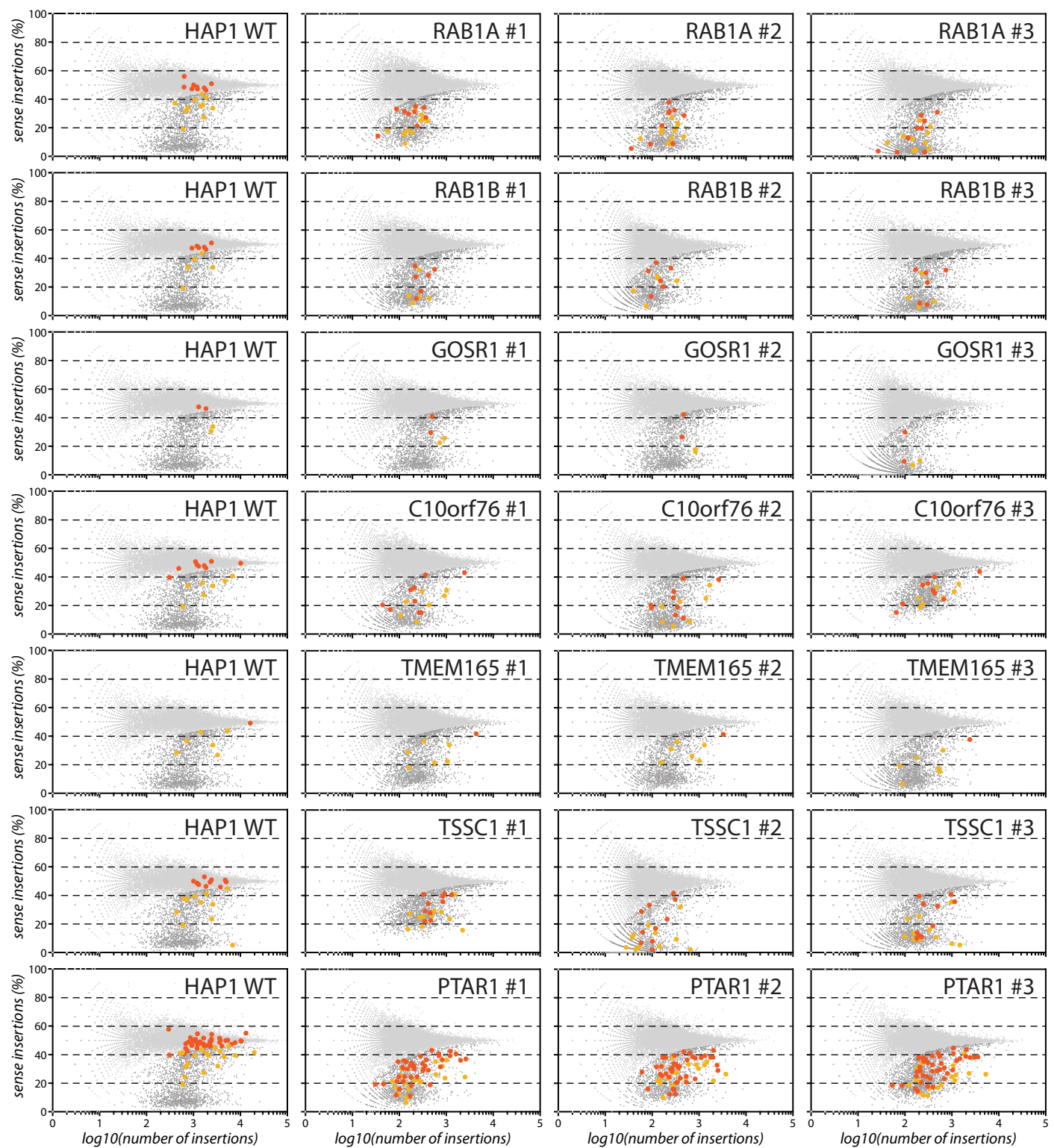


Fig. S15. Comprehensive overview of synthetic lethality screens. Genes with a significant change in essentiality as compared to four independent wild-type datasets are indicated on the non-normalized data for each genotype and independent replicate (#1, #2, #3). For statistical analysis the datasets are normalized according to gene essentiality distribution of the aggregated wild-type essentialome (left) and genes shifting from fitness-neutral to essential are colored in red, while essential genes with an increased depletion for sense-insertions are highlighted in yellow.

Figure S16-1

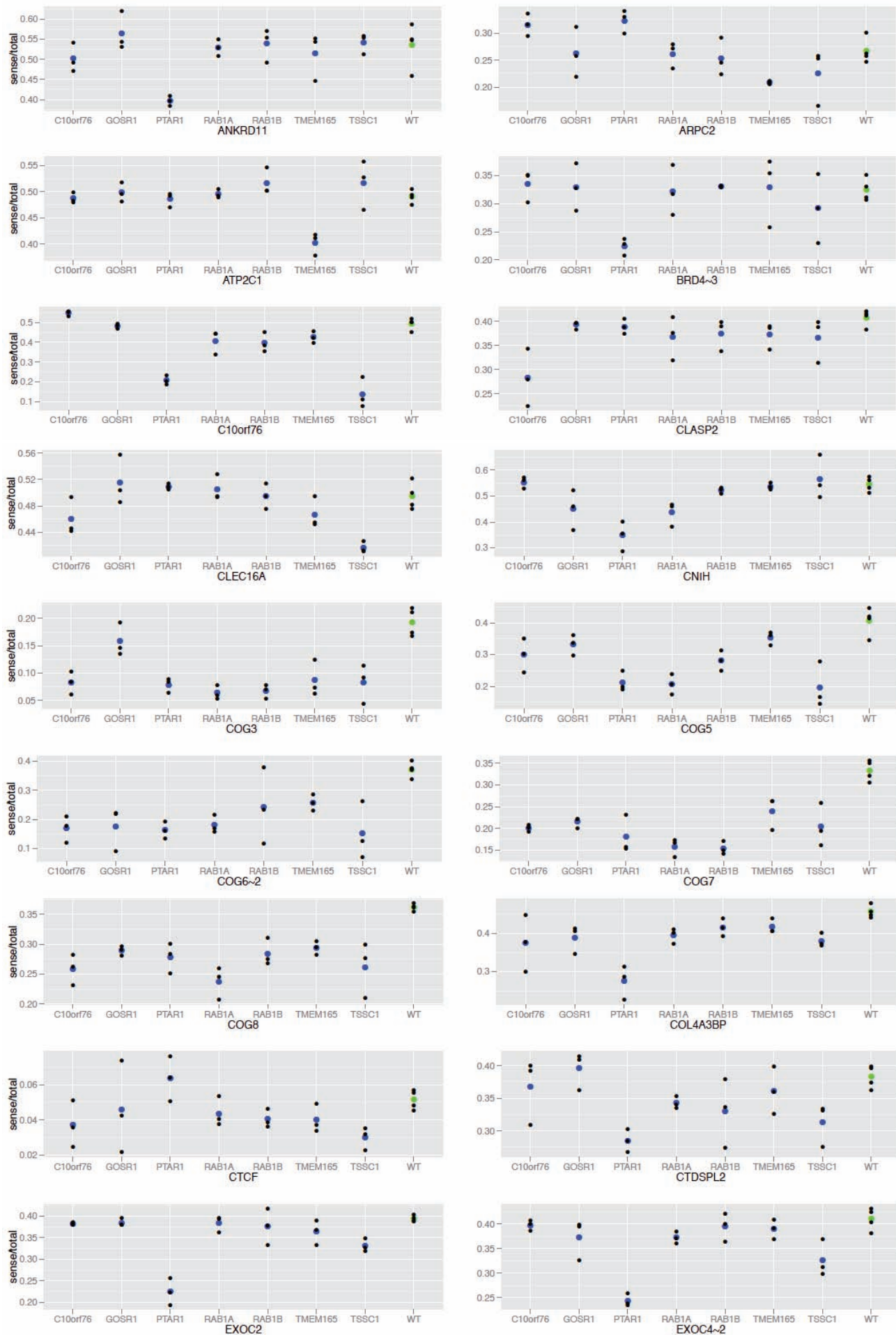


Figure S16-2

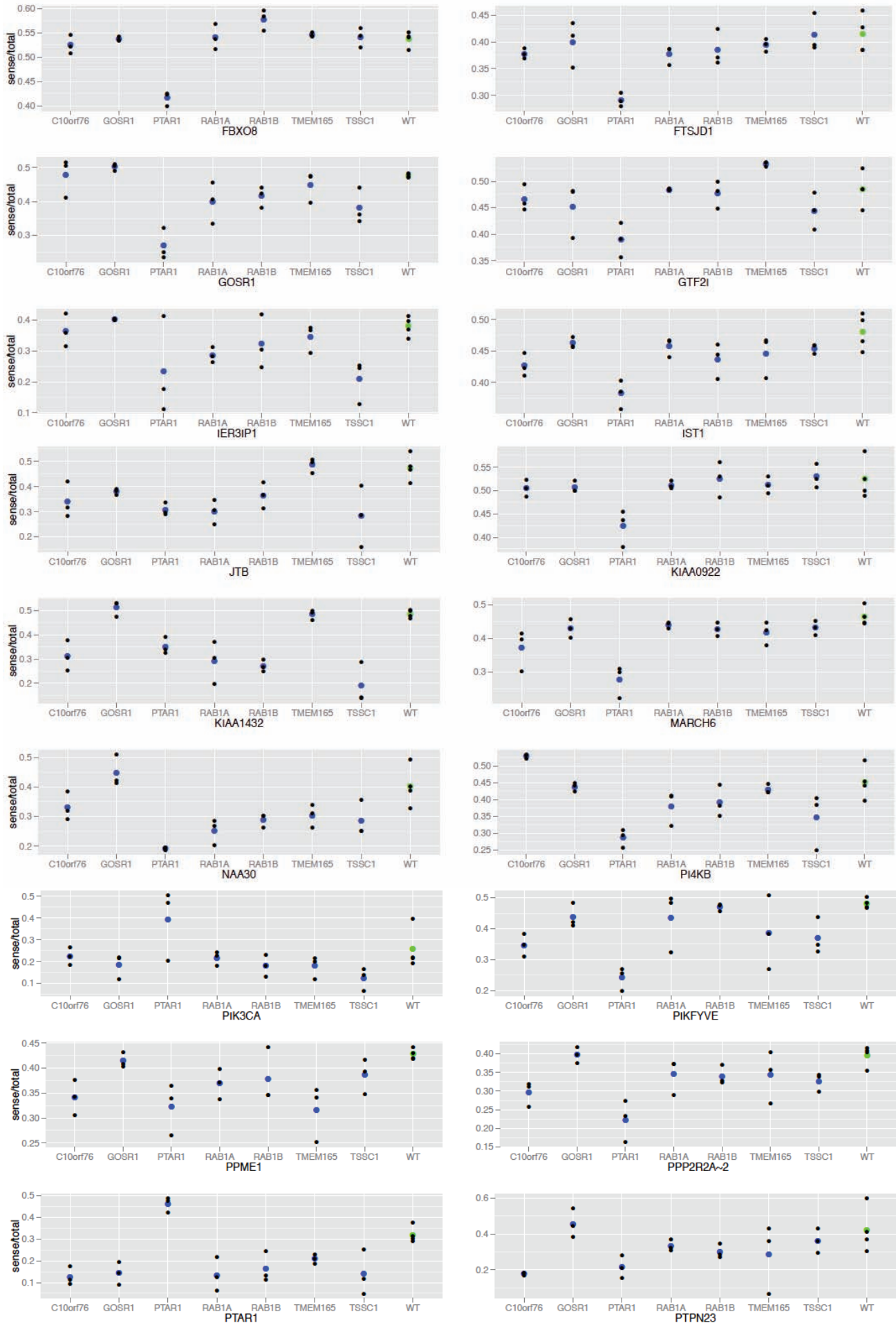


Figure S16-3

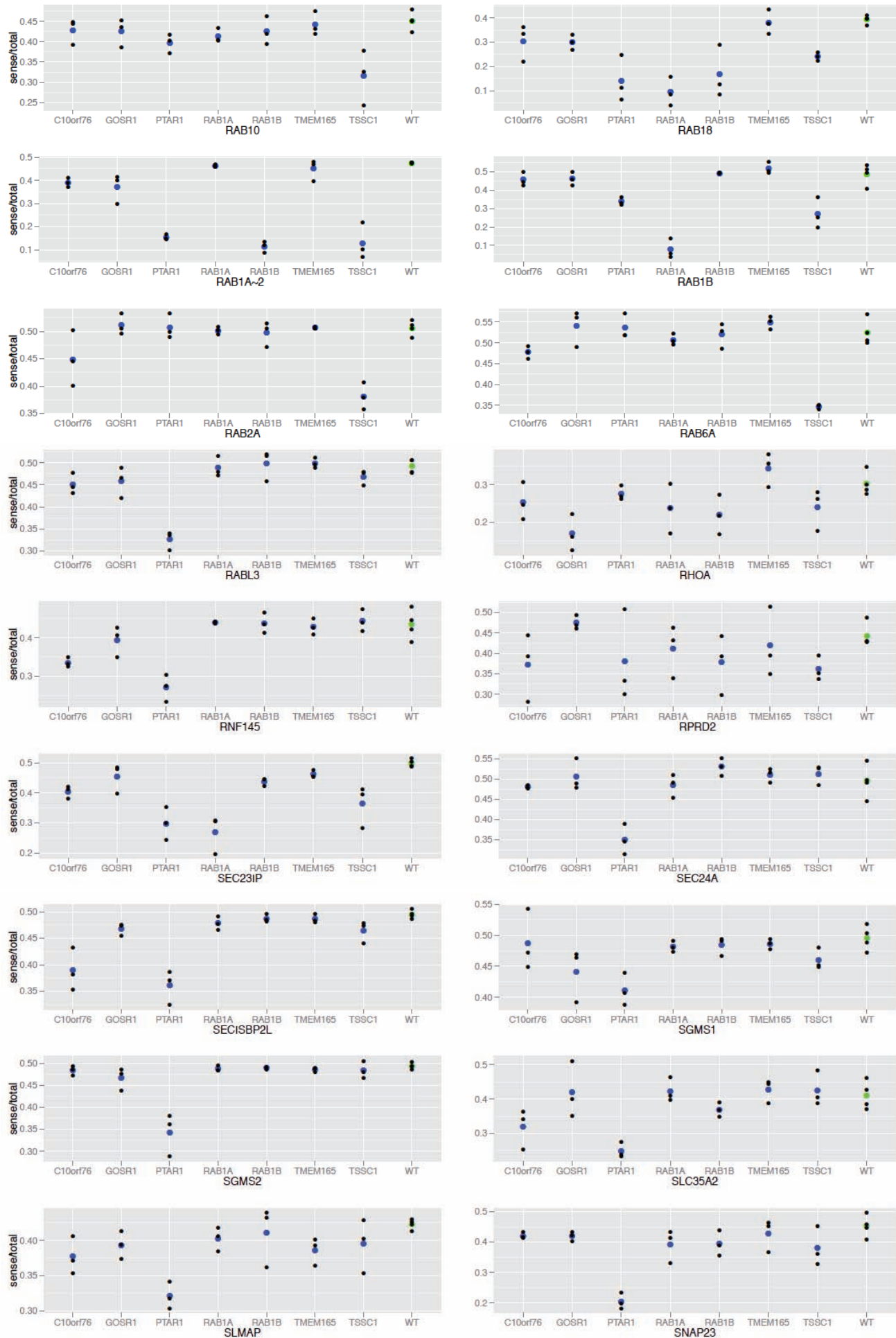


Figure S16-4

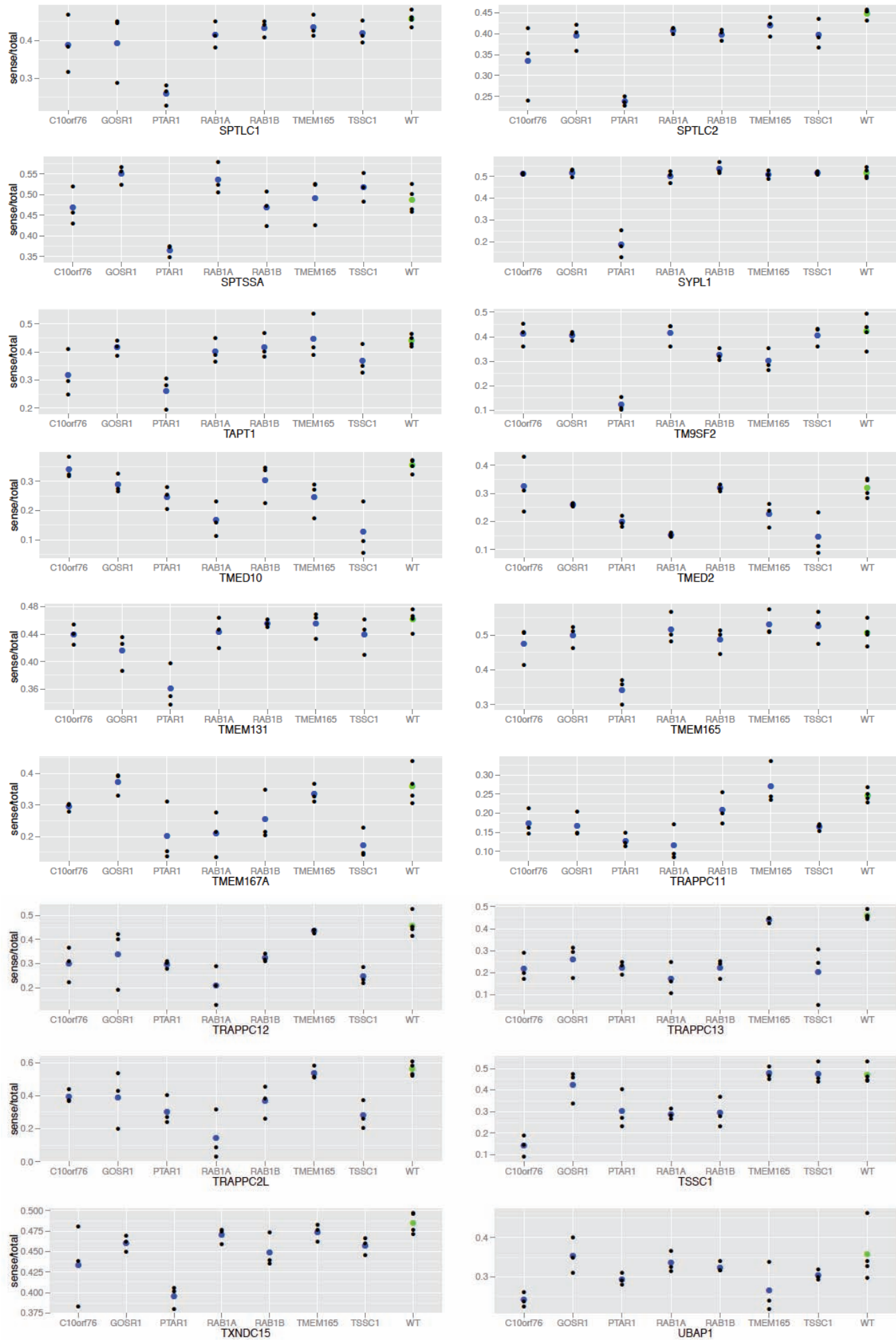


Figure S16-5

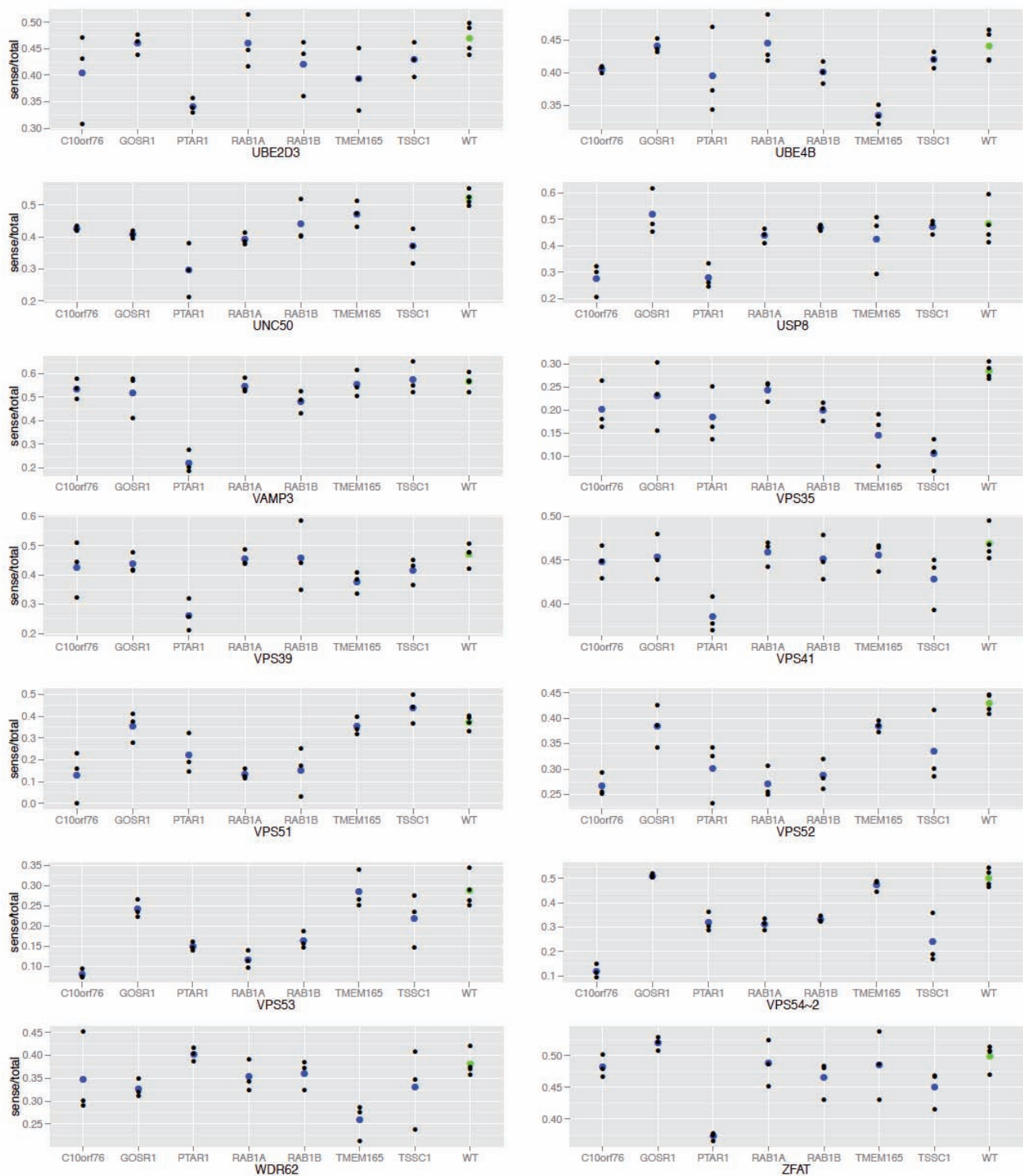
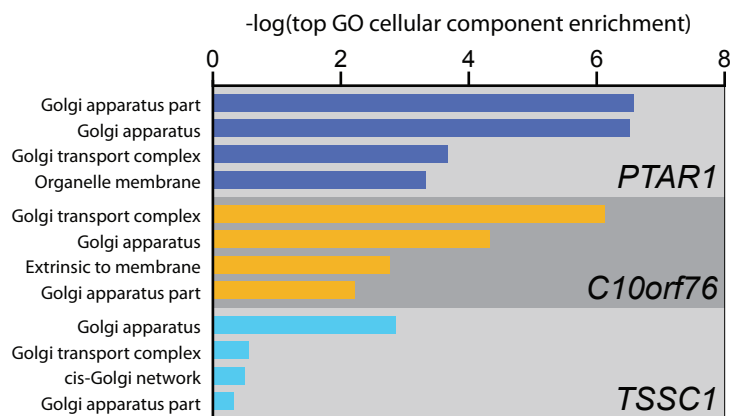


Fig. S16. Reproducibility of synthetic lethal interactions. Ratios of sense insertions in all biological replicates for all genes detected as synthetic lethal with at least one query gene are shown. Green dots represent average ratio in the wild-type HAP1 replicates and blue dots represent average ratios in query knockouts. The ~2 (~3) suffixes to the gene names indicate that the 2nd (3rd) transcript of a given gene was detected as synthetic lethal. If more than one transcript is detected as synthetic lethal, only the 1st transcript (without a ~ suffix in the name) is shown.

Figure S17**A****B**

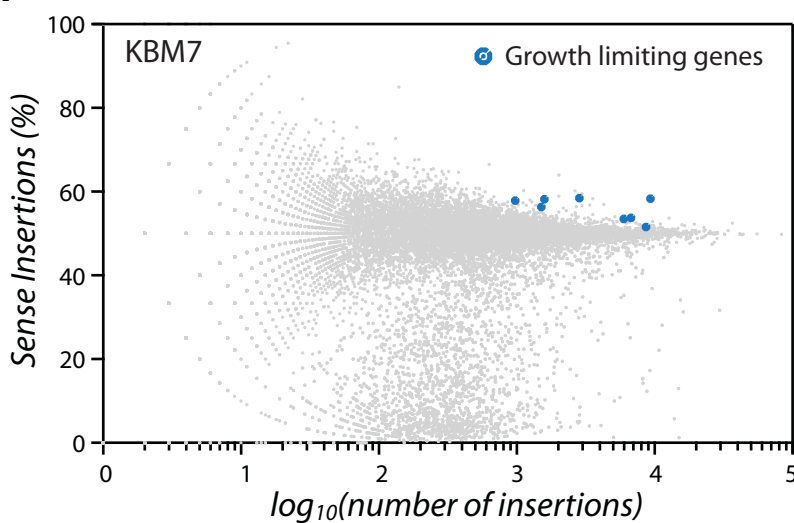
	SL interactions	neutral to fitness defect	increased fitness defect	% inter-connected	% connected to trafficking/secretion
C10orf76	16	9	7	81	94
GOSR1	4	2	2	75	75
PTAR1	60	42	18	33	78
RAB1A	20	9	11	90	100
RAB1B	11	6	5	100	100
TMEM165	7	1	6	29	71
TSSC1	21	10	11	57	86

Fig. S17. Properties of synthetic lethal (SL) interactions in the secretory pathway.

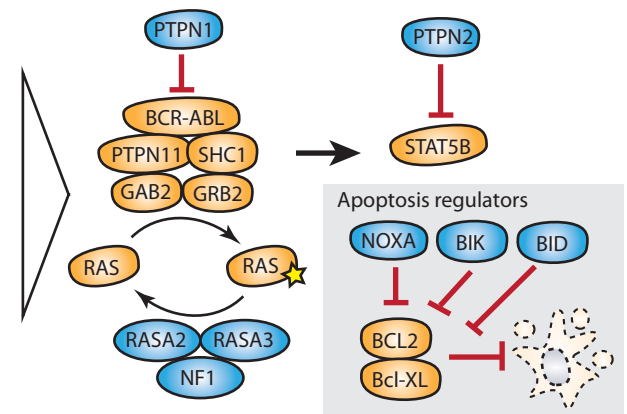
(A) The top-4 enriched gene annotation terms associated with interaction partners for the uncharacterized query genotypes *PTARI*, *C10orf76*, and *TSSC1* are provided with Benjamini-corrected *P*-values. **(B)** Summary of observed of synthetic lethal (SL) interactions in the secretory pathway. For each query genotype, the total number of SL interactions is subdivided into genes that shift from fitness-neutral to essential and genes for which the essentiality bias increases. The fraction of interacting genes with additional connections (% interconnected) and the percentage of interacting genes that function in the secretory pathway are also listed for every query genotype.

Figure S18

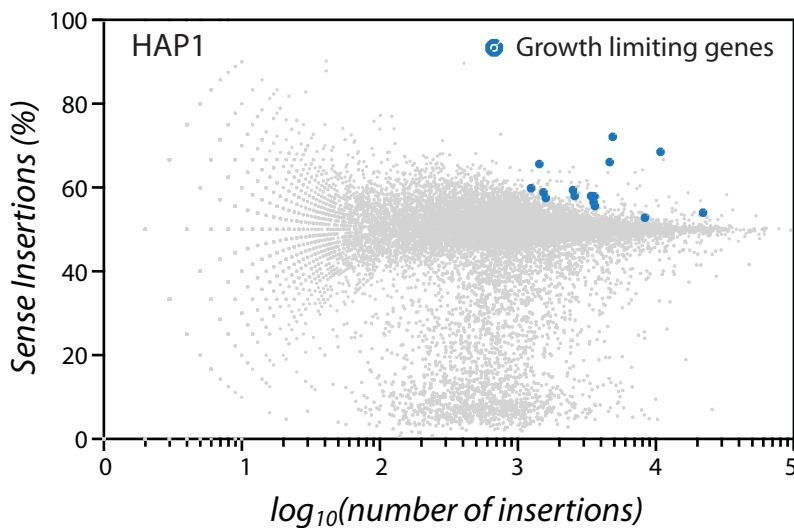
A



CML signaling regulators



B



Growth factor signaling regulators

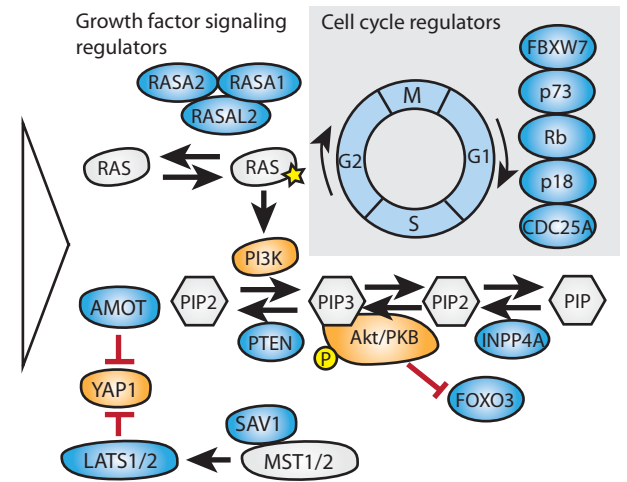


Fig. S18. Growth suppressive genes that are commonly enriched for sense orientation insertions in wild-type KBM7 or HAP1 cells. **(A)** Scatterplot showing orientation bias in KBM7 cells for commonly enriched genes. Numerous of these genes are well-studied negative regulators of growth-promoting signaling pathways, such as BCR-ABL signaling, and pro-apoptotic genes. **(B)** Similar plots for HAP1 cells, in which commonly enriched genes are known negative regulators of PI3K-signaling (e.g. *PTEN*), Hippo signaling (e.g. *SAVI*), and cell cycle inhibitors (e.g. *RBL*).

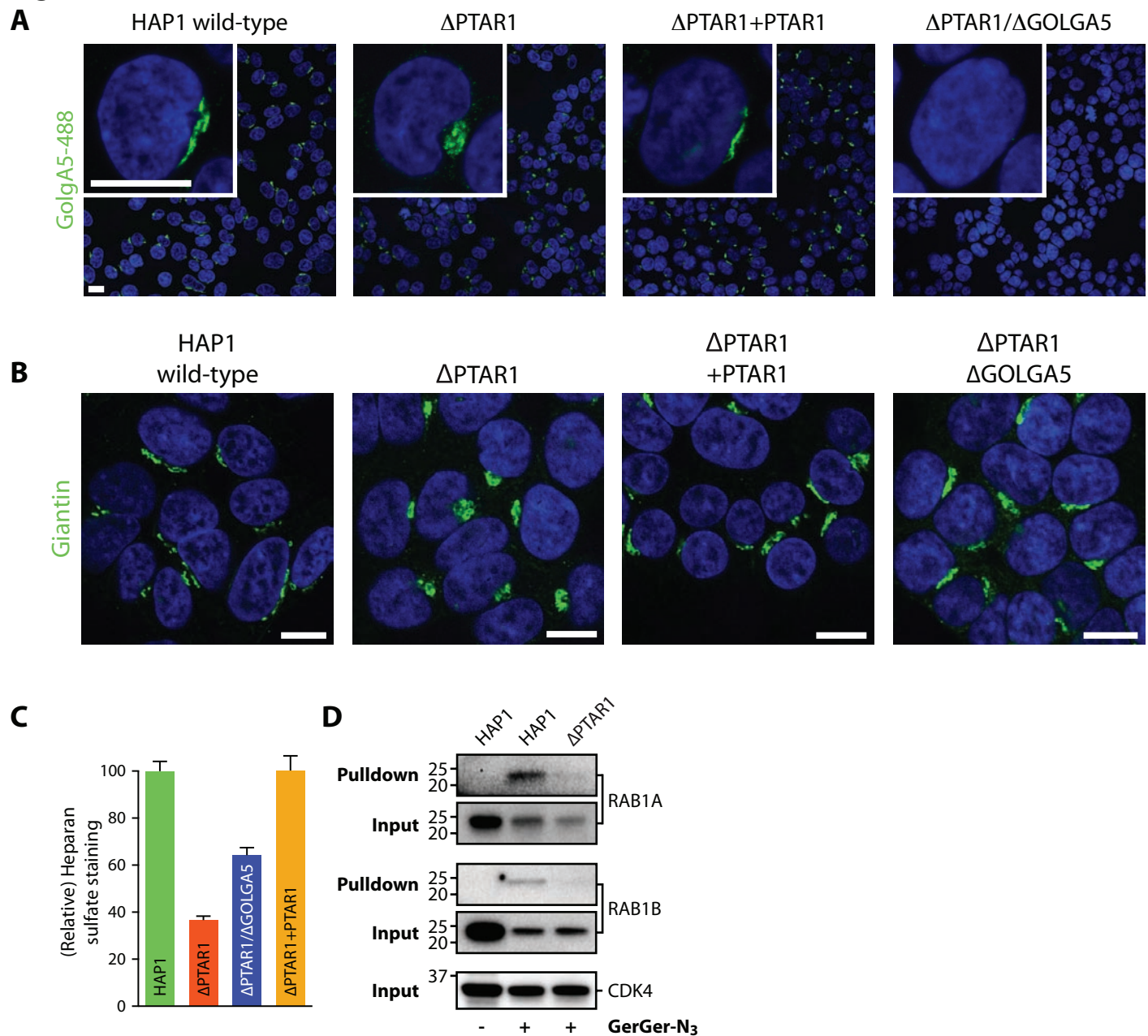
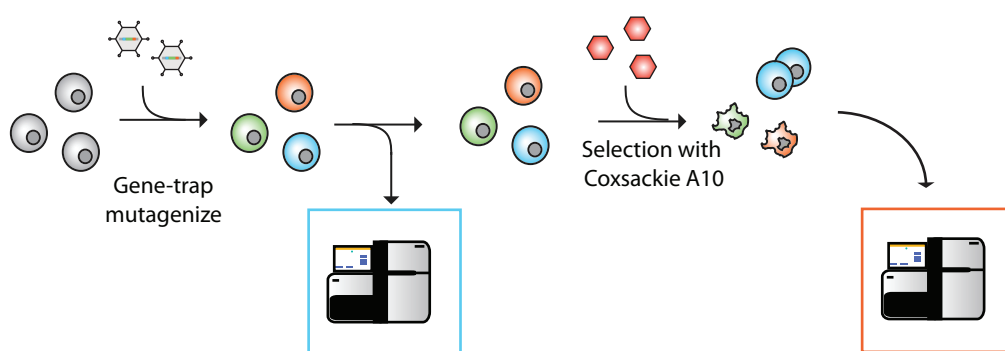
Figure S19

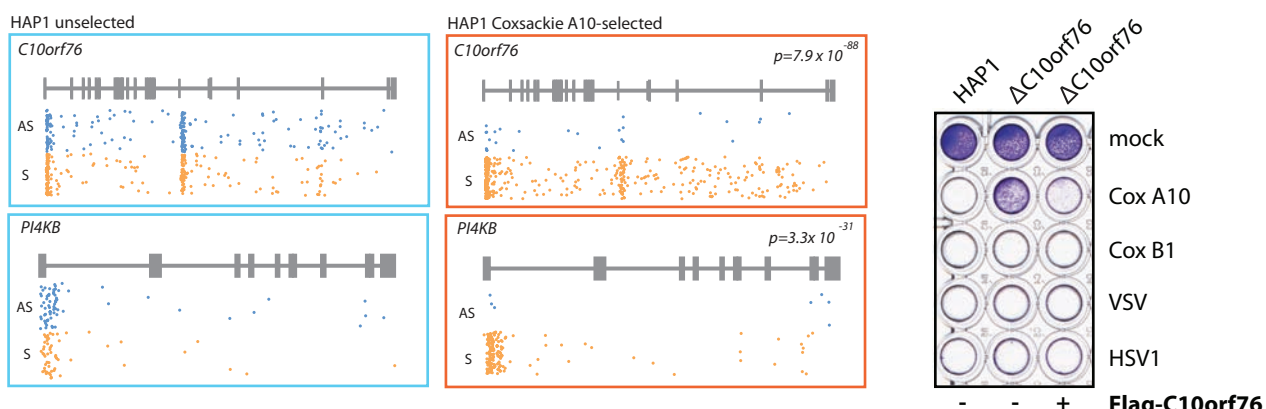
Fig. S19. GOLGA5 acts as suppressor for PTAR1 for Golgi morphology and function. (A) HAP1 cells, *PTAR1*-deficient cells, *PTAR1*-deficient cells complemented with a *PTAR1* cDNA and cells deficient for both *PTAR1* and *GOLGA5* were stained to determine expression levels and localization of GOLGA5 (green). As shown in Fig. 4 *PTAR1*-deficient cells display abnormal Golgi morphology, which could be restored by re-introduction of *PTAR1*. *PTAR1*-deficient cells show normal expression and Golgi localization of GOLGA5. Nuclei are stained in blue. Scale bars: 10μm. (B) The Golgi morphology in cells lacking *PTAR1* and in double-knockout cells for *PTAR1* and *GOLGA5* using immunofluorescence for the Golgi-resident protein Giantin (green). Wild-type cells and *PTAR1* knockout cells that were reconstituted with *PTAR1* were used as controls and the nuclei were stained in blue. (C) Cell surface glycosylation in cells deficient for *PTAR1* with an intact or mutated *GOLGA5* allele, or reconstituted with a virus directing the expression of *PTAR1* immunostained using an antibody specific for heparan sulfate and subjected to flow-cytometric analysis. The relative average staining intensity (compared to wild-type HAP1 cells) and standard deviation of three experiments is indicated. (D) Geranylgeranylation of RAB1A and RAB1B in wild-type and *PTAR1*-deficient cells detected after supplying cells with a clickable geranylgeranyl azide (GerGer-N₃). After cell lysis GerGer-N₃ was coupled to biotin using click chemistry and proteins were captured using streptavidin-coated beads. Eluted proteins were analyzed by immunoblotting. HAP1 cells not exposed to GerGer-N₃ were used as control.

Figure S20

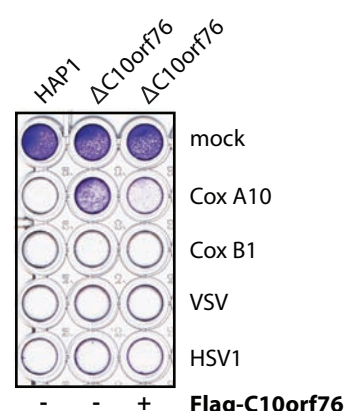
A



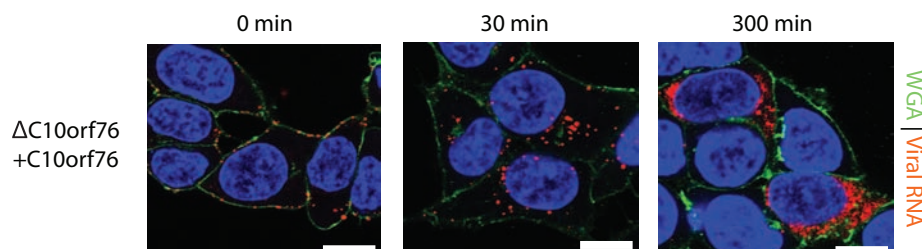
B



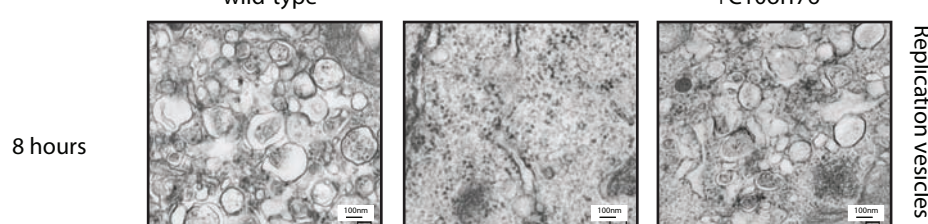
C



D



E

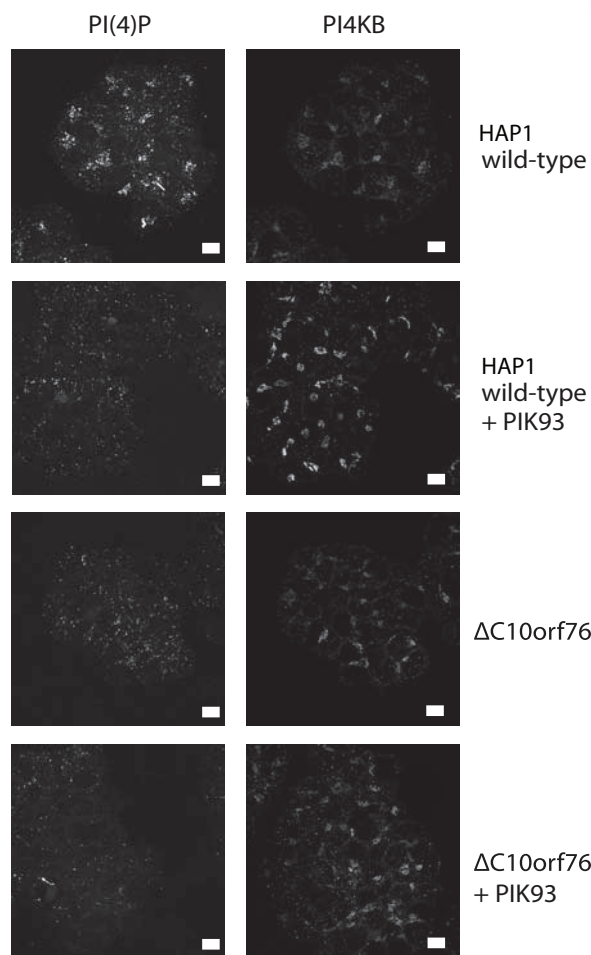


Replication vesicles

Fig. S20. A haploid genetic host factor survey for coxsackievirus A10 infection identifies C10orf76 as well as PI4KB. (A) Schematic outline of the haploid genetic screen. 100 million HAP1 cells were mutagenized with the gene-trap vector and expanded and exposed to coxsackievirus A10. Genomic DNA was isolated from mutagenized cells that had not been exposed to coxsackievirus A10 as well as from the virus-selected cell population. Gene-trap insertion sites were mapped and genes that showed an enrichment in sense-orientation gene-trap integrations in the virus-selected population but not in the control cell population were identified and this included *C10orf76* and *PI4KB*. (B) The orientation of gene-trap integrations in *C10orf76* and *PI4KB* in the virus-exposed population showed a bias towards insertions in the disruptive orientation, indicating virus-induced selective advantage for knockouts of these specific genotypes. (C) Viral sensitivity of wild-type cells, cells deficient for *C10orf76* and knockout cells reconstituted with the *C10orf76* cDNA were exposed to coxsackievirus A10 (Cox A10), coxsackievirus B1 (Cox B1), vesicular stomatitis virus (VSV) or herpes simplex virus (HSV1) as detected by crystal violet staining. Uninfected cells served as a control. (D) Coxsackievirus A10 amplification after restoration of *C10orf76* expression measured by single molecule fluorescent in situ hybridization (smFISH) to localize individual viral genomes (red). Intracellular viral RNA was first detected after 30 minutes. Increased RNA signal after 300 minutes indicates RNA replication. (E) Electron micrographs of wild-type cells, cells deficient for *C10orf76* and knockout cells reconstituted with the *C10orf76* cDNA exposed to coxsackievirus A10 indicating the absence of replication vesicles in the cytoplasm of *C10orf76*-deficient cells.

Figure S21

A



B

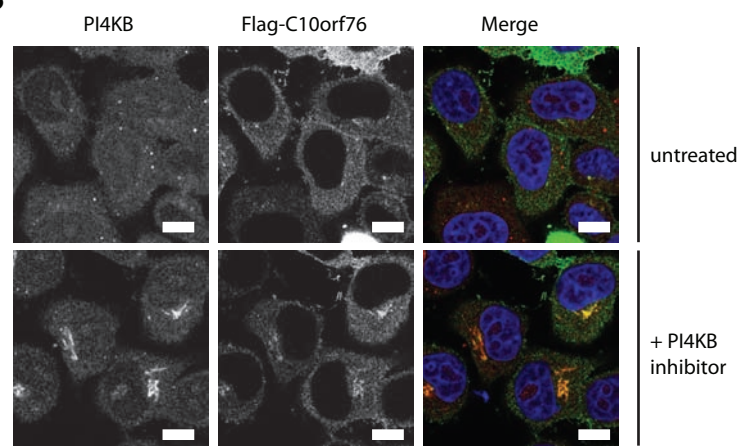
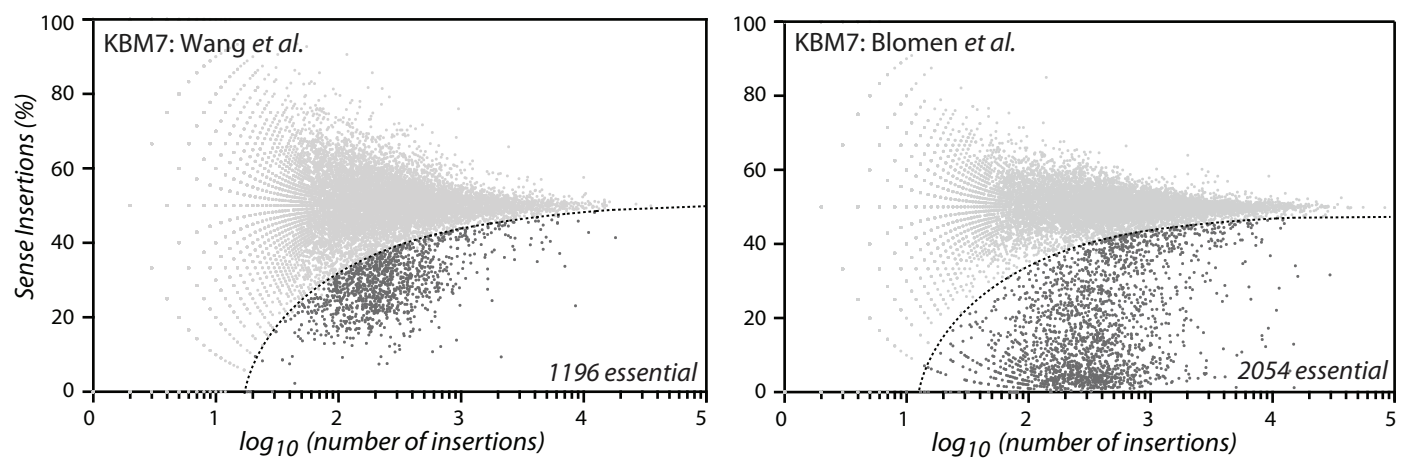


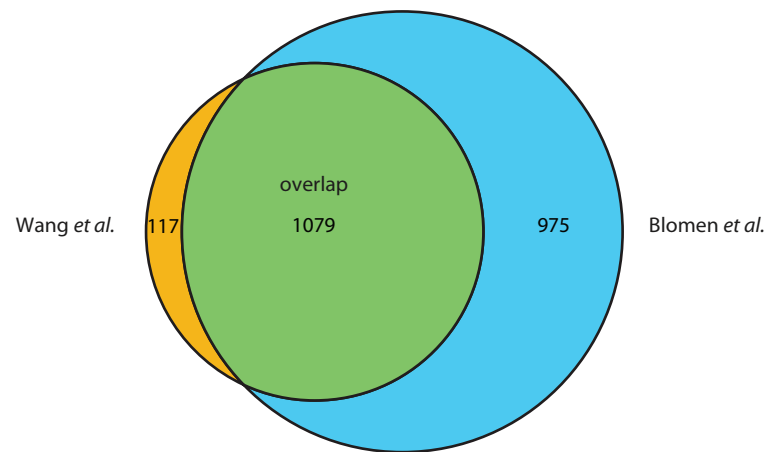
Fig. S21. Activity and localization of PI4KB and relocalization of C10orf76 following chemical inhibition **(A)** Golgi PI(4)P staining and inhibitor-induced localization of PI4KB in wild-type cells and *C10orf76*-deficient cells exposed to the PI4KB inhibitor PIK-93. **(B)** *C10orf76*-deficient cells were transduced with a retrovirus directing the expression of Flag-tagged C10orf76 and exposed to the PI4KB inhibitor PIK-93. Cells were analyzed by immunostaining using Flag antibodies and antibodies directed against PI4KB.

Figure S22

A



B



C

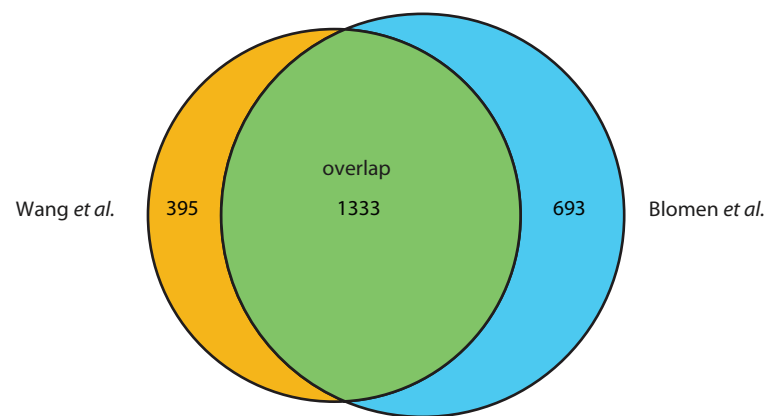
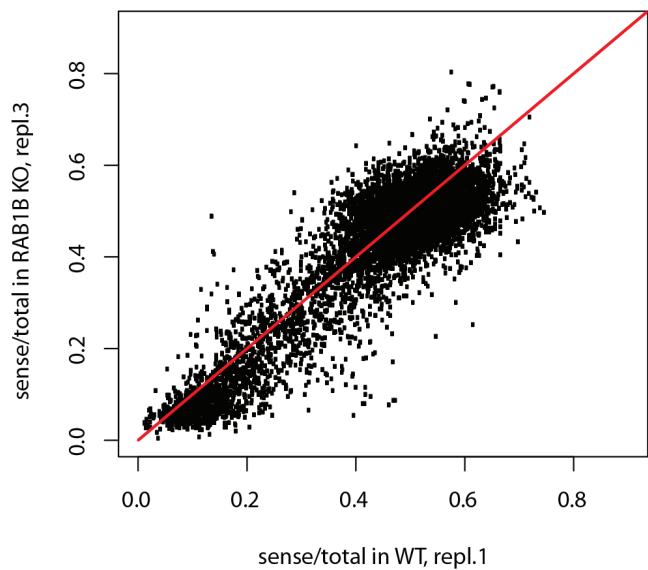


Fig. S22. Comparison of gene-trap and CRISPR datasets as presented by Wang *et al.* with gene-trap datasets obtained in this study in KBM7 cells. **(A)** Comparison of KBM7 datasets obtained using gene-trap mutagenesis between Wang *et al.* and Blomen *et al.* The significance threshold is based on noise modeling as described in the methods. **(B)** Venn diagram showing the overlap of the essential genes identified in (A). **(C)** Venn diagram showing the overlap of the essential genes identified using CRISPR-Cas (Wang *et al.*) or gene-trap mutagenesis (Blomen *et al.*) for the set of genes that can in principle be identified by both technologies (see supplemental discussion for details).

Figure S23

A

Raw data



B

Normalized data

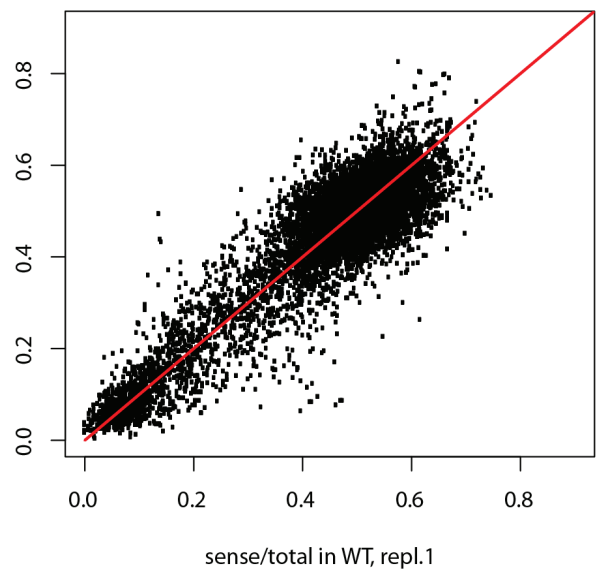


Fig. S23. Normalization of datasets for synthetic lethality analysis. **(A)** A scatterplot of ratio of sense insertions in wild-type replicate 1 versus in *RAB1B* knockout replicate 3. Only transcripts with at least 50 insertions are shown. The red diagonal marks identical ratios between the two replicates. The overall depletion is stronger in the *RAB1B*-3 replicate as the majority of transcripts with ratio < 0.5 lie under the red diagonal. **(B)** The observed data are re-centered back along the red diagonal after the median preserving normalization described in the method section.

Data table S1 (separate file). Essential Genes in KBM7 cells. For each gene we list insertion counts in sense and antisense orientation for the non-overlapping part of the gene's pre-mRNA. Biased genes that pass the noise-filter criterion for essentiality are listed with "YES" and the P-values and Q-values based on the noise-model are listed per gene. In addition, all insertion numbers for each independent replicate are listed in a separate tab.

Data table S2 (separate file). Essential Genes in HAP1 cells. For each gene we list insertion counts in sense and antisense orientation for the non-overlapping part of the gene's pre-mRNA. Biased genes that pass the noise-filter criterion for essentiality are listed with "YES" and the P-values and Q-values based on the noise-model are listed per gene. In addition, all insertion numbers for each independent replicate are listed in a separate tab.

Data table S3 (separate file). Shared and unique essential genes. A list of 'core' essential genes that are required for fitness of both HAP1 and KBM7 cells, in addition to genes that are essential uniquely in either cell type. Genes in orange are identified to have a fitness-effect in KBM7 cells and genes in green for HAP1.

Data table S4 (separate file). Essential genes and their yeast orthologs. A list of core essential genes that are detected via Ensembl to be homologous to genes essential in yeast or to genes important for fitness in yeast (*I*).

Data table S5 (separate file). Analysis of protein complexes with proteins encoded by essential genes. This table reports all the proteins identified in every pulldown with a multiple hypothesis-corrected P-value that was used to filter true from unlikely interactions. Bait AC = UniProtKB/Swissprot accession code of a bait; Prey AC = UniProtKB/Swissprot accession code of the preys; Interaction P-value = P-value according to the Decontaminator statistical model (see Materials and Methods); Prey adjusted P-value = a corrected P-value for the multiple hypotheses represented by the many potential preys identified for a bait; Bait and prey gene names are the official gene symbols; Replicate Ids = CeMM pulldown numbers identifying each replicate used in the data analysis; Spectral counts in replicates are the number of spectra identifying each protein in each replicate; Total spectral counts are the sums of the counts in each replicate; psm.mascot_scores=Mascot protein scores in each replicate; psm.phenyx_scores = Phenyx protein scores in each replicate; same columns for the negative control pulldowns; is_contaminant = known contaminants are marked with "TRUE"; is_carryover = when the bait of the previous pulldown is found as a prey for the next bait, this column contains a "TRUE" to indicate likely carryover due to high abundance in the previous sample; is_true_binder ="TRUE" if not a contaminant, not carryover, and the adjusted P-value<0.05.

Data table S6 (separate file). Overview of the number of mapped insertion sites pre-and post-normalization in each replicate for the synthetic lethality network. All datasets were normalized to the aggregated insertion counts of four wild-type HAP1 datasets; see Materials and Methods for normalization details. All gold transcripts of a

gene are listed here, the first transcript of each gene is identified by the gene name, any additional transcripts are distinguished with suffixes ~2, ~3, etc.

Data table S7 (separate file). Functional link of the identified network genes to the secretory pathway. Genes identified in the synthetic lethality network were analyzed for their function. This table lists genes that could be linked to the secretory pathway with a reference to the published literature or online databases.

Data table S8 (separate file). Summary of read counts for all performed screens and the number of mapped unique insertion sites.

References and Notes

1. G. Giaever, A. M. Chu, L. Ni, C. Connelly, L. Riles, S. Véronneau, S. Dow, A. Lucau-Danila, K. Anderson, B. André, A. P. Arkin, A. Astromoff, M. El-Bakkoury, R. Bangham, R. Benito, S. Brachat, S. Campanaro, M. Curtiss, K. Davis, A. Deutschbauer, K. D. Entian, P. Flaherty, F. Foury, D. J. Garfinkel, M. Gerstein, D. Gotte, U. Güldener, J. H. Hegemann, S. Hempel, Z. Herman, D. F. Jaramillo, D. E. Kelly, S. L. Kelly, P. Kötter, D. LaBonte, D. C. Lamb, N. Lan, H. Liang, H. Liao, L. Liu, C. Luo, M. Lussier, R. Mao, P. Menard, S. L. Ooi, J. L. Revuelta, C. J. Roberts, M. Rose, P. Ross-Macdonald, B. Scherens, G. Schimmack, B. Shafer, D. D. Shoemaker, S. Sookhai-Mahadeo, R. K. Storms, J. N. Strathern, G. Valle, M. Voet, G. Volckaert, C. Y. Wang, T. R. Ward, J. Wilhelmy, E. A. Winzeler, Y. Yang, G. Yen, E. Youngman, K. Yu, H. Bussey, J. D. Boeke, M. Snyder, P. Philippsen, R. W. Davis, M. Johnston, Functional profiling of the *Saccharomyces cerevisiae* genome. *Nature* **418**, 387–391 (2002). [Medline](#) [doi:10.1038/nature00935](https://doi.org/10.1038/nature00935)
2. A. H. Tong, M. Evangelista, A. B. Parsons, H. Xu, G. D. Bader, N. Pagé, M. Robinson, S. Raghibizadeh, C. W. Hogue, H. Bussey, B. Andrews, M. Tyers, C. Boone, Systematic genetic analysis with ordered arrays of yeast deletion mutants. *Science* **294**, 2364–2368 (2001). [Medline](#) [doi:10.1126/science.1065810](https://doi.org/10.1126/science.1065810)
3. S. Mnaimneh, A. P. Davierwala, J. Haynes, J. Moffat, W. T. Peng, W. Zhang, X. Yang, J. Pootoolal, G. Chua, A. Lopez, M. Trochesset, D. Morse, N. J. Krogan, S. L. Hiley, Z. Li, Q. Morris, J. Grigull, N. Mitsakakis, C. J. Roberts, J. F. Greenblatt, C. Boone, C. A. Kaiser, B. J. Andrews, T. R. Hughes, Exploration of essential gene functions via titratable promoter alleles. *Cell* **118**, 31–44 (2004). [Medline](#) [doi:10.1016/j.cell.2004.06.013](https://doi.org/10.1016/j.cell.2004.06.013)
4. J. E. Carette, M. Raaben, A. C. Wong, A. S. Herbert, G. Obernosterer, N. Mulherkar, A. I. Kuehne, P. J. Kranzusch, A. M. Griffin, G. Ruthel, P. Dal Cin, J. M. Dye, S. P. Whelan, K. Chandran, T. R. Brummelkamp, Ebola virus entry requires the cholesterol transporter Niemann-Pick C1. *Nature* **477**, 340–343 (2011). [Medline](#) [doi:10.1038/nature10348](https://doi.org/10.1038/nature10348)
5. J. E. Carette, C. P. Guimaraes, I. Wuethrich, V. A. Blomen, M. Varadarajan, C. Sun, G. Bell, B. Yuan, M. K. Muellner, S. M. Nijman, H. L. Ploegh, T. R. Brummelkamp, Global gene disruption in human cells to assign genes to phenotypes by deep sequencing. *Nat. Biotechnol.* **29**, 542–546 (2011). [Medline](#) [doi:10.1038/nbt.1857](https://doi.org/10.1038/nbt.1857)
6. J. E. Carette, C. P. Guimaraes, M. Varadarajan, A. S. Park, I. Wuethrich, A. Godarova, M. Kotecki, B. H. Cochran, E. Spooner, H. L. Ploegh, T. R. Brummelkamp, Haploid genetic screens in human cells identify host factors used by pathogens. *Science* **326**, 1231–1235 (2009). [Medline](#)
7. L. T. Jae, M. Raaben, M. Riemersma, E. van Beusekom, V. A. Blomen, A. Velds, R. M. Kerkhoven, J. E. Carette, H. Topaloglu, P. Meinecke, M. W. Wessels, D. J. Lefeber, S. P. Whelan, H. van Bokhoven, T. R. Brummelkamp, Deciphering the glycosylome of dystroglycanopathies using haploid screens for lassa virus entry. *Science* **340**, 479–483 (2013). [Medline](#) [doi:10.1126/science.1233675](https://doi.org/10.1126/science.1233675)
8. D. J. Kelleher, R. Gilmore, An evolving view of the eukaryotic oligosaccharyltransferase. *Glycobiology* **16**, 47R–62R (2006). [Medline](#) [doi:10.1093/glycob/cwj066](https://doi.org/10.1093/glycob/cwj066)

9. A. Dumax-Vorzet, P. Roboti, S. High, OST4 is a subunit of the mammalian oligosaccharyltransferase required for efficient N-glycosylation. *J. Cell Sci.* **126**, 2595–2606 (2013). [Medline doi:10.1242/jcs.115410](#)
10. O. Parnas, M. Jovanovic, T. M. Eisenhaure, R. H. Herbst, A. Dixit, C. J. Ye, D. Przybylski, R. J. Platt, I. Tirosh, N. E. Sanjana, O. Shalem, R. Satija, R. Raychowdhury, P. Mertins, S. A. Carr, F. Zhang, N. Hacohen, A. Regev, A Genome-wide CRISPR Screen in Primary Immune Cells to Dissect Regulatory Networks. *Cell* **162**, 675–686 (2015). [Medline doi:10.1016/j.cell.2015.06.059](#)
11. G. Reiss, S. te Heesen, R. Gilmore, R. Zufferey, M. Aebi, A specific screen for oligosaccharyltransferase mutations identifies the 9 kDa OST5 protein required for optimal activity in vivo and in vitro. *EMBO J.* **16**, 1164–1172 (1997). [Medline doi:10.1093/emboj/16.6.1164](#)
12. A. H. Tong, G. Lesage, G. D. Bader, H. Ding, H. Xu, X. Xin, J. Young, G. F. Berriz, R. L. Brost, M. Chang, Y. Chen, X. Cheng, G. Chua, H. Friesen, D. S. Goldberg, J. Haynes, C. Humphries, G. He, S. Hussein, L. Ke, N. Krogan, Z. Li, J. N. Levinson, H. Lu, P. Ménard, C. Munyana, A. B. Parsons, O. Ryan, R. Tonikian, T. Roberts, A. M. Sdicu, J. Shapiro, B. Sheikh, B. Suter, S. L. Wong, L. V. Zhang, H. Zhu, C. G. Burd, S. Munro, C. Sander, J. Rine, J. Greenblatt, M. Peter, A. Bretscher, G. Bell, F. P. Roth, G. W. Brown, B. Andrews, H. Bussey, C. Boone, Global mapping of the yeast genetic interaction network. *Science* **303**, 808–813 (2004). [Medline doi:10.1126/science.1091317](#)
13. J. L. Hartman 4th, B. Garvik, L. Hartwell, Principles for the buffering of genetic variation. *Science* **291**, 1001–1004 (2001). [Medline doi:10.1126/science.291.5506.1001](#)
14. C. Boone, H. Bussey, B. J. Andrews, Exploring genetic interactions and networks with yeast. *Nat. Rev. Genet.* **8**, 437–449 (2007). [Medline doi:10.1038/nrg2085](#)
15. M. Schuldiner, S. R. Collins, N. J. Thompson, V. Denic, A. Bhamidipati, T. Punna, J. Ihmels, B. Andrews, C. Boone, J. F. Greenblatt, J. S. Weissman, N. J. Krogan, Exploration of the function and organization of the yeast early secretory pathway through an epistatic miniaarray profile. *Cell* **123**, 507–519 (2005). [Medline doi:10.1016/j.cell.2005.08.031](#)
16. S. M. Nijman, S. H. Friend, Cancer. Potential of the synthetic lethality principle. *Science* **342**, 809–811 (2013). [Medline doi:10.1126/science.1244669](#)
17. J. Tischler, B. Lehner, A. G. Fraser, Evolutionary plasticity of genetic interaction networks. *Nat. Genet.* **40**, 390–391 (2008). [Medline doi:10.1038/ng.114](#)
18. V. N. Subramaniam, F. Peter, R. Philp, S. H. Wong, W. Hong, GS28, a 28-kilodalton Golgi SNARE that participates in ER-Golgi transport. *Science* **272**, 1161–1163 (1996). [Medline doi:10.1126/science.272.5265.1161](#)
19. D. Demaegd, F. Foulquier, A. S. Colinet, L. Gremillon, D. Legrand, P. Mariot, E. Peiter, E. Van Schaftingen, G. Matthijs, P. Morsomme, Newly characterized Golgi-localized family of proteins is involved in calcium and pH homeostasis in yeast and human cells. *Proc. Natl. Acad. Sci. U.S.A.* **110**, 6859–6864 (2013). [Medline doi:10.1073/pnas.1219871110](#)
20. E. L. Huttlin, L. Ting, R. J. Bruckner, F. Gebreab, M. P. Gygi, J. Szpyt, S. Tam, G. Zarzaga, G. Colby, K. Baltier, R. Dong, V. Guarani, L. P. Vaites, A. Ordureau, R. Rad, B. K. Erickson, M. Wühr, J. Chick, B. Zhai, D. Kolippakkam, J. Mintseris, R. A. Obar, T.

Harris, S. Artavanis-Tsakonas, M. E. Sowa, P. De Camilli, J. A. Paulo, J. W. Harper, S. P. Gygi, The BioPlex Network: A Systematic Exploration of the Human Interactome. *Cell* **162**, 425–440 (2015). [Medline doi:10.1016/j.cell.2015.06.043](#)

21. A. Diao, D. Rahman, D. J. Pappin, J. Lucocq, M. Lowe, The coiled-coil membrane protein golgin-84 is a novel rab effector required for Golgi ribbon formation. *J. Cell Biol.* **160**, 201–212 (2003). [Medline doi:10.1083/jcb.200207045](#)
22. W. L. Charng, S. Yamamoto, M. Jaiswal, V. Bayat, B. Xiong, K. Zhang, H. Sandoval, G. David, S. Gibbs, H. C. Lu, K. Chen, N. Giagtzoglou, H. J. Bellen, Drosophila Tempura, a novel protein prenyltransferase α subunit, regulates notch signaling via Rab1 and Rab11. *PLOS Biol.* **12**, e1001777 (2014). [Medline doi:10.1371/journal.pbio.1001777](#)
23. A. Rejman Lipinski, J. Heymann, C. Meissner, A. Karlas, V. Brinkmann, T. F. Meyer, D. Heuer, Rab6 and Rab11 regulate Chlamydia trachomatis development and golgin-84-dependent Golgi fragmentation. *PLOS Pathog.* **5**, e1000615 (2009). [Medline doi:10.1371/journal.ppat.1000615](#)
24. A. L. Greninger, G. M. Knudsen, M. Betegon, A. L. Burlingame, J. L. DeRisi, ACBD3 interaction with TBC1 domain 22 protein is differentially affected by enteroviral and kobuviral 3A protein binding. *MBio* **4**, e00098–e00013 (2013). [Medline doi:10.1128/mBio.00098-13](#)
25. T. R. Graham, C. G. Burd, Coordination of Golgi functions by phosphatidylinositol 4-kinases. *Trends Cell Biol.* **21**, 113–121 (2011). [Medline doi:10.1016/j.tcb.2010.10.002](#)
26. N. Y. Hsu, O. Ilnytska, G. Belov, M. Santiana, Y. H. Chen, P. M. Takvorian, C. Pau, H. van der Schaar, N. Kaushik-Basu, T. Balla, C. E. Cameron, E. Ehrenfeld, F. J. van Kuppeveld, N. Altan-Bonnet, Viral reorganization of the secretory pathway generates distinct organelles for RNA replication. *Cell* **141**, 799–811 (2010). [Medline doi:10.1016/j.cell.2010.03.050](#)
27. H. M. van der Schaar, L. van der Linden, K. H. Lanke, J. R. Strating, G. Pürstinger, E. de Vries, C. A. de Haan, J. Neyts, F. J. van Kuppeveld, Coxsackievirus mutants that can bypass host factor PI4KIII β and the need for high levels of PI4P lipids for replication. *Cell Res.* **22**, 1576–1592 (2012). [Medline doi:10.1038/cr.2012.129](#)
28. J. Seebacher, A. C. Gavin, SnapShot: Protein-protein interaction networks. *Cell* **144**, 1000–1000.e1, 1000.e1 (2011). [Medline doi:10.1016/j.cell.2011.02.025](#)
29. M. Newmann, *Networks: An Introduction*. (Oxford University Press, ed. 1 edition 2010), pp. 720.
30. C. M. Toledo, J. A. Herman, J. B. Olsen, Y. Ding, P. Corrin, E. J. Girard, J. M. Olson, A. Emili, J. G. DeLuca, P. J. Paddison, BuGZ is required for Bub3 stability, Bub1 kinetochore function, and chromosome alignment. *Dev. Cell* **28**, 282–294 (2014). [Medline doi:10.1016/j.devcel.2013.12.014](#)
31. H. Jiang, X. He, S. Wang, J. Jia, Y. Wan, Y. Wang, R. Zeng, J. Yates 3rd, X. Zhu, Y. Zheng, A microtubule-associated zinc finger protein, BuGZ, regulates mitotic chromosome alignment by ensuring Bub3 stability and kinetochore targeting. *Dev. Cell* **28**, 268–281 (2014). [Medline doi:10.1016/j.devcel.2013.12.013](#)

32. T. Blondal, A. Thorisdottir, U. Unnsteinsdottir, S. Hjorleifsdottir, A. Aevarsson, S. Ernstsson, O. H. Fridjonsson, S. Skirnisdottir, J. O. Wheat, A. G. Hermannsdottir, S. T. Sigurdsson, G. O. Hreggvidsson, A. V. Smith, J. K. Kristjansson, Isolation and characterization of a thermostable RNA ligase 1 from a *Thermus scotoductus* bacteriophage TS2126 with good single-stranded DNA ligation properties. *Nucleic Acids Res.* **33**, 135–142 (2005). [Medline](#) [doi:10.1093/nar/gki149](#)
33. B. Langmead, C. Trapnell, M. Pop, S. L. Salzberg, Ultrafast and memory-efficient alignment of short DNA sequences to the human genome. *Genome Biol.* **10**, R25 (2009). [Medline](#) [doi:10.1186/gb-2009-10-3-r25](#)
34. J. Harrow, A. Frankish, J. M. Gonzalez, E. Tapanari, M. Diekhans, F. Kokocinski, B. L. Aken, D. Barrell, A. Zadissa, S. Searle, I. Barnes, A. Bignell, V. Boychenko, T. Hunt, M. Kay, G. Mukherjee, J. Rajan, G. Despacio-Reyes, G. Saunders, C. Steward, R. Harte, M. Lin, C. Howald, A. Tanzer, T. Derrien, J. Chrast, N. Walters, S. Balasubramanian, B. Pei, M. Tress, J. M. Rodriguez, I. Ezkurdia, J. van Baren, M. Brent, D. Haussler, M. Kellis, A. Valencia, A. Reymond, M. Gerstein, R. Guigó, T. J. Hubbard, GENCODE: The reference human genome annotation for The ENCODE Project. *Genome Res.* **22**, 1760–1774 (2012). [Medline](#) [doi:10.1101/gr.135350.111](#)
35. F. P. Breitwieser, A. Müller, L. Dayon, T. Köcher, A. Hainard, P. Pichler, U. Schmidt-Erfurth, G. Superti-Furga, J. C. Sanchez, K. Mechtler, K. L. Bennett, J. Colinge, General statistical modeling of data from protein relative expression isobaric tags. *J. Proteome Res.* **10**, 2758–2766 (2011). [Medline](#) [doi:10.1021/pr1012784](#)
36. Z. Dosztányi, V. Csizmok, P. Tompa, I. Simon, IUPred: Web server for the prediction of intrinsically unstructured regions of proteins based on estimated energy content. *Bioinformatics* **21**, 3433–3434 (2005). [Medline](#) [doi:10.1093/bioinformatics/bti541](#)
37. T. Bürckstümmer, C. Banning, P. Hainzl, R. Schobesberger, C. Kerzendorfer, F. M. Pauer, D. Chen, N. Them, F. Schischlik, M. Rebsamen, M. Smida, F. Fece de la Cruz, A. Lapao, M. Liszt, B. Eizinger, P. M. Guenzl, V. A. Blomen, T. Konopka, B. Gapp, K. Parapatics, B. Maier, J. Stöckl, W. Fischl, S. Salic, M. R. Taba Casari, S. Knapp, K. L. Bennett, C. Bock, J. Colinge, R. Kralovics, G. Ammerer, G. Casari, T. R. Brummelkamp, G. Superti-Furga, S. M. Nijman, A reversible gene trap collection empowers haploid genetics in human cells. *Nat. Methods* **10**, 965–971 (2013). [Medline](#) [doi:10.1038/nmeth.2609](#)
38. W. Huang, B. T. Sherman, R. A. Lempicki, Systematic and integrative analysis of large gene lists using DAVID bioinformatics resources. *Nat. Protoc.* **4**, 44–57 (2009). [Medline](#) [doi:10.1038/nprot.2008.211](#)
39. W. Huang, B. T. Sherman, R. A. Lempicki, Bioinformatics enrichment tools: Paths toward the comprehensive functional analysis of large gene lists. *Nucleic Acids Res.* **37**, 1–13 (2009). [Medline](#) [doi:10.1093/nar/gkn923](#)
40. H. Hermjakob, L. Montecchi-Palazzi, C. Lewington, S. Mudali, S. Kerrien, S. Orchard, M. Vingron, B. Roechert, P. Roepstorff, A. Valencia, H. Margalit, J. Armstrong, A. Bairoch, G. Cesareni, D. Sherman, R. Apweiler, IntAct: An open source molecular interaction database. *Nucleic Acids Res.* **32**, D452–D455 (2004). [Medline](#) [doi:10.1093/nar/gkh052](#)

41. C. Stark, B. J. Breitkreutz, T. Reguly, L. Boucher, A. Breitkreutz, M. Tyers, BioGRID: A general repository for interaction datasets. *Nucleic Acids Res.* **34**, D535–D539 (2006). [Medline doi:10.1093/nar/gkj109](#)
42. T. S. Keshava Prasad, R. Goel, K. Kandasamy, S. Keerthikumar, S. Kumar, S. Mathivanan, D. Telikicherla, R. Raju, B. Shafreen, A. Venugopal, L. Balakrishnan, A. Marimuthu, S. Banerjee, D. S. Somanathan, A. Sebastian, S. Rani, S. Ray, C. J. Harrys Kishore, S. Kanth, M. Ahmed, M. K. Kashyap, R. Mohmood, Y. L. Ramachandra, V. Krishna, B. A. Rahiman, S. Mohan, P. Ranganathan, S. Ramabadran, R. Chaerkady, A. Pandey, Human Protein Reference Database—2009 update. *Nucleic Acids Res.* **37** (Database), D767–D772 (2009). [Medline doi:10.1093/nar/gkn892](#)
43. I. Xenarios, D. W. Rice, L. Salwinski, M. K. Baron, E. M. Marcotte, D. Eisenberg, DIP: The database of interacting proteins. *Nucleic Acids Res.* **28**, 289–291 (2000). [Medline doi:10.1093/nar/28.1.289](#)
44. A. Chatr-aryamontri, A. Ceol, L. M. Palazzi, G. Nardelli, M. V. Schneider, L. Castagnoli, G. Cesareni, MINT: The Molecular INTeraction database. *Nucleic Acids Res.* **35** (Database), D572–D574 (2007). [Medline doi:10.1093/nar/gkl950](#)
45. D. J. Lynn, G. L. Winsor, C. Chan, N. Richard, M. R. Laird, A. Barsky, J. L. Gardy, F. M. Roche, T. H. Chan, N. Shah, R. Lo, M. Naseer, J. Que, M. Yau, M. Acab, D. Tulpan, M. D. Whiteside, A. Chikatamarla, B. Mah, T. Munzner, K. Hokamp, R. E. Hancock, F. S. Brinkman, InnateDB: Facilitating systems-level analyses of the mammalian innate immune response. *Mol. Syst. Biol.* **4**, 218 (2008). [Medline doi:10.1038/msb.2008.55](#)
46. G. Launay, R. Salza, D. Multedo, N. Thierry-Mieg, S. Ricard-Blum, MatrixDB, the extracellular matrix interaction database: Updated content, a new navigator and expanded functionalities. *Nucleic Acids Res.* **43** (D1), D321–D327 (2015). [Medline doi:10.1093/nar/gku1091](#)
47. A. Ruepp, B. Waegele, M. Lechner, B. Brauner, I. Dunger-Kaltenbach, G. Fobo, G. Frishman, C. Montrone, H. W. Mewes, CORUM: The comprehensive resource of mammalian protein complexes—2009. *Nucleic Acids Res.* **38** (Database), D497–D501 (2010). [Medline doi:10.1093/nar/gkp914](#)
48. C. F. Schaefer, K. Anthony, S. Krupa, J. Buchoff, M. Day, T. Hannay, K. H. Buetow, PID: The Pathway Interaction Database. *Nucleic Acids Res.* **37** (Database), D674–D679 (2009). [Medline doi:10.1093/nar/gkn653](#)
49. S. Powell, D. Szklarczyk, K. Trachana, A. Roth, M. Kuhn, J. Muller, R. Arnold, T. Rattei, I. Letunic, T. Doerks, L. J. Jensen, C. von Mering, P. Bork, eggNOG v3.0: Orthologous groups covering 1133 organisms at 41 different taxonomic ranges. *Nucleic Acids Res.* **40** (D1), D284–D289 (2012). [Medline doi:10.1093/nar/gkr1060](#)
50. T. Glatter, A. Wepf, R. Aebersold, M. Gstaiger, An integrated workflow for charting the human interaction proteome: Insights into the PP2A system. *Mol. Syst. Biol.* **5**, 237 (2009). [Medline doi:10.1038/msb.2008.75](#)
51. L. T. Jae, M. Raaben, A. S. Herbert, A. I. Kuehne, A. S. Wirchnianski, T. K. Soh, S. H. Stubbs, H. Janssen, M. Damme, P. Saftig, S. P. Whelan, J. M. Dye, T. R. Brummelkamp,

- Lassa virus entry requires a trigger-induced receptor switch. *Science* **344**, 1506–1510 (2014). [Medline doi:10.1126/science.1252480](#)
52. E. Campeau, V. E. Ruhl, F. Rodier, C. L. Smith, B. L. Rahmberg, J. O. Fuss, J. Campisi, P. Yaswen, P. K. Cooper, P. D. Kaufman, A versatile viral system for expression and depletion of proteins in mammalian cells. *PLOS ONE* **4**, e6529 (2009). [Medline doi:10.1371/journal.pone.0006529](#)
53. E. L. Rudashevskaya, R. Sacco, K. Kratochwill, M. L. Huber, M. Gstaiger, G. Superti-Furga, K. L. Bennett, A method to resolve the composition of heterogeneous affinity-purified protein complexes assembled around a common protein by chemical cross-linking, gel electrophoresis and mass spectrometry. *Nat. Protoc.* **8**, 75–97 (2013). [Medline doi:10.1038/nprot.2012.133](#)
54. M. Varjosalo, R. Sacco, A. Stukalov, A. van Drogen, M. Planyavsky, S. Hauri, R. Aebersold, K. L. Bennett, J. Colinge, M. Gstaiger, G. Superti-Furga, Interlaboratory reproducibility of large-scale human protein-complex analysis by standardized AP-MS. *Nat. Methods* **10**, 307–314 (2013). [Medline doi:10.1038/nmeth.2400](#)
55. M. L. Huber, R. Sacco, K. Parapatics, A. Skucha, K. Khamina, A. C. Müller, E. L. Rudashevskaya, K. L. Bennett, abFASP-MS: Affinity-based filter-aided sample preparation mass spectrometry for quantitative analysis of chemically labeled protein complexes. *J. Proteome Res.* **13**, 1147–1155 (2014). [Medline doi:10.1021/pr4009892](#)
56. D. N. Perkins, D. J. Pappin, D. M. Creasy, J. S. Cottrell, Probability-based protein identification by searching sequence databases using mass spectrometry data. *Electrophoresis* **20**, 3551–3567 (1999). [Medline doi:10.1002/\(SICI\)1522-2683\(19991201\)20:18<3551::AID-ELPS3551>3.0.CO;2-2](#)
57. J. Colinge, A. Masselot, M. Giron, T. Dessingy, J. Magnin, OLAV: Towards high-throughput tandem mass spectrometry data identification. *Proteomics* **3**, 1454–1463 (2003). [Medline doi:10.1002/pmic.200300485](#)
58. A. Pichlmair, K. Kandasamy, G. Alvisi, O. Mulhern, R. Sacco, M. Habjan, M. Binder, A. Stefanovic, C. A. Eberle, A. Goncalves, T. Bürckstümmer, A. C. Müller, A. Fauster, C. Holze, K. Lindsten, S. Goodbourn, G. Kochs, F. Weber, R. Bartenschlager, A. G. Bowie, K. L. Bennett, J. Colinge, G. Superti-Furga, Viral immune modulators perturb the human molecular network by common and unique strategies. *Nature* **487**, 486–490 (2012). [Medline doi:10.1038/nature11289](#)
59. M. Lavallée-Adam, P. Cloutier, B. Coulombe, M. Blanchette, Modeling contaminants in AP-MS/MS experiments. *J. Proteome Res.* **10**, 886–895 (2011). [Medline doi:10.1021/pr100795z](#)
60. L. Cong, F. A. Ran, D. Cox, S. Lin, R. Barretto, N. Habib, P. D. Hsu, X. Wu, W. Jiang, L. A. Marraffini, F. Zhang, Multiplex genome engineering using CRISPR/Cas systems. *Science* **339**, 819–823 (2013). [Medline doi:10.1126/science.1231143](#)
61. T. O. Auer, K. Duroure, A. De Cian, J. P. Concorde, F. Del Bene, Highly efficient CRISPR/Cas9-mediated knock-in in zebrafish by homology-independent DNA repair. *Genome Res.* **24**, 142–153 (2014). [Medline doi:10.1101/gr.161638.113](#)

Gene essentiality and synthetic lethality in haploid human cells

Vincent A. Blomen, Peter Májek, Lucas T. Jae, Johannes W. Bigenzahn, Joppe Nieuwenhuis, Jacqueline Staring, Roberto Sacco, Ferdy R. van Diemen, Nadine Olk, Alexey Stukalov, Caleb Marceau, Hans Janssen, Jan E. Carette, Keiryn L. Bennett, Jacques Colinge, Giulio Superti-Furga and Thijm R. Brummelkamp

Science 350 (6264), 1092-1096.

DOI: 10.1126/science.aac7557 originally published online October 15, 2015

Zeroing in on essential human genes

More powerful genetic techniques are helping to define the list of genes required for the life of a human cell. Two papers used the CRISPR genome editing system and a gene trap method in haploid human cells to screen for essential genes (see the Perspective by Boone and Andrews). Wang *et al.*'s analysis of multiple cell lines indicates that it may be possible to find tumor-specific dependencies on particular genes. Blomen *et al.* investigate the phenomenon in which nonessential genes are required for fitness in the absence of another gene. Hence, complexity rather than robustness is the human strategy.

Science, this issue p. 1096 and p. 1092; see also p. 1028

ARTICLE TOOLS

<http://science.sciencemag.org/content/350/6264/1092>

SUPPLEMENTARY MATERIALS

<http://science.sciencemag.org/content/suppl/2015/10/14/science.aac7557.DC1>

RELATED CONTENT

<http://stke.sciencemag.org/content/sigtrans/8/404/ec345.abstract>
<http://science.sciencemag.org/content/sci/350/6264/1028.full>
<http://science.sciencemag.org/content/sci/350/6264/1096.full>

REFERENCES

This article cites 61 articles, 16 of which you can access for free
<http://science.sciencemag.org/content/350/6264/1092#BIBL>

PERMISSIONS

<http://www.sciencemag.org/help/reprints-and-permissions>

Use of this article is subject to the [Terms of Service](#)